The AdS / CFT Correspondence:

bulk to boundary map and applications

by

Fernando Michell Falieri Nogueira

B.Sc., Federal University of Minas Gerais, 2007
M.Sc., Federal University of Minas Gerais, 2009

A THESIS SUBMITTED IN PARTIAL FULFILLMENT OF
THE REQUIREMENTS FOR THE DEGREE OF

DOCTOR OF PHILOSOPHY

in

The Faculty of Graduate and Postdoctoral Studies

(Physics)

THE UNIVERSITY OF BRITISH COLUMBIA

(Vancouver)

August 2014

Abstract

The holographic principle connects theories with gravity to lower dimensional theories without gravity. Notably, the AdS/CFT correspondence — the first concrete realization of the holographic principle — provides a one to one map between string theory in Anti de Sitter space, and a strongly coupled, large $\mathcal{N}$, SU(N) super Yang-Mills gauge theory in one less dimension.

In this thesis, within the context of holographic field theories, I improve on the current understanding of the map between gravity (bulk) and gauge theory (boundary) degrees of freedom. Furthermore, I explore some of the applications of the AdS/CFT correspondence to the study of strongly coupled field theories.

I study the map between bulk and boundary degrees of freedom mainly by trying to determine what is the gravity dual of a subset of the boundary field theory. In the process of doing so I show how extremal surfaces, entanglement entropy, hyperbolic black holes, and boson stars are fundamental tools in this quest.

Next, I explore a few examples of direct applications of the correspondence as a model building device. I discuss how AdS/CFT can be used to construct quasi realistic strongly coupled physical systems ranging from relativistic fluids to plasmas and high temperature superconductors. Finally, I compare some of the results obtained in this thesis with known standard field theory results.

Preface

Chapter 1 is the sole work of the candidate.

Chapter 2 is an edited version of the work by Bartlomiej Czech, Joanna L. Karczmarek, Fernando Nogueira, and Mark Van Raamsdonk. The Gravity Dual of a Density Matrix. *Class.Quant.Grav.*, 29:155009, 2012.. It was a collaboration between the candidate's supervisor, co-supervisor, postdoctoral fellow Bartlomiej Czech, and the candidate.

Chapter 3 is an edited version of the work by Fernando Nogueira. Extremal Surfaces in Asymptotically AdS Charged Boson Stars Backgrounds. *Phys.Rev.*, D87(10):106006, 2013. And it is the sole work of the candidate.

Chapter 4 is an edited version of the work by Bartlomiej Czech, Joanna L. Karczmarek, Fernando Nogueira, and Mark Van Raamsdonk. Rindler Quantum Gravity. *Class.Quant.Grav.*, 29:235025, 2012.. It was a collaboration between the candidate's supervisor, co-supervisor, postdoctoral fellow Bartlomiej Czech, and the candidate.

Chapter 5 is the sole work of the candidate.

Chapter 6 is an edited version of the work by Fernando Nogueira and Jared B. Stang. Density versus chemical potential in holographic field theories. *Phys.Rev.*, D86:026001, 2012.. It was an even collaboration between fellow Ph.D. candidate Jared B. Stang and the candidate.

Chapter 7 is an edited version of the work by Pallab Basu, Fernando Nogueira, Moshe Rozali, Jared B. Stang, and Mark Van Raamsdonk. Towards A Holographic Model of Color Superconductivity. *New J. Phys.*, 13:055001, 2011. It was a collaboration between the candidate's supervisor, professor Moshe Rozali, postdoctoral fellow Pallab Basu, fellow Ph.D. candidate Jared B. Stang, and the candidate.

Chapter 8 is the sole work of the candidate.

Table of Contents

Appendices

List of Tables

List of Figures

Acknowledgements

I would like to thank my advisors Mark Van Raamsdonk and Joanna Karczmarek for all the invaluable help given throughout the years, all the postdoctoral fellows that were part of the string theory group, in particular Bartlomiej Czech and Pallab Basu, and all other members of the String Theory group that in one way or another helped in this journey, in particular Jared Stang, Charles Rabideau, Michael B. McDermott, Connor Behan and Philippe Sabella-Garnier.

I would also like to thank all my office colleagues with whom I shared many laughs and many memorable moments, and Oliva Dela Cruz-Cordero, the graduate program coordinator for all the help, in particular with all the international student bureaucracy.

And I would also like to thank my family and friends, specially Crystal, for being by my side all these years.

Dedication

I dedicate this thesis to my parents, without whom I could not have completed it.

Chapter 1

Introduction

1.1 Holography and AdS/CFT

The holographic principle is a remarkable idea relating theories with gravity to theories without gravity [129, 133]. The best understood example of holography is the AdS/CFT correspondence which proposes a one to one relation between a gravitational theory in anti-de Sitter space (bulk theory) and a strongly coupled, large N conformal field theory living on the conformal boundary of AdS [92, 140] (boundary theory). It advocates that each state of the boundary field theory should correspond to a configuration (not necessarily classical) of the bulk gravitational theory. This correspondence has been extensively used to study a variety of strongly coupled field theories and has led to the formulation of successful formalisms such as AdS/QCD and AdS/CMT.

In this thesis I address a particular gap in our understanding of AdS/CFT that could shine light on a myriad of long standing problems in quantum gravity and the nature of space-time. In addition, I explore some of the vast number of applications of AdS/CFT, in particular, holographic fluids, holographic field theories at finite temperature and chemical potential, and QCD like models.

First, I will show how the correspondence can be used to answer some deep questions about quantum gravity and the nature of spacetime. In particular, I argue that entanglement entropy and its holographic formulation can be seen as fundamental building blocks of holographic spacetimes. This discussion will pave the way to tackling one of the major questions surrounding the holographic principle: what is the exact map between bulk and boundary degrees of freedom.

Understanding the connection between bulk and boundary degrees of freedom is one of the main barriers in the way of the gauge / gravity duality fulfilling its potential of answering long standing problems in quantum gravity by recasting them in field-theoretic language. In order to improve this situation, further investigation of the map between bulk and boundary degrees of freedom is necessary. Optimistically, one should be able to ex-

press any variation of the boundary theory state in terms of a well defined perturbation of the bulk geometry in a one to one fashion.

Second, I will use the AdS/CFT correspondence directly to construct models for a variety of physical systems. In particular, I will show how relativistic conformal fluids arise naturally from perturbations of the bulk metric, and try to generalize this discussion hoping to elucidate how certain bulk features are connected to boundary observables. Moreover, I will use the AdS/CFT correspondence in a bottom up approach to create a model for relativistic field theories at finite temperature and chemical potential and study the main properties of these theories. Finally, as a special case of holographic field theories, I will show how a richer model can be used to describe the phenomenon of colour superconductivity and the various phase transitions expected to take place.

In the remainder of this chapter I will describe the basic tools that will be used throughout this thesis. I start by discussing how the correspondence was originally formulated and limits of its applicability. That is followed by a quick review on how to generalize holographic models to finite temperature and chemical potential regimes, and the definitions of important tools such as the holographic entanglement entropy.

1.1.1 Two sides, one theory

The most fundamental object in string theory — a string — can either be open or closed. Closed strings are free to propagate throughout space, their internal degrees of freedom are subject to (anti)periodic boundary conditions and give rise to tachyonic (negative squared mass), massless and massive excitations. The endpoints of open strings, however, can be subject to Dirichlet boundary conditions, in which case the strings require an object to which their ends can attach to, these objects are called Dp-branes.

Branes can extend in an arbitrary number p of spacial dimensions and provide a $(1+p)$ dimensional sub manifold to which open strings end points can attach to. Nevertheless, these objects are more than mere open strings hangers, branes also have mass, charge, interact with each other, and play a central role in the AdS/CFT correspondence.

While today AdS/CFT — and, more generally, the holographic principle — is believed to apply to a myriad of different scenarios, the original argument for the correspondence involved low energy excitations of D3-branes in type IIB string theory.

Let us consider type IIB string theory on a ten dimensional flat Minkowski space. Let us consider also a stack of N parallel D3-branes extending along

a $(1+3)$ dimensional hyper plane embedded within this ten dimensional space.

In the low energy limit, string theory in this background has only two kinds of excitations, massless closed strings, describing excitations of empty space, and massless open strings, describing excitations of the D-branes. It is known that the low energy effective Lagrangian of these states is that of type IIB supergravity for massless closed strings, and $\mathcal{N} = 4$ $U(N)$ super Yang Mills for massless open strings.

The full effective action of the massless modes is therefore written as

$$S = S_{bulk} + S_{brane} + S_{int}, \tag{1.1}$$

where S_{bulk} is the effective action of ten dimensional supergravity in addition to possible higher derivative corrections. S_{brane} is the brane effective action defined on the $(1+3)$ dimensional hyper plane covered by the branes, which not only includes $\mathcal{N} = 4$ $U(N)$ super Yang Mills, but also possible higher derivative corrections. And S_{int} is the effective action for the interaction between bulk and brane modes.

The total effective action in equation (1.1) can be understood as the effective description of the system once all the massive modes are integrated out. While in this general form the action is quite complicated — and, in fact, non renormalizable — in the low energy limit it simplifies greatly. In this limit, all the higher derivative terms disappear, and the interaction sector can also be neglected, leaving as a final product two decoupled systems, namely, free gravity in the bulk and a four dimensional gauge theory.

The same stack of D-branes in flat Minkowski space can be studied from a different perspective. As mentioned before, D-branes are massive objects, when their number is large ($N \to \infty$) they backreact with the background metric and are described as a black p-brane, a well known classical supergravity solution. The metric for a black p-brane is given by

$$ds^2 = f^{-1/2}\left(-dt^2 + dx_1^2 + dx_2^2 + dx_3^2\right) + f^{1/2}\left(dr^2 + r^2 d\Omega_5^2\right), \tag{1.2}$$

with

$$f = 1 + \frac{R^4}{r^4}, \quad \text{and} \quad R^4 = 4\pi g_s l_s^4 N, \tag{1.3}$$

where g_s is the string coupling, l_s is the string length and N the number of branes[1].

[1] N is related to the total flux of the $(3+1)$-form potential F_5 that will be omitted in the present discussion.

From equation (1.2) we see that E, the energy of an object measured by an observer at a given position r and, E_∞, the energy of the same object measured by another observer at infinity, are related by the red shift factor,

$$E_\infty = f^{-1/4} E. \tag{1.4}$$

Due to this red shift factor we see that from the point of view of an observer at infinity there are two kinds of low energy excitations. Long wavelength, massless particles propagating in the bulk, and arbitrary energy excitations **near** $r = 0$. Note that for large enough wavelengths, massless particles in the bulk are effectively blind to the existence of branes whose typical size is of order R; conversely, the closer we bring higher energy excitations to $r = 0$, the deeper the potential well becomes, effectively trapping them. In other words, these two types of low energy excitation decouple, leaving on the one hand free bulk supergravity, and on the other arbitrary excitations in the near horizon ($r \to 0$) limit.

The near horizon limit of the black p-brane metric in equation 1.2 is just

$$ds^2 = \frac{r^2}{R^2}\left(-dt^2 + dx_1^2 + dx_2^2 + dx_3^2\right) + R^2 \frac{dr^2}{r^2} + R^2 d\Omega_5^2, \tag{1.5}$$

which turns out to be the geometry of $AdS_5 \times S^5$. Therefore in the near horizon limit we are left with string theory in $AdS_5 \times S^5$.

Notice that the above discussion was merely two different ways of looking at the same system. While the effective descriptions we arrived at are strikingly different, our starting points were precisely the same, and in both cases we restricted our attention to the same low energy limit. Therefore, we are led to believe that these might, indeed, represent two equivalent mathematical descriptions of the same physical system. Moreover, since in both instances we found two decoupled sectors, one of which being free bulk supergravity, we are compelled to make an even stronger statement and equate $\mathcal{N} = 4$ $U(N)$ super Yang Mill in 1+3 dimensions with type IIB string theory on $AdS_5 \times S^5$.

Coupling strength dichotomy

In the above discussion I showed how on one side the decoupling between supergravity modes and super Yang Mills gauge theory, and on the other side the decoupling between supergravity modes and string theory modes in the near horizon limit of black p-branes was central to the AdS/CFT correspondence. The argument behind the decoupling involved taking the low energy limit in both cases, which, in the black p-brane scenario, involved

taking the near horizon limit and the long wavelength limit. In addition, in both cases the supergravity approximation can only be achieved in the large N limit of the number of branes.

From the coupling parameter g_{YM} of Yang Mills theories and the gauge group parameter N the 't Hooft coupling parameter given by $g^2_{YM}N$ can be constructed. In order to treat Yang Mills theories with gauge group SU(N) perturbatively both the 't Hooft coupling needs to be small, as well as the gauge field parameter N has to be large, i.e.: $g^2_{YM}N \ll 1$ while $N \gg 1$.

Alternatively, in the context of string theory, quantum gravity effects can only be dismissed when the spacetime curvature R is much larger than the string scale l_s. However, from equation 1.3 and the fact that the string coupling g_s is proportional to g^2_{YM} we conclude that working on the perturbative regime of SYM would require the field theory and gravity parameters to obey

$$g^2_{YM}N \sim g_sN \sim \frac{R^4}{l_s^4} \ll 1, \tag{1.6}$$

where R is the radius of the AdS_5 space. Conversely, ensuring that the classical gravity description of string theory is reliable requires that

$$\frac{R^4}{l_s^4} \sim g_sN \sim g^2_{YM}N \gg 1, \tag{1.7}$$

therefore, the conclusion is these two limits are incompatible. This incompatibility is precisely what makes the AdS/CFT correspondence such a useful tool. It provides both a way of dealing with strongly coupled gauge theories (albeit in the large N limit only) by exploring their classical gravity duals, or, alternatively, a way of dealing with quantum gravity by exploring its weakly coupled field theory dual.

While the above mentioned limits of the duality are specially interesting, broadly speaking the consequences of the AdS/CFT are deep. The precise equivalence between a quantum gravity theory and a lower dimensional quantum field theory imposes strong constraints on the global and local behaviour of these two theories. Ranging from the loss of information inside a black hole, to the phase transitions of sub-atomic matter, the knowledge that these two, while at first sight completely different physical systems, are in fact equivalent to each other, offers a completely new approach to such questions and many others.

1.1.2 The bulk to boundary map

Understanding the exact connection between bulk and boundary degrees of freedom is among the most fundamental questions surrounding the AdS/CFT correspondence. A better understanding of such map would allow recasting long standing quantum gravity problems in a field theoretic language. Therefore, further investigation of the map between bulk and boundary degrees of freedom is necessary. Optimistically, it should be possible to express any variation of the boundary theory state in terms of a well defined perturbation of the bulk geometry; conversely, any changes in the bulk should be related to a particular deformation of the boundary state in a one to one fashion.

In part I of this thesis I will improve on the current understanding of the relation between boundary and bulk degrees of freedom in holographic duals. By examining how information contained in a portion of the boundary theory is encoded in the bulk and how certain theories respond to small perturbations, I hope to gain insight into the elusive bulk to boundary dictionary. To do so I will tackle this problem in a few different ways, both from bulk as well as boundary perspectives.

The goal is to investigate how degrees of freedom inside a subregion of a holographic field theory correlate to those in the bulk gravity dual. A good understanding of how to describe seemingly local degrees of freedom in gravity theories, specially in the context of the gauge / gravity duality, remains elusive. Therefore, by examining the question of what bulk region should contain enough information to be dual to a particular subregion of the boundary, I can shed some light on how degrees of freedom, both local and non local, in these dual theories relate to each other.

While there are a myriad of possible ways to investigate the bulk to boundary dictionary, in this thesis I will focus on sub-regions of the field theory and investigate the properties of gravity duals when only partial information is available. These subregions can be constructed by considering accelerated bulk observers and will naturally lead to entanglement entropy and its holographic dual as I will discuss in the next section. Below I will argue that from a purely field theoretic perspective it is easy to see how entanglement entropy and incomplete knowledge of a theory's state are closely related. Combined with the Ryu-Takayanagi[118] proposal (also discussed below), I can use the holographic prescription of EE (entanglement entropy) to directly connect, and in special cases even quantify, boundary and bulk statements regarding the amount of information contained in a given region and how it is translated between bulk and boundary languages.

Entanglement entropy and partial Boundary Information

The general picture in the AdS/CFT correspondence is that of a field theory defined on the conformal boundary of AdS space, with each state of the field theory being dual to a particular geometry of the bulk[2]. In its most well understood form, the field theory is the large N, strongly coupled limit of supersymmetric $U(N)$ Yang Mills. In this limit the gravity theory simplifies to classical supergravity, and its dynamics is given by Einstein's equations.

Among the extensive list of progress made in the direction of better understanding this duality is the proposal for a holographic dual of entanglement entropy. For a quantum system with Hilbert space $\mathcal{H} = \mathcal{H}_A \otimes \mathcal{H}_B$ and density matrix ρ, the entanglement entropy of the subsystem A is defined as $S_A = -\mathrm{Tr}_A \rho_A \log \rho_A$, where $\rho_A = \mathrm{Tr}_B \rho$ is the reduced density matrix for the subsystem A. The holographic version of this physical quantity was proposed by Ryu and Takayanagi [118] and is given by the area of the minimal surface $\gamma_{\delta A}$ that is anchored at the boundary of A, δA, and extends into the bulk space-time[3] as can be seen in figure 1.1.

Since these extremal surfaces are related to entanglement entropy of the boundary subregion A, they comprise a good measure of the amount of information encoded as entanglement between degrees of freedom inside A and in its complement $\bar{A}$. Naturally one should expect that these minimal areas surfaces play a role at understanding how boundary degrees of freedom are related to bulk degrees of freedom.

In AdS/CFT, the expectation values of field theory operators are related to boundary conditions of the bulk fields, hence, given the knowledge of the expectation values of certain operators of the field theory, one should be able to determine the bulk field (via integration), at least very near the boundary. Obviously, if all possible expectation values are known in a Cauchy surface of the boundary ($A \cup \bar{A}$ in the example above), full knowledge of the gravity theory is expected, however that is not the case if only partial boundary information is available.

Clearly one can see that any bulk field in a region causally connected to $\bar{A}$ can not be fully determined since its boundary value problem is not well defined. Nevertheless, while this maximum bound is clear, and while a

[2] In general the geometrical picture will be highly quantum mechanical and a classical, well behaved metric does not usually exist.

[3] Given the negatively curved nature of anti de-Sitter space, a minimal area surface that is anchored at the boundary will necessarily extend into the bulk. Note, however, that the area of such surfaces is formally infinite, nevertheless we can regularize it by imposing a IR cutoff, which, in turn, is related to the UV cutoff normally imposed on the field theory entanglement entropy (which is also infinite).

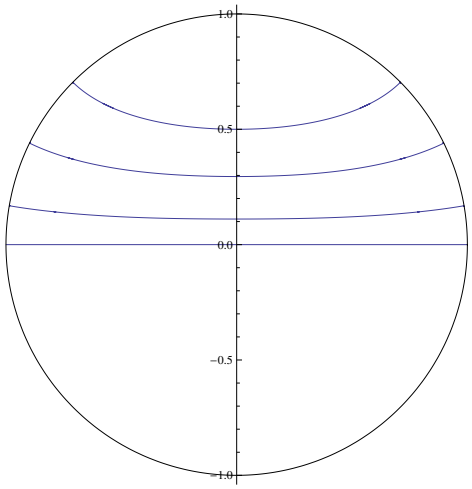

Figure 1.1: A number of extremal surfaces anchored at the boundary of a time slice of global AdS space. The boundary region A is the hemisphere bounded by the endpoints of one of the extremal surfaces γ_A (blue lines), and the boundary of A, δA, is the boundary circle to which the surface attaches to.

minimum amount of bulk information is guaranteed from any set of data, the exact bulk dual to a piece of boundary data, say, the region A, is still unknown.

Accelerated bulk observers

One way of modelling an observer with limited access to boundary information, and putting the ideas outlined above to test, is to consider bulk accelerated observer and wedges of AdS. Similarly to Rindler wedges in Minkowski space, Rindler wedges of AdS are the portions of the full manifold accessible to constantly accelerating observers. From the boundary perspective, such incomplete access to boundary data is tantamount to partially tracing over some of the field theory's degrees of freedom, therefore Rindler AdS immediately provides a quantitative formulation of the ideas in the previous section.

The metric describing such an accelerated observer is that of a hyperbolic black hole in AdS. This metric has a horizon, therefore a temperature associated with it, and its boundary is in the same conformal class as Rindler space and hyperbolic spacetime. It is interesting to note that for a special

temperature ($T = \frac{1}{2\pi R}$), the metric of the AdS Rindler wedge is diffeomorphic to that of pure AdS itself. That is, while from the accelerated observer's point of view the manifold he is embeded in has a horizon, this is nothing but a coordinate pathology, and the analytic extension of this particular metric simply restores AdS.

This is specially relevant since the state of the total field theory is known to be the vacuum state, hence the quantum state dual to the wedge of the accelerated observer is the partial trace over the boundary region complementary to the boundary of the Rindler AdS wedge. It can immediately be seen how entanglement entropy and its holographic formulation enter the problem.

Once the general picture between hyperbolic black holes and boundary Rindler wedges is established, the temperature of the black hole can be varied while the behaviour of physical observers such as the energy momentum tensor is being tracked. By doing so, considerable insight on the interplay between boundary entanglement and the properties of the bulk geometry can be obtained.

1.2 Phenomenological applications

Earlier in this Introduction I discussed how the coupling of the gravity dual and its field theory counterpart are inversely related. In particular, when the gauge theory is strongly coupled, a regime where perturbation theory methods are not applicable, the bulk dynamics is in its simplest form, i.e.: classical general relativity. This is arguably the single most compelling feature of the AdS/CFT correspondence: not only does it provide an abstract relation between generic field theories and gravity systems, but it also provides a tool box to tackle notoriously difficult problems in the study of strongly coupled field theories.

In addition to offering the means to study aspects of strongly coupled field theories that are usually beyond the scope of standard quantum field theory methods, the AdS/CFT correspondence enables one to go even further and easily generalize theses systems to finite temperature and finite chemical potential cases. Therefore, the range of applications of the duality to phenomenological toy models is vast, including the behaviour of high temperature quark plasmas, strongly coupled electrons, high temperature superconductors, and even low energy configurations of QCD.

In part II of this thesis I will address examples of some of the applications mentioned above, and I will show how rich even basic holographic models

can be. A few basic concepts behind some of the systems and examples mentioned above are introduced bellow.

1.2.1 Holographic fluids and metric perturbations

Studying the behaviour of small perturbations of certain metrics in General Relativity leads to a remarkable conformal fluid interpretation when viewed in the context of the Gauge / Gravity duality. From the modelling of high temperature relativistic plasma [21, 123], to the emergence of Einstein's Equations from boundary field theory considerations [44, 88], the applications are plenty. The investigation of small metric perturbations is usually conducted iteratively; at each step the perturbed metric is corrected in such a way that it solves Einstein's Equation to a desired order of accuracy. While certain problems allow for analytic solutions at any order, a numerical approach can come in handy.

In line with the aforementioned results, small metric perturbations can be used to investigate to what degree a slight variation of the state of the boundary theory can alter the bulk metric. In particular, certain patterns of the field theory state will inexorably lead to a pathological bulk geometry. This constrains the class of physically allowed boundary states by imposing certain smooth geometrical conditions on the bulk theory.

In this thesis I investigate what kind of information about the bulk and boundary theories can be uncovered by small metric (or, from the boundary perspective, state) perturbations, using both analytical and numerical methods. In particular I focus on the relation between the boundary theory energy momentum tensor and the bulk metric, and how one can be used to deduce the other.

1.2.2 Finite temperature in holographic field theories

The study of field theories at finite temperature is hard and many of the methods suitable for the zero temperature case can not be used to tackle finite temperature questions. Luckily AdS/CFT provides a natural and relatively easy way of modelling a holographic field theory at finite temperature.

The correspondence connects a spacetime with a black hole to a boundary field theory on a thermal state whose temperature is just the Hawking temperature of the black hole. The Hawking temperature is found from the euclideanized bulk metric

$$ds^2 = \alpha(r)d\tau^2 + \frac{dr^2}{\beta(r)}$$

with periodic $\tau = it$ coordinate and $\alpha(r_+) = \beta(r_+) = 0$, by demanding regularity at the horizon, ultimately leading to

$$T = \frac{\sqrt{\alpha'(r_+)\beta'(r_+)}}{4\pi}.$$

This strikingly simple connection between black holes and thermal states of conformal field theories is extremely useful for building phenomenological models as well as for studying basic aspects of quantum gravity.

1.2.3 Finite density in holographic field theories

Similar to the finite temperature case, finite chemical potential also poses a challenge to standard methods in quantum field theory. Not only is the analytical analysis particularly hard, but even numerical approaches using lattice techniques fail to tackle this problem.

The holographic dictionary dictates that a conserved charge in the field theory is dual to a massless $U(1)$ gauge field A in the bulk. The chemical potential and the charge density are encoded in the asymptotic behaviour of the time-component of the gauge field as

$$\mu = A_t(\infty), \tag{1.8}$$

and

$$\rho = \left(\frac{1}{d-2}\right) \frac{\partial \mathcal{L}}{\partial(\partial_r A_t)}\bigg|_{r=\infty}, \tag{1.9}$$

where r is the radial direction in the bulk, with the boundary living at $r = \infty$. After writing down the gravitational lagrangian, our prescription for computing the charge density at a given chemical potential is to solve the equations of motion with a fixed boundary condition for the gauge field, equation (1.8), before reading off the density using equation (1.9).

1.2.4 Holographic QCD

Quantum Chromodynamics is believed to display a rich phase structure at finite temperature and chemical potential, with phase transitions associated with deconfinement, nuclear matter condensation, the breaking of (approximate) flavor symmetries, and the onset at high density of quark matter phases displaying color superconductivity. However, apart from the regimes of asymptotically large temperature or chemical potential, a direct analytic study of the thermodynamic properties of the theory is not possible.

A modern route to understanding properties of strongly coupled gauge theories, that would be otherwise inaccessible, is via the AdS/CFT correspondence, or gauge theory / gravity duality. A bottom-up approach can be used to generate a holographic system (starting with a gravity action) describing a confining gauge theory that exhibit a quark-matter phase with colour (or flavour) superconductivity at large chemical potential.

Part I

Nature of Spacetime

Chapter 2

Dual of a Density Matrix

2.1 Introduction

The AdS/CFT correspondence [1, 92] relates states of a field theory on some fixed spacetime **B** to states of a quantum gravity theory for which the spacetime metric is asymptotically locally AdS with boundary geometry **B**. The field theory provides a nonperturbative description of the quantum gravity theory that is manifestly local on the boundary spacetime: for a given spacelike slice of the boundary spacetime **B**, the degrees of freedom in one subset are independent from the degrees of freedom in another subset. On the gravity side, identifying independent degrees of freedom is much more difficult; for example, the idea of black hole complementarity [131] suggests that local excitations inside the horizon of a black hole cannot be independent of the physics outside the horizon. It is therefore interesting to ask whether we can use our knowledge of independent field theory degrees of freedom to learn anything about which degrees of freedom on the gravity side may be considered to be independent.

In this chapter, we consider the following question: Given a CFT on **B** in a state $|\Psi\rangle$ dual to a spacetime M with a geometrical description, and given a subset A of a spatial slice of **B**, what part of the spacetime M can be fully reconstructed from the density matrix ρ_A describing the state of the subset of the field theory degrees of freedom in A?

An immediate question is why we expect there to be any region that can be reconstructed if we know only about the degrees of freedom on a subset of the boundary. If the map between boundary degrees of freedom and the bulk spacetime is sufficiently non-local, it could be that information from every region of the boundary spacetime is needed to reconstruct any particular subset of M. However, there are various reasons to be more optimistic. It is well known that the asymptotic behavior of the fields in the bulk spacetime is given directly in terms of expectation values of local operators in the field theory (together with the field theory action). Equipped with

this boundary behavior of the bulk fields in some region of the boundary[4] and the bulk field equations, we should be able to integrate these field equations to find the fields in some bulk neighborhood of this boundary region. We can also compute various other field theory quantities (e.g. correlation functions, Wilson loops, entanglement entropies) restricted to the region A or its domain of dependence. According to the AdS/CFT dictionary, these give us direct information about nearby regions of the bulk geometry.

The notion that particular density matrices can be associated with certain patches of spacetime was advocated in [135, 137].[5] There, it was pointed out that a given density matrix may arise from many different states of the full system, or from a variety of different quantum systems that contain this set of degrees of freedom as a subset. Different pure states that give rise to the same density matrix for the subset correspond to different spacetimes with a region in common; this common region can be considered to be the dual of the density matrix.[6]

In the bulk of this chapter, we seek to understand in general the region of a bulk spacetime M that can be directly associated with the density matrix describing a particular subset of the field theory degrees of freedom. We begin in Section 2 by reviewing some relevant facts from field theory and arguing that the density matrix associated with a region A may be more naturally associated with the domain of dependence D_A (defined below). In Section 3, we outline in more detail the basic question considered in the chapter. In Section 4, we propose several basic constraints on the region $R(A)$ dual to a density matrix ρ_A. In Section 5, we consider two regions that are plausibly contained in $R(A)$. First, we argue that $z(D_A)$, the intersection of the causal past and causal future of D_A, satisfies our constraints and should be contained in $R(A)$, as should its domain of dependence, $\hat{z}(D_A)$.[7] We note that in some special cases, $R(A)$ cannot be larger than $\hat{z}(D_A)$. However, in generic spacetimes, we argue that entanglement observables

[4] As we recall below, knowledge of the field theory density matrix for a spatial region A allows us to compute any field theory quantities localized to a particular codimension-zero region of the boundary, the domain of dependence of A.

[5] For an earlier discussion of mixed states in the context of AdS/CFT, see [47].

[6] As a particular example, it was pointed out in [135, 137] that a CFT on S^d in a thermal density matrix, commonly understood to be dual to an AdS/Schwarzchild black hole, cannot possibly know whether the whole spacetime is the maximally extended black hole; only the region outside the horizon is common to all states of larger systems for which the CFT on S^d forms a subset of degrees of freedom described by a thermal density matrix.

[7] We denote domains of dependence in the boundary with $D_\cdot$ (for example, D_A), while domains of dependence in the bulk are marked with a hat $\hat{}$.

that can be calculated from the density matrix ρ_A certainly allow us to probe regions of spacetime beyond $\hat{z}(D_A)$.[8] This motivates us to consider another region, $w(D_A)$, defined as the union of surfaces used to calculate these entanglement observables (defined more precisely below) according to the holographic entanglement entropy proposal [73, 118]. We show that $w(D_A)$ (or more precisely, its domain of dependence $\hat{w}(D_A)$) also satisfies our constraints, and that for a rather general class of spacetimes, there is a sense in which $R(A)$ cannot be larger than $\hat{w}(D_A)$. On the other hand, we show that in some examples, $R(A)$ must be larger than $\hat{w}(D_A)$. We conclude in Section 6 with a summary and discussion.

2.2 Field theory considerations

To begin, consider a field theory on some globally hyperbolic spacetime $\mathbf{B}$, and consider a spacelike slice Σ that forms a Cauchy surface. Then, classically, the fields on this hypersurface and their derivatives with respect to some timelike future-directed unit vector orthogonal to the hypersurface determine the complete future evolution of the field. Quantum mechanically, the fields on this hypersurface can be taken as the basic set of variables for quantization and conjugate momenta defined with respect to the timelike normal vector.

Now consider some region A of the hypersurface Σ. Since the field theory is local, the degrees of freedom in A are independent from the degrees of freedom in the complement $\bar{A}$ of A on Σ. Thus, the Hilbert space can be decomposed as a tensor product $\mathcal{H} = \mathcal{H}_A \otimes \mathcal{H}_{\bar{A}}$, and we can associate a density matrix $\rho_A = \mathrm{tr}\left((|\Psi\rangle\langle\Psi|)\right)_{\bar{A}}$ to the degrees of freedom in A. This density matrix captures all information about the state of the degrees of freedom in A and can be used to compute any observables localized to A.

In fact, the density matrix ρ_A allows us to compute field theory observables localized to a larger region D_A known as the domain of dependence of A. The domain of dependence D_A is the set of points p in $\mathbf{B}$ for which every (inextensible) causal curve through p intersects A (see Figure 2.1). Classically, the region D_A is the subspace of $\mathbf{B}$ in which the field values are completely determined in terms of the initial data on A. Quantum mechanically, any operator in D_A can be expressed in terms of the fields in A alone and therefore computed using the density matrix ρ_A.

As can be seen from Figure 2.1, any other spacelike surface $\tilde{A}$ homologous

[8] It is an open question whether these observables are enough to reconstruct the spacetime beyond $\hat{z}(D_A)$, so we cannot say with certainty that $R(A)$ is larger than $\hat{z}(D_A)$.

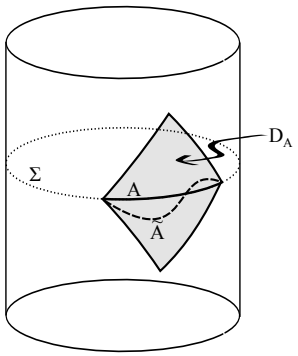

Figure 2.1: A spacelike slice Σ of a boundary manifold $\mathbf{B}$ ($= S^1 \times$ time) with a region A and its domain of dependence D_A. The same domain of dependence arises from any spacelike boundary region $\tilde{A}$ homologous to A with $\partial A = \partial \tilde{A}$.

to A with boundary $\partial \tilde{A} = \partial A$ shares its domain of dependence.[9] Thus, in some other quantization of the theory based on a hypersurface $\tilde{\Sigma}$ with $\tilde{A} \subset \tilde{\Sigma}$, we expect that the density matrix $\rho_{\tilde{A}}$ contains the same information as the density matrix ρ_A. It is then perhaps more natural to associate density matrices directly with domain of dependence regions. This observation is important for our considerations below: in constructing the bulk region dual to a density matrix ρ_A, it is more natural to use the boundary region D_A as a starting point, rather than the surface A.

It is useful to note that a quantum field theory on a particular domain of dependence can be thought of as a complete quantum system, independent of the remaining degrees of freedom of the field theory. The observables of this field theory are the set of all operators built from the fields on A. The state of the theory is specified by a density matrix ρ_A, which allows us to compute any such observable. The spectrum of this density matrix, and associated observables such as the von Neumann entropy, give additional information about the system. We can interpret this in a thermodynamic way as giving information about the ensemble of pure states described by the density matrix. Alternatively, viewing this system as a subset of a larger

[9] To see this, we note that since A and $\tilde{A}$ are homologous, we can deform A into $\tilde{A}$ and define $\mathcal{B}$ to be the volume bound by A and $\tilde{A}$. Then for any point p in $\mathcal{B}$, consider an inextensible causal curve through p. Such a curve must necessarily pass through A. But it cannot pass through A twice, since A is spacelike. On the other hand, the curve must intersect the boundary of the region $\mathcal{B}$ twice (on the past boundary and on the future boundary), so it must have an intersection with $\tilde{A}$.

system that we assume is in a pure state, we can interpret this additional information as telling us about the entanglement between the degrees of freedom in our causal development region with other parts of the system.

2.3 The gravity dual of ρ_A

In this section, we consider the question of how much information the density matrix ρ_A carries about the dual spacetime. We restrict the discussion to states of the full system that are dual to some spacetime M with a good classical description. Specifically, we ask the question

Question: *Suppose that a field theory on a spacetime* **B** *in a state* $|\Psi\rangle$ *has a dual spacetime* M *with a good geometrical description (e.g. a solution to some low-energy supergravity equations). How much of* M *can be reconstructed given only the density matrix* ρ_A *for the degrees of freedom in a subset* A *of some spacelike slice of the boundary?*

Alternatively, we can ask:

Consider all states $|\Psi_\alpha\rangle$ *with dual spacetimes* M_α *that give rise to a particular density matrix* ρ_A *for region* A *of the boundary spacetime. What is the largest region common to all the* M_α*s?*

We recall that knowledge of the density matrix ρ_A allows us to calculate any field theory observable involving operators localized in the domain of dependence D_A, plus additional quantities such as the entanglement entropy associated with the degrees of freedom on any subset of A. According to the AdS/CFT dictionary, these observables give us a large amount of information about the bulk spacetime, particularly near the boundary region D_A, so it is plausible that at least some region of the bulk spacetime can be fully reconstructed from this data. We will refer to this region as $R(A)$. We expect that in general the density matrix ρ_A carries additional information about some larger region $G(A)$, but this additional information does not represent the complete information about $G(A) - R(A)$.

In this chapter, we do not attempt to come up with a procedure to reconstruct the region $R(A)$; rather we will attempt to use general arguments to constrain how large $R(A)$ can be.

2.4 Constraints on the region dual to ρ_A

Before considering specific proposals for $R(A)$, it will be useful to point out various constraints that $R(A)$ should satisfy. First, since the density matrices for any two subsets A and $\tilde{A}$ with the same domain of dependence D correspond to the same information in the field theory, we expect that the region of spacetime that can be reconstructed from ρ_A is the same as the region that can be reconstructed from $\rho_{\tilde{A}}$. Thus we have:

Constraint 1: *If A and $\tilde{A}$ have the same domain of dependence D, then $R(A) = R(\tilde{A})$.*

For a particular boundary field theory, the bulk spacetime will be governed by some specific low-energy field equations. We assume that we are working with a known example of AdS/CFT so that these equations are known. If we know all the fields in some region R of the bulk spacetime M, we can use these field equations to find the fields everywhere in the bulk domain of dependence of R (which we denote by $\hat{R}$). Since $R(A)$ is defined to be the largest region of the bulk spacetime that we can reconstruct from ρ_A, we must have:

Constraint 2: $\hat{R}(A) = R(A)$.

Now, suppose we consider two non-intersecting regions A and B on some spacelike slice of the boundary spacetime. The degrees of freedom in A and B are completely independent, so it is possible to change the state $|\Psi\rangle$ such that ρ_B changes but ρ_A does not.[10] Changes in ρ_B will generally affect the region $R(B)$ in the bulk spacetime, but as a consequence can also affect any region in the causal future $J^+(R(B))$ or causal past $J^-(R(B))$ of $R(B)$. But these changes can have no effect on the region $R(A)$ since this region can be reconstructed from ρ_A, which does not change. Thus, we have:

Constraint 3: *If A and B are non-intersecting regions of a spacelike slice of the boundary spacetime, then $R(A)$ cannot intersect $J(R(B))$.*

Here we have defined $J(R) = J^-(R) \cup J^+(R)$. Note that whatever $R(B)$ is, it certainly includes D_B so as a corollary, we can say that $R(A)$ cannot intersect $J(D_B)$. Taking $B = \bar{A}$ (i.e. as large as possible without intersecting A), we get a definite upper bound on the size of $R(A)$: it cannot be larger than the complement of $J(D_{\bar{A}})$.

[10] Further, we expect that for some subset of these variations, the dual spacetime continues to have a classical geometric description.

2.5 Possibilities for $R(A)$

Let us now consider some physically motivated possibilities for the region $R(A)$. An optimistic expectation is that we could reconstruct the entire region $G(A)$ of the bulk spacetime M used in calculating any field theory observable localized in D_A (for example, all points touched by any geodesic with boundary points in D_A). However, this cannot be a candidate for $R(A)$, since it is easy to find examples of non-intersecting A and B on some spacelike slice of a boundary spacetime such that geodesics with endpoints in B intersect with geodesics with endpoints in A.[11] Thus, $G(A) \cap G(B) \neq \emptyset$ (which implies $G(A) \cap J(G(B)) \neq \emptyset$) and so Constraint 3 is violated.

A lesson here is that even if field theory observables calculated from a boundary region D_A probe a certain region of the bulk, they cannot necessarily be used to reconstruct that region. Generally, we will have $R(A) \subset G(A) \subset M$, where ρ_A contains complete information about $R(A)$, some information about $G(A)$ and no information about $\bar{G}(A)$.

2.5.1 The causal wedge $z(D_A)$

A simple region that is quite plausibly included in $R(A)$ is the set of points $z(D_A)$ in the bulk that a boundary observer restricted to D_A can communicate with (i.e. send a light signal to and receive a signal back). For example, such an observer could easily detect the presence or absence of an arbitrarily small mirror placed at any point in $z(D_A)$. Formally, this region in the bulk is defined as the intersection of the causal past of D_A with the causal future of D_A in the bulk, $z(D_A) \equiv J^+(D_A) \cap J^-(D_A)$, as shown in Figure 2.2.[12] These observations correspond to perturbing the spacetime at one point in the asymptotic region and observing the asymptotic fields at another point at a later time. In the field theory language, such observations correspond to calculating response functions, in which the fields are perturbed at one point in D_A and observed at another point in D_A. Such calculations can be done using only the density matrix ρ_A, thus we expect that $z(D_A)$ is included in the region $R(A)$.

[11] For example, suppose we consider the vacuum state of a CFT on a cylinder and take A and B to be the regions $\theta \in (0, \pi/2) \cup (\pi, 3\pi/2)$ and $\theta \in (\pi/2, \pi) \cup (3\pi/2, 2\pi)$ on the $\tau = 0$ slice. Then the lines of constant θ are spatial geodesics in the bulk, and the region covered by such geodesics anchored in A clearly intersects the region of such geodesics anchored in B.

[12] Recall that the causal future $J^+(D_A)$ of D_A in the bulk is the set of points reachable by causal curves starting in D_A while the causal past $J^-(D_A)$ of D_A is the set of points, from which D_A can be reached along a causal curve.

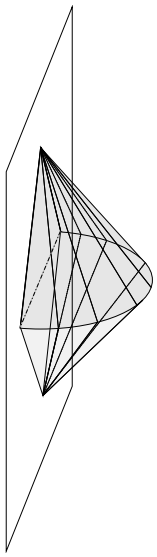

Figure 2.2: Causal wedge $z(D_A)$ associated with a domain of dependence D_A.

By condition 2, we can extend this expectation to the proposal that $\hat{z}(D_A) \subset R(A)$. It is straightforward to check that $\hat{z}(D_A)$ also satisfies condition 3.[13] Thus, the suggestion that $\hat{z}(D_A) \subset R(A)$ is consistent with our Constraints 1, 2 and 3.

The boundary of the region $z(D_A)$ in the interior of the spacetime is a horizon with respect to the boundary region D_A. Thus, the statement that we can reconstruct the region $z(D_A)$ is equivalent to saying that the information in D_A is enough to reconstruct the spacetime outside this horizon. This horizon can be an event horizon for a black hole, but in general is simply a horizon for observers restricted to the boundary region D_A.

In certain simple examples, it is straightforward to argue that $R(A)$ cannot be larger than $z(D_A)$ or $\hat{z}(D_A)$. For example, if M is pure global AdS spacetime and A is a hemisphere of the $\tau = 0$ slice of the boundary cylinder, then $z(D_A)$ is the region bounded by the lightcones from the past

[13] Suppose subsets A and B of a boundary slice do not intersect and suppose $p \in J(\hat{z}(D_B))$. Then there exists a causal curve through p that intersects $\hat{z}(D_B)$ and therefore intersects some q in $z(D_B)$. If p is also in $\hat{z}(D_A)$, this same causal curve through p must intersect a point r in $z(D_A)$. Thus, there is a causal curve from q in $z(D_B)$ to r in $z(D_A)$. By definition of z, we must be able to extend this curve to a causal curve connecting D_A to D_B. But in this situation, perturbations to the fields in D_A could affect the fields in D_B (or vice versa), and this would violate field theory causality.

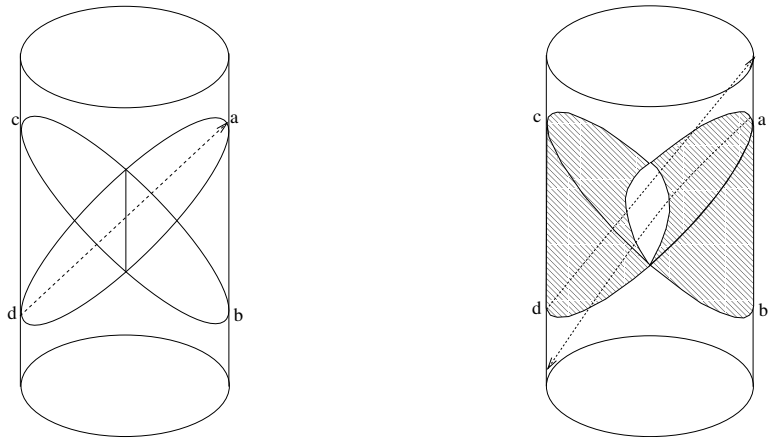

Figure 2.3: In pure global AdS, causal wedges of complementary hemispherical regions of the $\tau = 0$ slice intersect along a codimension-two surface. In generic asymptotically AdS spacetimes, they intersect only at the boundary.

and future tips of D_A and the spacetime boundary, as shown in Figure 2.3. Any point outside this region is in the causal future or causal past of the boundary region $D_{\bar{A}}$,[14] so by Constraint 3 (and the consequences discussed afterwards) such points cannot be in $R(A)$.

Information beyond the causal wedge $z(D_A)$

We might be tempted to guess that $R(A) = \hat{z}(D_A)$ in general, but we will now see that ρ_A typically contains significant information about the spacetime outside the region $\hat{z}(D_A)$. Consider the same example of a CFT on the cylinder with the same regions A and $\bar{A}$, but now consider some other state for which the dual spacetime is not pure AdS. A key observation[15] is that, generically, the wedges $z(D_A)$ and $z(D_{\bar{A}})$ do not intersect, except at the boundary of A. This follows from a result of Gao and Wald [49] that light rays through the bulk of a generic asymptotically AdS spacetime generally take longer to reach the antipodal point of the sphere than light rays along the boundary. Thus, the backward lightcone from the point a in the right panel of Figure 2.3 is different from the forward lightcone from point d. We

[14] This relies on the fact that for pure global AdS, the forward lightcone from the past tip of D_A (point b in Figure 2.3) is the same as the backward lightcone from the future tip of $D_{\bar{A}}$ (point c) and the backward lightcone from the future tip of D_A (point a in Figure 2.3) is the same as the forward lightcone from the past tip of $D_{\bar{A}}$ (point d).

[15] We are grateful to Veronika Hubeny and Mukund Rangamani for pointing this out.

can still argue that $R(A)$ cannot overlap with the region $J^+(D_{\bar{A}}) \cup J^-(D_{\bar{A}})$, but the complement of this region no longer coincides with $\hat{z}(D_A)$. Thus, it is possible that $R(A)$ is larger than $\hat{z}(D_A)$ in these general cases.[16]

To see that the density matrix ρ_A typically does contain information about the spacetime outside the region $z(D_A)$, we can take inspiration from Hubeny [70], who argued that in many examples, the field theory observables that probe deepest into the bulk of the spacetime are those computed by extremal codimension-one surfaces in the bulk.

According to the proposal of Ryu and Takayanagi [118] and the covariant generalization by Hubeny, Rangamani, and Takayanagi [73], the von Neumann entropy of a density matrix ρ_C corresponding to any spatial region C of the boundary gives the area of a surface $W(C)$ in the bulk defined either as

- the extremal codimension-two surface W in the bulk whose boundary is the boundary of C. In cases where more than one such extremal surface exists, we take the one with minimal area, or
- the surface of minimal area such that the light sheets from this surface intersect the boundary exactly at ∂D_C.

In each case, it is assumed that the surface W is homologous to C. In [73], it is argued that these two definitions are equivalent.

Now, consider the surface $W(A)$ that computes the entanglement entropy of the full density matrix ρ_A. From the second definition, it is clear that the surface W cannot have any part in the interior of $z(D_A)$. Otherwise, the light rays from any such point would reach the boundary in the interior of region D_A, and it would not be true that the light sheet from W intersects the boundary at ∂D_A. By the same argument, the surface $W(\bar{A})$ that computes the entanglement entropy of $\rho_{\bar{A}}$ cannot have any part in the interior of $z(D_{\bar{A}})$. But by the first definition, the surface $W(\bar{A})$ is the same as the surface $W(A)$, since $\partial\bar{A} = \partial A$.[17] Since $z(D_A)$ and $z(D_{\bar{A}})$ generally have no overlap in the bulk of the spacetime, it is now clear that the surface W lies outside at least one of $z(D_A)$ and $z(D_{\bar{A}})$.

[16] As an explicit example of a spacetime with this property, we can take a static spacetime with a spherically symmetric configuration of ordinary matter in the interior, e.g. the boson stars studied in [11].

[17] The equivalence of these surfaces and hence their areas is consistent with the fact that for a pure state in a Hilbert space $\mathcal{H} = \mathcal{H}_A \otimes \mathcal{H}_{\bar{A}}$, the spectrum of eigenvalues of ρ_A must equal the spectrum of eigenvalues of $\rho_{\bar{A}}$. Thus, the entanglement entropies $S(\rho_A)$ and $S(\rho_{\bar{A}})$ must agree. We do not consider here the case where the entire theory is in a mixed state.

To summarize, the area of surface W may be computed as the von Neumann entropy of either the density matrix ρ_A or the density matrix $\rho_{\bar{A}}$. In the generic case where $z(D_A)$ and $z(D_{\bar{A}})$ do not intersect in the bulk, the surface W must lie outside at least one of $z(D_A)$ and $z(D_{\bar{A}})$. Thus, we can say that either the density matrix ρ_A carries some information about the spacetime outside $z(D_A)$ or the density matrix $\rho_{\bar{A}}$ carries information about the spacetime outside $z(D_{\bar{A}})$.[18]

2.5.2 The wedge of minimal-area extremal surfaces $w(D_A)$.

Based on these observations, and the observation of Hubeny that the extremal surfaces probe deepest into the bulk in various examples, it is natural to define a second candidate for the region $R(A)$ based on extremal surfaces.

The surface $W(A)$ calculates the entanglement entropy associated with the entire domain of dependence D_A (equivalently, the largest spacelike surface in D_A). We can also consider the entanglement entropy associated with any smaller causal development region within D_A. For any such region C, there will be an associated surface $W(C)$ (as defined above) whose area computes the entanglement entropy (according to the proposal). Define a bulk region $w(D_A)$ as the set of all points contained on some minimal-area[19] extremal codimension-two surface whose boundary coincides with the boundary of a spacelike codimension-one region in D_A. The area of each such codimension-two surface is (according to [73]) equal to the entanglement entropy of the corresponding boundary region. Thus, the region $w(D_A)$ directly corresponds to the region of the bulk whose geometry is probed by entanglement observables. As we have seen, the region $w(D_A)$ generally extends beyond the region $z(D_A)$.

From the region $w(D_A)$, we can define a larger region $\hat{w}(D_A)$ as the domain of dependence of the region $w(D_A)$. As discussed above, knowing the geometry (and other fields) in $w(D_A)$ and the bulk gravitational equations should allow us to reconstruct the geometry in $\hat{w}(D_A)$.

We would now like to understand whether the region $\hat{w}(D_A)$ obeys the constraints outlined above. Constraints 1 and 2 are satisfied by definition. It is straightforward to show that Constraint 3 is satisfied assuming that the

[18] Again, it is easy to check this in specific examples. For explicit examples of spherically symmetric static star geometries asymptotic to global AdS with A equal to a hemisphere of the $\tau = 0$ slice, the surface $W(A)$ lies at $\tau = 0$ and passes through the center of the spacetime, while the regions $z(D_A)$ and $z(D_{\bar{A}})$ do not reach the center.

[19] Here, we mean minimal area among the set of extremal surfaces with the same boundary.

following conjecture holds:

Conjecture C1: *If D_A and D_B are domains of dependence for non-intersecting regions A and B of a spacelike slice of the boundary spacetime, then $w(D_A)$ and $w(D_B)$ are spacelike separated.*

Supposing that this holds, if p is in $J(\hat{w}(D_B))$, then there exists a causal curve through p intersecting $\hat{w}(D_B)$, and by definition of $\hat{w}$, this causal curve also intersects $w(D_B)$. If p is also in $\hat{w}(D_A)$, then every causal curve through p intersects $w(D_A)$. Thus, there exists a causal curve that intersects both $w(D_B)$ and $w(D_A)$, which violates **C1**. We conclude that $\hat{w}(D_A)$ satisfies Constraints 1, 2 and 3 assuming that Conjecture **C1** holds.

Aside: proving Conjecture C1

While a proof (or refutation) of Conjecture **C1** is left to future work, we make a few additional comments here.

For the case of static spacetimes, it is straightforward to prove a result similar to **C1**.

Let A_1 and A_2 be two non-intersecting regions of the $t = 0$ boundary slice of a static spacetime, with B_1 and B_2 spacelike regions in A_1 and A_2, respectively. Let $W(B_1)$ and $W(B_2)$ be the minimal surfaces in the $t = 0$ slice of the bulk spacetime with $\partial W(B_1) = \partial B_1$ and $\partial W(B_2) = \partial B_2$. Then $W(B_1)$ and $W(B_2)$ cannot intersect.

To show this, consider the part of $W(B_1)$ contained in the region of the $t = 0$ slice bounded by $W(B_2)$ and B_2, and the part of $W(B_2)$ contained in the region of the $t = 0$ slice bounded by $W(B_1)$ and B_1. If these two pieces have different areas, then by swapping the two pieces, either the new surface $W(B_1)$ or the new surface $W(B_2)$ will have a smaller area than before, contradicting the assumption that these were minimal-area surfaces. If the two pieces have the same area, the modified surfaces will have the same area as before, but the new surfaces will be cuspy[20], such that we can decrease the area by smoothing the cusps.

In attempting a more general proof, it may be useful to note that Conjecture **C1** is equivalent to the following statement (with some mild assumptions):

[20]The surfaces $W(B_1)$ and $W(B_2)$ cannot be tangent at their intersection because there should be a unique extremal surface passing through a given point with a specified tangent plane to the surface at this point.

Conjecture C2: *For any spacelike boundary region C, the surface $W(C)$ is spacelike separated from the rest of $w(D_C)$.*

To see the equivalence, assume first that **C1** holds and let $A = C$ and $B = \bar{C}$. If we assume the generic case that $W(C)$ is the same as $W(\bar{C})$, then $W(C) = W(B) \subset w(D_B)$ must be spacelike separated from $w(D_A) = w(D_C)$. Conversely, for two disjoint regions A and B, let C be any region such that $A \subset C$ and $B \subset \bar{C}$. By definition, we have that $w(D_A) \subset w(D_C)$ and $w(D_B) \subset w(D_{\bar{C}})$. Assuming again that $W(C) = W(\bar{C})$, Conjecture **C2** implies that there is a spacelike path connecting any point in $w(D_A) \subset w(D_C)$ with any point p in $W(C)$, and that there also exists a spacelike path connecting any point in $w(D_B) \subset w(D_{\bar{C}})$ with the same point p. Therefore, there is a spacelike path (through p) connecting any point in $w(D_A)$ with any point in $w(D_B)$, as required for **C1**.

While **C1** is immediately more useful, **C2** might be easier to prove. Consider any boundary region C and any point p in $w(D_C)$. Then there exists a spacelike codimension-one region I_p in the domain of dependence D_C such that $p \in W(I_p)$. I_p can be extended to a spacelike surface A_I homologous with C, with the same boundary as C, $\delta_{A_I} = \delta_C$. The surface which calculates entanglement entropy is the same for A_I and C: $W(A_I) = W(C)$. Consider now a one-parameter family of surfaces $S(\lambda)$, which continuously interpolate between $A_I = S(0)$ and $I_p = S(1)$, and the corresponding family of bulk minimal surfaces $W(S(\lambda))$ interpolating between $W(C)$ and $W(I_p)$. It is plausible that these bulk minimal surfaces change smoothly and that their deformations are spacelike; following the flow, we can find a spacelike path from p to $W(C)$, which would complete the proof of the Conjecture **C2**.

We leave further investigation of the general validity of **C1** as a question for future work.[21]

[21] We note here that the restriction to minimal extremal surfaces (rather than all extremal surfaces) is essential for the validity of this conjecture. In static spacetimes with metric of the form $ds^2 = -f(r)dt^2 + dr^2/g(r) + r^2 d\Omega^2$ where $g(0) = 1$ and $g(r) \to r^2$, it is possible that extremal surfaces bounded on one hemisphere intersect extremal surfaces bounded on the other hemisphere in cases where $g(r)$ is not monotonically increasing. For these examples, **C1** would fail if the definition of w did not restrict to minimal surfaces.

Possible connection between the geometry of $W(A)$ and the spectrum of ρ_A

To summarize the discussion so far, the region $\hat{w}(D_A)$ satisfies conditions 1, 2 and 3 assuming that Conjecture **C1** is correct. Thus, $\hat{w}(D_A)$ is a possible candidate for the region $R(A)$. A rather nice feature of this possibility is that $\hat{w}(D_A)$ intersects $\hat{w}(D_{\bar{A}})$ along the codimension-two surface $W(A) = W(\bar{A})$ defined above. Thus, the surface W represents the information in the bulk common to $\hat{w}(D_A)$ and $\hat{w}(D_{\bar{A}})$. The area of this surface corresponds to the von Neumann entropy of ρ_A, which is the simplest information shared by ρ_A and $\rho_{\bar{A}}$. We might then conjecture that the full spectrum of ρ_A (which is the same as the spectrum of $\rho_{\bar{A}}$ and represents the largest set of information common to ρ_A and $\rho_{\bar{A}}$) encodes the full geometry of the surface W (i.e. the largest set of information common to $\hat{w}(D_A)$ and $\hat{w}(D_{\bar{A}})$).

Reconstructing bulk metrics from extremal surface areas

Before proceeding, let us ask whether it is even possible that the areas of extremal surfaces with boundary in some region D_A carry enough information to reconstruct the geometry in $w(D_A)$.

Consider the simple case of a 1+1 dimensional CFT on a cylinder with D_A a diamond-shaped region on the boundary. Given any state for the CFT, we could in principle compute the entanglement entropy associated with any smaller diamond-shaped region bounded by the past lightcone of some point in D_A and the forward lightcone of some other point. This would give us one function of four variables, since each of the two points defining the smaller diamond-shaped region is labeled by two coordinates. Assuming the state has a geometrical bulk dual description, the bulk geometry will be described by a metric which consists of several functions of three variables.[22] These functions allow us to determine the entanglement entropy from the geometry in the wedge $w(D_A)$ via the Takayanagi et. al. proposal, so we have a map from the space of metrics to the space of entropy functions. Small changes in the geometry of the wedge $w(D_A)$ will generally affect the areas of some of the minimal surfaces, while small changes in the geometry outside the wedge will generally not affect these areas. It is at least plausible that the entanglement information could be used to fully reconstruct the geometry in the wedge in some cases, since the map from wedge geometries into the entanglement information is a map from finitely many functions of three variables to a function of four variables, and it is possible for such a map to

[22] We are ignoring the possible extra compact dimensions in the bulk.

be an injection.

A proven result of this form in the mathematics literature [113] is that for two-dimensional *simple*[23] compact Riemannian manifolds with boundary, the bulk geometry is completely fixed by the distance function $d(x, y)$ between points on the boundary (the lengths of the shortest geodesics connecting various points). This implies that for static three-dimensional spacetimes, the spatial metric of the bulk constant time slices can be reconstructed in principle if the entanglement entropy is known for arbitrary subsets of the boundary. However, we are not aware of any results about the portion of a space that can be reconstructed if the distance function is known only on a subset of the boundary, or of any results that apply to Lorentzian spacetimes.

Cases when $R(A)$ cannot be larger than $\hat{w}(D_A)$

We saw above that in special cases, $z(D_A)$ together with $J(z(D_{\bar{A}}))$ cover the entire spacetime, so Constraint 3 is just barely satisfied for z (or $\hat{z}$). For these examples, if $z(D_{\bar{A}})$ is in $R(\bar{A})$ then $R(A)$ cannot possibly be larger than $z(D_A)$. On the other hand, for generic spacetimes, we argued that only a portion of the spacetime is covered by $z(D_A)$ and $J(z(D_{\bar{A}}))$, leaving the possibility that $R(A)$ could be larger than $z(D_A)$. In these examples, extremal surfaces from A typically extend into the region not covered by $z(D_A)$ or $z(D_{\bar{A}})$ (or the causal past/future of these), and this motivated us to consider $\hat{w}(D_A)$ as a larger possibility for $R(A)$.

We will now see that in a much wider class of examples, $\hat{w}(D_A)$ together with $J(w(D_{\bar{A}}))$ do cover the entire spacetime. To see this, recall that the surfaces $W(A)$ and $W(\bar{A})$ computing the entanglement entropy of the entire regions A and $\bar{A}$ are the same by definition, as long as A and $\bar{A}$ are homologous in the bulk.[24] Now, suppose that for a one-parameter family of boundary regions $B(\lambda) \subset A$ interpolating between A and a point (assuming A is contractible), the surfaces $W(B(\lambda))$ change smoothly. Similarly, suppose that for a one-parameter family of boundary regions $B'(\lambda) \subset \bar{A}$ interpolating between $\bar{A}$ and a point (assuming $\bar{A}$ is contractible), the surfaces $W(B'(\lambda))$ change smoothly. Then the union of all surfaces $W(B(\lambda))$ and $W(B'(\lambda))$ covers an entire slice of the bulk spacetime. In this case, for any point p in the bulk spacetime, either there is a causal curve through

[23] See [113] for the definition of a simple manifold.

[24] The only possible exception would be the case where there are two extremal surfaces with equal area having boundary ∂A. In this case, we might call one $W(A)$ and the other $W(\bar{A})$.

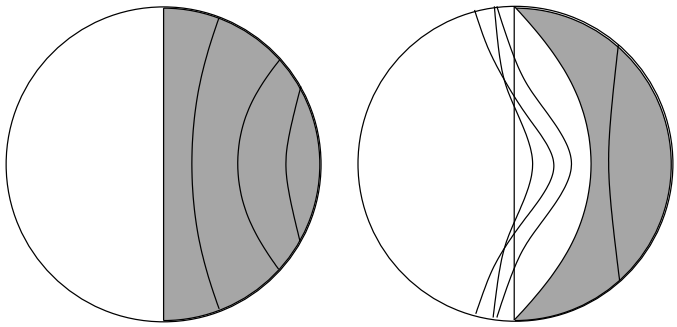

Figure 2.4: Different possible behaviors of extremal surfaces in spherically symmetric static spacetimes. Shaded region indicates $w(D_A)$ where A is the right hemisphere. The boundary of the shaded region on the interior of the spacetime is the minimal area extremal surface bounded by the equatorial S^{d-1}.

p that intersects $\cup_\lambda W(B(\lambda)) \subset w(D_A)$ or else every causal curve through p intersects $\cup_\lambda W(B'(\lambda)) \subset w(D_{\bar{A}})$. This shows that $\hat{w}(D_A)$ together with $J(w(D_{\bar{A}}))$ cover the entire spacetime.

To summarize, in cases where $W(B)$ varies smoothly with B as described above, we have that $\hat{w}(D_A)$ together with $J(w(D_{\bar{A}}))$ cover the entire spacetime. Thus, by Constraint 3, *with this smoothness condition*, if $\hat{w}(\bar{A}) \subset R(\bar{A})$ then $R(A)$ cannot be larger than $\hat{w}(D_A)$.[25] While there are many examples of spacetimes for which this smooth variation does not occur (e.g. as described in the next section), spacetimes satisfying the condition are not particularly special.

An example where $R(A)$ is strictly larger than $\hat{w}(D_A)$

We have seen that $\hat{w}(D_A)$ is in some sense a maximally optimistic proposal for $R(A)$ in cases where a particular smoothness condition is satisfied or when $w(D_A) \cup w(D_{\bar{A}})$ includes a Cauchy surface. We will now see that these conditions can fail to be true in some cases, and that in these cases, $R(A)$ must be larger than $\hat{w}(D_A)$ for some choice of A.

Consider the simple example of static spherically symmetric spacetimes with metric of the form $ds^2 = -f(r)dt^2 + dr^2/g(r) + r^2 d\theta^2$ where $g(0) = 1$ and $g(r) \to r^2$ for large r. For any spacetime of this form, the extremal codimension-two surfaces bounded by spherical regions on the boundary

[25] An alternative condition that leads to the same conclusion is that $w(D_A) \cup w(D_{\bar{A}})$ includes a Cauchy surface.

will be constant-time surfaces in the bulk that can easily be computed. By symmetry, there always exists an extremal surface through the center of the spacetime whose boundary is an equatorial S^{d-1} of the boundary S^d. Now, moving out towards the boundary along some radial geodesic, there will be a unique extremal surface passing through each point and normal to the radial line.

In some cases (e.g. pure AdS), the boundary spheres for these extremal surfaces shrink monotonically as we approach the boundary, as shown in the left half of Figure 2.4. However, there are other cases for which $g(r)$ is not monotonic where the extremal surfaces shrink in the opposite direction, then grow, then shrink again, as shown in the right half of Figure 2.4.[26] In these cases, boundary spheres with angular radius in a neighborhood of $\pi/2$ will bound multiple extremal surfaces in the bulk. The extremal surface of minimum area in these cases is always one that is contained within one half of the bulk space (otherwise we could construct intersecting minimal surfaces bounding disjoint regions of the boundary). Considering only the minimal surfaces, we find that there exists a spherical region in the middle of the spacetime penetrated by no such surface. Thus, even if we choose D_A to be the entire spacetime boundary, the region $w(D_A)$ excludes the region $r < r_0$ for some r_0. In this case, we have all information about the field theory (assumed to be a pure state), so $R(A)$ should be the entire spacetime.

More generally, the region $w(D_A)$ in these cases will have a "hole" if A is chosen to be any boundary sphere with angular radius between $\pi/2$ and π, as shown in Figure 2.5. Note, however, that the central region is included in $z(D_A)$ for sufficiently large A, so $z(D_A) \not\subset w(D_A)$ in these cases.

2.6 Discussion

In this note, we have presented various consistency constraints on the region $R(A)$ of spacetime which can in principle be reconstructed from the density matrix ρ_A for a spatial region A of the boundary with domain of dependence D_A. We have argued that the $z(D_A) \equiv J^+(D_A) \cap J^-(D_A)$ and its domain of dependence $\hat{z}(D_A)$ should be contained in $R(A)$ and that $\hat{z}(D_A)$ satisfies our consistency constraints. Since entanglement observables calculated

[26] As an explicit example, we have considered the case of a charged massive scalar field coupled to gravity, with scalar field of the form $\phi(r) = e^{i\omega t} f(r)$. Spherically-symmetric configurations of this type with non-zero charge are known as "boson-stars" [11]. We find that for fixed $\psi(0)$, the metric function $g(r)$ is monotonically increasing for sufficiently small values of the scalar field mass, while for sufficiently large values we can have the behavior shown on the right in Figure 2.4.

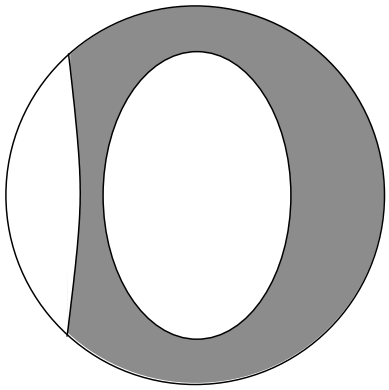

Figure 2.5: Region $w(D_A)$ (shaded) where A is a boundary sphere of angular size greater than π. No minimal surface with boundary in A penetrates the unshaded middle region.

from ρ_A correspond to extremal surfaces that typically probe a region of spacetime beyond $\hat{z}(D_A)$, we have also considered the union of these surfaces $w(D_A)$ and its domain of dependence $\hat{w}(D_A)$ as a possibility for $R(A)$ that is often larger than $\hat{z}(D_A)$. We have seen that $\hat{w}(D_A)$ also satisfies our constraints (assuming Conjecture **C1**), and that if $\hat{w}(D_A) \subset R(A)$ generally, then $R(A) = \hat{w}(D_A)$ for a broad class of spacetimes.

A false constraint

The constraints discussed in this note are essentially consistency requirements that do not make use of details of the AdS/CFT correspondence. It is interesting to ask whether there exist any more detailed conditions that could constrain the region $R(A)$ further.

It may be instructive to point out a somewhat plausible constraint that turns out to be false. For two non-intersecting regions A and B of the boundary spacetime, it may seem that the region $G(B)$ of the spacetime used to construct field theory observables in B should not intersect the region $R(A)$ dual to the density matrix ρ_A. The argument might be that if the physics in $R(A)$ is the bulk manifestation of information in ρ_A, we cannot expect to learn anything about this region knowing only ρ_B. It would seem that this would be telling us directly about ρ_A knowing only ρ_B. Perhaps surprisingly, it is easy to find an example where neither $w(D_A)$ nor $z(D_A)$ satisfies this constraint, see Figure 2.6.

In the planar AdS black hole geometry, take the region A to be a ball-

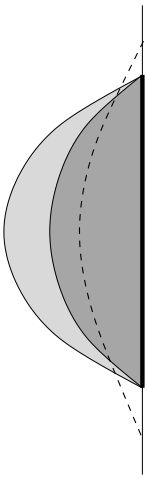

Figure 2.6: Spatial $t = 0$ slice of $w(D_A)$ (light shaded plus dark shaded) and $z(D_A)$ (dark shaded) for a planar AdS black hole. The dashed curve is a spatial geodesic with endpoints in $\bar{A}$. Knowledge of observables obtained from $\rho_{\bar{A}}$ alone allow us to compute the length of this geodesic.

shaped region on the boundary. In this case, it is straightforward to check that spatial geodesics with endpoints in $\bar{A}$ intersect both $w(D_A)$ and $z(D_A)$. Thus, the constraint $R(A) \cap G(\bar{A}) = \emptyset$ can't be correct if $z(D_A) \subset R(A)$. In hindsight, it is not difficult to understand the reason. Knowledge of the density matrix $\rho_{\bar{A}}$ allows us to reconstruct $R(\bar{A})$. There could be many states of the full theory that give rise to the same density matrix $\rho_{\bar{A}}$. For any such state with a classical gravity dual description, the dual spacetime geometry must be such that spatial geodesics anchored in $D_{\bar{A}}$ have the same lengths as in the original spacetime we were considering. But there can be many such spacetimes. So using the information in $\rho_{\bar{A}}$, we are not learning directly about ρ_A, only about the family of density matrices ρ_A^α such that the pair $(\rho_{\bar{A}}, \rho_A^\alpha)$ can arise from a pure state $|\Psi\rangle$ that has a geometrical gravity dual.[27]

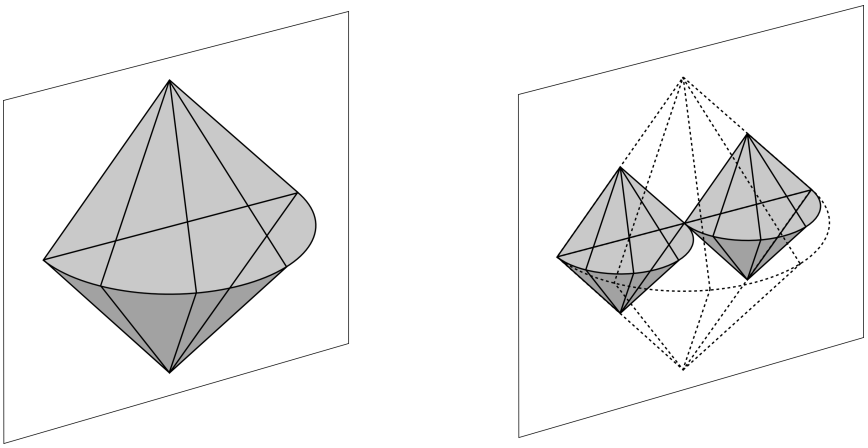

Figure 2.7: The region of spacetime reconstructible from density matrices ρ_B and ρ_C (shaded, right hand side picture) is smaller than that reconstructible from $\rho_{B\cup C}$ (shaded, left hand side picture). Reconstruction of $R(B \cup C) - (R(B) \cup R(C))$ (interior of dotted frame outside of the two shaded regions) requires knowledge of entanglement between degrees of freedom in B and C.

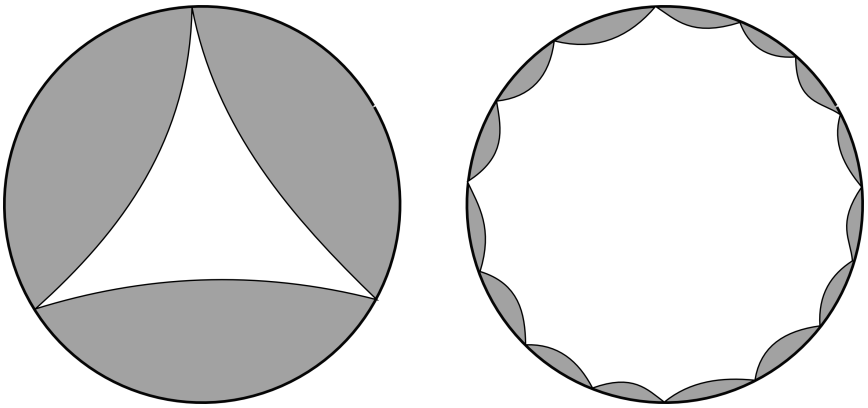

Figure 2.8: The region of spacetime reconstructible from density matrices ρ_{A_i} lies arbitrarily close to the boundary (illustrated here on a spatial slice). The ability to reconstruct the bulk geometry depends entirely on the knowledge of entanglement among the various boundary regions.

Spacetime emergence and entanglement

The observations in this note highlight the importance of entanglement in the emergence of the dual spacetime. Consider a collection $\{A_i\}$ of subsets on the boundary such that $\cup A_i$ covers an entire boundary Cauchy surface. In a classical system, knowing the configuration and time derivatives of the fields in each of these regions would give us complete information about the physical system. Quantum mechanically, however, complete information about the system consists of two ingredients: (i) the density matrices ρ_{A_i}, and (ii) the entanglement between the various regions.

If we subdivide a set $A \to \{B, C\}$ and pass from $\rho_A \to \{\rho_B, \rho_C\}$, we lose information about the entanglement between B and C. In the bulk picture, the region of spacetime that we can reconstruct (for any R satisfying our constraints) is significantly smaller than before, as we see in Figure 2.7. The region of spacetime that we can no longer reconstruct corresponds to the information about the entanglement between the degrees of freedom in B and C that we lost when subdividing.

As we divide the boundary into smaller and smaller sets A_i, we retain information about entanglement only at successively smaller scales, while the bulk space $\cup R(A_i)$ that can be reconstructed retreats ever closer to the boundary (Figure 2.8). Conversely, knowledge of the bulk geometry at successively greater distance from the boundary requires knowledge of entanglement at successively longer scales.[28] In the limit where A_i become arbitrarily small, we know nothing about the bulk spacetime even if we know the precise state for each of the individual degrees of freedom via the matrices ρ_{A_i}. In this sense, the bulk spacetime is entirely encoded in the entanglement of the boundary degrees of freedom.

[27] Don Marolf has pointed out to us that the connection between two-point functions and the lengths of spatial geodesics has been argued to fail for spacetimes that do not satisfy certain analyticity properties [91]. It is likely that demanding such properties imposes even stronger constraints connecting ρ_A and $\rho_{\bar{A}}$.

[28] A very similar picture was advocated in [132].

Chapter 3

Boson Stars

3.1 Introduction

In this chapter we construct solutions of asymptotically asymptotically AdS boson stars coupled to a $U(1)$ gauge field in 3 and 4 dimensions, compute the star's charge and mass as functions of the scalar field central density and study the behaviour of extremal surfaces in these backgrounds. In particular, we determine conditions under which minimal area, codimension 2 spacelike surfaces fail to cover the whole spacetime. To understand the motivation for doing so, let us digress for a moment and consider some intricate open questions regarding the holographic principle in anti de Sitter spacetimes.

The holographic principle is a remarkable idea relating theories with gravity to theories without gravity [129, 133]. The best understood example of holography is the AdS/CFT correspondence which proposes a one to one correspondence between a gravitational theory on anti-de Sitter space and a strongly coupled, large N, conformal field theory living on the conformal boundary of AdS [92, 140]. This correspondence has been extensively used to study a variety of strongly coupled field theories and has led to the formulation of successful formalisms such as AdS/QCD and AdS/CMT [29], however, the potential use of the gauge gravity duality to tackle problems in quantum gravity has yet to show comparable progress.

The intrinsic non local aspect of the bulk theory is particularly challenging when trying to understand the exact connection between bulk and boundary degrees of freedom. It stands as one of the major barriers in the way of the gauge / gravity duality fulfilling its potential of answering long standing problems in quantum gravity by recasting them in field-theoretic language. In order to improve this situation, the issue of understanding the map between bulk and boundary degrees of freedom must be addressed. Optimistically, we should be able to express any variation of the boundary theory state in terms of a well defined perturbation of the bulk geometry; conversely, any changes in the bulk should be related to a particular pertur-

[29] For an extensive review, refer to [58, 101].

bation of the boundary state in a one to one fashion.

An important question related to establishing the dictionary between bulk and boundary is to understand what information about the bulk is contained in a certain region of the boundary field theory. In other words, let a local field theory defined on the conformal boundary **B** of a spacetime $\mathcal{M}$ be in a generic state ρ. Assume this theory has a well defined gravity dual and consider, with respect to some arbitrary time slicing, a spacelike subregion A of the boundary. Which portion of the bulk $R(A)$ is dual to the reduced density matrix ${\rho_A}$[30], is a question closely related to the issue of characterizing the bulk-boundary degree of freedom map.

The Ryu-Takayanagi proposal [119] suggests that the entanglement entropy of a sub-region A of a field theory with a well behaved, static, gravity dual, is proportional to the area of the minimal area surface anchored at the boundary δA of A. Using this proposal we can construct a family of minimal surfaces by considering the surface dual to the entanglement entropy of ρ_A and all the surfaces dual to the partial traces of ρ_A with respect to arbitrary subregions within A. This family of surfaces defines a region in the bulk we will call $w(A)$ and is a possible candidate for $R(A)$ as proposed in [33] and further explored in [139][31].

Despite meeting several conditions for a suitable candidate for $R(A)$ [33, 139], when $A = B$, the whole boundary slice, $w(B)$ does not cover the entire spacetime in general. It was pointed out in [33] that there are spacetimes for which no minimal surfaces reach certain areas of the bulk that are, nevertheless, causally connected to the boundary, leading us to the conclusion that, at least for such cases, $w(A)$ cannot be the elusive region $R(A)$.

An explicit example of minimal surfaces that do not cover the bulk is found in asymptotically AdS boson star backgrounds. Boson stars are solutions to Einstein's equation coupled to a complex scalar field that have attracted the interest of physicists for over 40 years. Beginning with the work of Kaup [83] and others [117], the fields of general relativity, cosmology, and even particle physics have shown great interest in fully understanding these solitonic objects. Some of the standard reviews are [78, 89, 90, 124].

In this chapter we compute the physical charge and mass of asymptotically AdS, charged boson stars as a function of the scalar field central density, investigate numerically the behaviour of extremal surfaces on these

[30] Where ρ_A is the partial trace of ρ over the complement of A, $\bar{A}$.

[31] Formally we should extend the discussion to D_A, the causal development of A, however, for clarity and objectivity's sake we choose to omit it in the Introduction.

backgrounds, and determine the conditions for which $w(A)$ fails to fully cover the bulk, which we will call hollow phases. Furthermore we compare the conditions for the existence of hollow phases with that of known physical instabilities in four dimensional charged boson star systems, and argue that such hollow configurations are likely unstable and therefore physically forbidden, thus providing further evidence that $w(A)$ may be the correct proposal for $R(A)$.

This chapter is organized as follows: in section 2 we present the action, the metric and fields ansatz and equations of motion that follow, in addition we discuss boundary conditions and the free parameters we are left with once these are imposed. In section 3 we explore the relation between the star mass, charge, the scalar field central density, and the stability of charged boson stars. We present some numerical results, compare them to what is known from the literature, and argue that for a certain range of parameters the solutions we find are unstable in $D \geq 4$ dimensions. In section 4 we review and extend the above discussion as well as outline the numerical strategy to extract information about extremal surfaces and present the reader with preliminary results. In section 5 we construct phase diagrams displaying the relation between the free parameters, the transition between solid and hollow regimes, and the transition between stable and unstable configurations. We conclude with a few final remarks and future directions in section 6.

3.2 Equations of motion

We start by considering the Einstein-Maxwell action with a negative cosmological constant minimally coupled to a massive complex scalar field in D spacetime dimensions[32]

$$S = \frac{1}{8\pi G_D}\int d^D x\sqrt{-g}\left[\frac{1}{2}R + \frac{(D-2)(D-1)}{2} - \frac{1}{4}F^2 - |(\partial_i - iqA_i)\Psi|^2 - m^2|\Psi|^2\right]. \tag{3.1}$$

We want to restrict our attention to stationary, spherically symmetric configurations and allow for electric charges only, therefore we will let the metric be of the form

$$ds^2 = -f(r)dt^2 + \frac{dr^2}{g(r)} + r^2 d\Omega_{D-2}, \tag{3.2}$$

[32]Since the main goal of this chapter is to discuss numerical solutions of this action, the Hawking-Gibbons surface term can be neglected for it does not alter the equations of motion.

and adopt the following ansatz for the scalar and gauge fields

$$\Psi = \psi(r)\mathrm{e}^{-i\omega t}, \tag{3.3}$$
$$A_0 = A(r), \tag{3.4}$$
$$A_{i\neq 0} = 0. \tag{3.5}$$

To include the gravitational contribution from both the scalar and gauge fields we write the total energy momentum tensor as

$$T_{ij} = T_{ij}^{SF} + T_{ij}^{GF}, \tag{3.6}$$

the sum of the scalar's energy momentum tensor

$$T_{ij}^{SF} = \nabla_i\Psi^*\nabla_j\Psi + \nabla_i\Psi\nabla_j\Psi^* - g_{ij}\left(|\nabla\Psi|^2 + m^2\,|\Psi|^2\right), \tag{3.7}$$

where ∇_i is the covariant derivative $(\partial_i - iqA_i)$, and the gauge field energy momentum tensor

$$T_{ij}^{GF} = F_{ik}F_j^k - \frac{1}{4}g_{ij}F^2. \tag{3.8}$$

Additionally, note that the action 3.1 is invariant under the global $U(1)$ rotation $\Psi \to \mathrm{e}^{i\alpha}\Psi$, implying the existence of the conserved current

$$J^j = ig^{jk}((\nabla_k\Psi)^*\Psi - (\nabla_k\Psi)\Psi^*), \tag{3.9}$$

which will act as a source for the gauge field.

With the above definitions in hand we obtain four linearly independent equations of motion from the tt and rr components of Einstein's equation

$$R_{ij} - \frac{1}{2}g_{ij}R - \frac{(D-2)(D-1)}{2}g_{ij} = T_{ij}, \tag{3.10}$$

the Klein-Gordon equation

$$\nabla^2\phi - m^2\phi = 0, \tag{3.11}$$

and Maxwell's equations

$$\nabla_i F^{ij} = qJ^j. \tag{3.12}$$

In terms of the functions defined in our ansatz, the D dimensional equations of motion from the tt and rr components of Einstein's equation are

$$\begin{aligned} &-q^2r^2A(r)^2\psi(r)^2 - 2qr^2\omega A(r)\psi(r)^2 - \frac{1}{2}(D-2)r^{D-3}f(r)g'(r) - \\ &\frac{1}{2}(D-3)(D-2)f(r)g(r) + \frac{1}{2}(D-2)(D-1)r^2f(r) - r^2g(r)A'(r)^2 + \\ &\frac{1}{2}(D-3)(D-2)f(r) - r^2f(r)g(r)\psi'(r)^2 - m^2r^2f(r)\psi(r)^2 - r^2\omega^2\psi(r)^2 = 0, \end{aligned} \tag{3.13}$$

and

$$\begin{aligned} q^2r^2A(r)^2\psi(r)^2 + 2qr^2\omega A(r)\psi(r)^2 - \frac{1}{2}(D-2)r^{D-3}f'(r)g(r) - \\ \frac{1}{2}(D-3)(D-2)f(r)g(r) + \frac{1}{2}(D-2)(D-1)r^2f(r) - r^2g(r)A'(r)^2 + \\ \frac{1}{2}(D-3)(D-2)f(r) + r^2f(r)g(r)\psi'(r)^2 - m^2r^2f(r)\psi(r)^2 + r^2\omega^2\psi(r)^2 &= 0. \end{aligned} \tag{3.14}$$

While from the Klein-Gordon equation we find

$$\begin{aligned} 2q^2rA(r)^2\psi(r) + 2(D-2)f(r)g(r)\psi'(r) + rg(r)f'(r)\psi'(r) + \\ rf(r)g'(r)\psi'(r) + 2rf(r)g(r)\psi''(r) - 2m^2rf(r)\psi(r) + 2r\omega^2\psi(r) &= 0, \end{aligned} \tag{3.15}$$

and Maxwell's equations give

$$\begin{aligned} -2rf(r)g(r)A''(r) - 2(D-2)f(r)g(r)A'(r) + rg(r)A'(r)f'(r) - \\ rf(r)A'(r)g'(r) + 4q^2rA(r)f(r)\psi(r)^2 + 4qr\omega f(r)\psi(r)^2 &= 0. \end{aligned} \tag{3.16}$$

These comprise a set of two first order and two second order ordinary differential equations and allow for a six parameter family of solutions, one of which is empty AdS. However, we are not interested in any generic solution of the above set of equations, but only in those that are asymptotically AdS and regular at $r = 0$.

By requiring the solution to be regular at the origin, the near $r = 0$ analysis of the equations of motion leads to the following constraints

$$g(0) = 1, \quad g'(0) = 0, \quad f(0) = f_0, \quad f'(0) = 0, \tag{3.17}$$

$$A(0) = A_0, \quad A'(0) = 0, \quad \psi(0) = \psi_0, \quad \psi'(0) = 0, \tag{3.18}$$

leaving three undetermined parameters. We can use the following symmetry of the equations of motion

$$f \to \gamma^2 f, \quad A \to \gamma A, \quad \omega \to \gamma\omega, \quad t \to \frac{1}{\gamma}t, \tag{3.19}$$

to fix $A(0) = 1$. In addition, the value of f_0 is chosen to ensure that our solutions asymptote to global AdS, that is as $r \to \infty$, $f(r) \to 1 + r^2$, and

similarly for $g(r)$. This leaves us with one free parameter, ψ_0, and the task of studying a one parameter family of solutions of equations 6.72-6.75.

However, before we move forward, we are still left with the issue of guaranteeing that the scalar field showcases the correct asymptotic fall off. In general, the large r behaviour of $\psi(r)$ is given by

$$\psi(r) = \frac{\psi_1}{r^{\lambda_+}} + \frac{\psi_2}{r^{\lambda_-}}, \tag{3.20}$$

with

$$\lambda_\pm = \frac{1}{2}\left((D-1) \pm \sqrt{(D-1)^2 + 4m^2}\right), \tag{3.21}$$

where m^2 is the scalar field mass in the lagrangian 3.1, and ψ_1 and ψ_2 are constants. For $m^2 > 0$, $\psi(r)$ has a non normalizable term that can be set to zero by picking a solution for which $\psi_1 = 0$, while for $(D-1)^2/4 < m^2 < 0$ both terms are normalizable and therefore allowed in principle.

To pick the desired fall off of $\psi(r)$ we will look for the lowest value of ω, the phase of $\Psi(t)$, for which we observe $\psi_1 = 0$. We do so by using ω as a shooting parameter and imposing the boundary condition $\psi_1 < 10^{-10}$. Once ω is fixed we are left with only m^2 and q (the scalar charge) as free theory parameters. Henceforth in this chapter we will numerically study the one parameter family of solutions of equations 6.72-6.75, their dependence on the solution's parameter $\psi(0)$, the central density of the scalar field, as well as on the theory's parameters m^2 and q. Later we will apply these results to investigate the behaviour of extremal surfaces living in charged, asymptotically AdS boson star backgrounds and how their behaviour depend on the free parameters we just discussed as well as the star's mass, charge and the scalar's central density studied in detail in the next section.

3.3 Mass, charge and scalar central density

Before we start the discussion of how the solutions of equations 6.72-6.75 and the families of minimal surfaces depend of the free parameters discussed above, lets take some time to look at how the total mass and total charge of the star are calculated and how they depend on the central density of the scalar field, $\psi(0)$.

The metric (4.29) describes a spherically symmetric body whose mass can be extracted from the asymptotic behaviour of the metric function $g(r)$. At large r we expect the metric to approach that of a charged, massive star

in AdS with no scalar field, i.e.:

$$g(r) \xrightarrow{r\to\infty} 1 + r^2 - \frac{2M}{r^{D-3}} + \frac{Q^2}{r^{2(D-2)}}, \tag{3.22}$$

where M is the mass of the star and Q its charge, which is simply the total number of scalar particles times the charge q, i.e.:

$$Q = q \int d^{D-1}x J^0 \sqrt{-g}. \tag{3.23}$$

However, the existence of a scalar field allows for the possibility of scalar hair, therefore we should expect that our metric, while still approaching 3.22 at large r, will receive higher order corrections. Ergo we choose to write the general metric as

$$g(r) = 1 + r^2 - \frac{2M(r)}{r^{D-3}} + \frac{Q(r)^2}{r^{2(D-2)}}, \tag{3.24}$$

where the large r behaviour of the function $M(r)$ is given by

$$M(r) \sim M + \mathcal{O}\left(1/r^{\alpha}\right), \tag{3.25}$$

with α being is a positive constant, and similarly for $Q(r)$.

The behaviour of the mass and charge of a boson star as a function of the scalar's central density has been extensively studied in the literature both for asymptotically flat and asymptotically AdS spacetimes [12, 69]. In particular, in AdS space, the existence of a variety of new solutions and the presence of a zero temperature phase transition have recently been shown to exist [27, 40, 50, 69]. Furthermore the stability of boson stars has also been the subject of numerous studies and found to correlate with certain aspects of the behaviour between mass, charge and central density [12, 77] as we discuss below.

Since later in this chapter the question of whether the solutions we find displaying hollow configurations of minimal area surfaces are physically stable will be particularly important, we should take a closer look at the behaviour of the mass and charge of our solutions as a function of the central density $\psi(0)$ and compare it to what is known from the literature. Our analysis here will rely solely on previously known results and educated guesses, so we will refrain from a formal study of the stability of the solutions as it lies outside the scope of this work.

For $D \geq 4$ dimensions it has been found that for models with no gauge field in both zero and negative cosmological constants background, and with

a gauge field in a zero cosmological constant background, the star mass as a function of the scalar field central density $M(\psi(0))$ reaches a maximum value for a finite $\psi(0) = \psi_c$. Even though the numerical value for the maximum mass and ψ_c change for each case, they correspond to the threshold between dynamically stable ($\psi(0) < \psi_c$) and unstable ($\psi(0) > \psi_c$) regimes[33].

The $D = 3$ case has attracted considerably less attention and consequently, to the extent of the author's knowledge, no formal result is available. Nevertheless, in the context of strongly self interacting boson stars, there is evidence for the existence of a maximum mass as well as some discussion regarding the positive binding energy of these objects possibly being an indicator of instabilities [121, 122]. Despite the existence of such partial results we will refrain from making any statements regarding the stability of the three dimensional solutions.

With the above discussion in mind we numerically solve equations 6.72-6.75, compute the physical mass and charge of the configurations using 3.25 and 3.23 for different values of $\psi(0)$ and compare to what is known from the literature. We find qualitatively similar results in $D = 4$ to that of pure boson stars (without gauge field), more importantly we observe the existence of a maximum value for M as can be seen in figure 3.1.

Given the proximity of the models considered in the literature and ours, together with the qualitative agreement between results, we are led to believe that our model is also unstable past the central density threshold ψ_c for $D \geq 4$ dimensions. We will assume this conjecture is indeed true in the reminder of this chapter and use it to understand better the conditions for the existence of a hollow $w(D_A)$ in the upcoming sections.

In $D = 3$ dimensions we again observe qualitatively similar results to those found in [12] (figure 3.2). Most notably we would like to highlight the absence of a maximum mass within the central density range investigated[34] as it showcases a considerably different behaviour than that expected for $D \geq 4$ dimensions.

[33] At maximum mass ($\psi(0) = \psi_c$) the pulsation equation arising from the analysis of the time evolution of infinitesimal radial perturbations has a zero mode indicating that ψ_c is a boundary between stable and unstable equilibrium configurations [77].

[34] Our numerical solution is untrustworthy past the $\psi(0) = 0.8$ mark in $D = 3$ dimensions, therefore precluding us from investigating the mass versus central density relation any further.

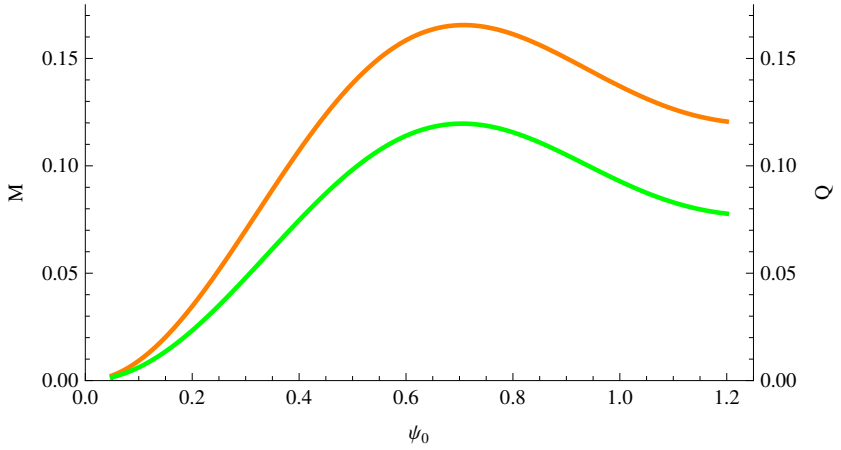

Figure 3.1: Plot of the star's mass (orange) and charge (green) versus the central value of the scalar field ψ_0 with $m^2 = 0$ and $q = 0.2$ in $D = 4$ dimensions.

3.4 Overlapping extremal surfaces

Our main goal in this section is to construct extremal surfaces in the background of charged, asymptotically AdS boson stars found in section 2. Before we do so, it is instructive to further solidify the motivations for studying such objects and how it can help shedding light on the discussion presented in the introduction. However, to accomplish this task, we will need to employ more general tools. In particular, while we started our discussion in the introduction addressing the question of what is the bulk region $R(A)$ dual to a given boundary region A, here we will consider instead the bulk region $R(D_A)$ dual to the causal development of A, D_A, defined as the union of all boundary points connected to A by a causal curve.

A natural candidate for $R(D_A)$ would be to consider the causal wedge $z(D_A) = J^+(D_A) \cap J^-(D_A)$[35], the region in the bulk a boundary observer restricted to D_A is causally connected to. Intuitively speaking, we expect $z(D_A)$ to be at least the minimal portion of the bulk accessible to a boundary

[35]Where $J^+(D_A)$, defined as all points accessible by causal curves arising from D_A, is the causal future of D_A, while $J^-(D_A)$, defined as the set of points from which D_A can be reached following a causal curve, is its causal past.

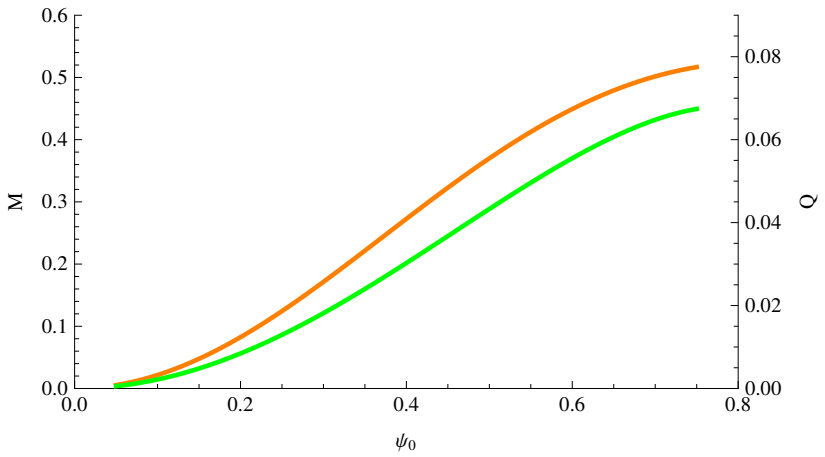

Figure 3.2: Plot of the star's mass (orange) and charge (green) versus the central value of the scalar field ψ_0 with $m^2 = 0$ and $q = 0.2$ in $D = 3$ dimensions.

observer living in D_A. The reason being that its complete causal connection to D_A allows for the detection of any perturbation of the bulk metric inside $z(D_A)$.

While $z(D_A)$ seems to be a natural guess, and it certainly imposes a lower bound on the size of $R(D_A)$, examples for which $z(D_A) \subset w(D_A)$ while $z(D_A) \not\supseteq w(D_A)$[36], are easy to find[37] and demonstrate how the region $z(D_A)$ alone cannot, in general, hold all the information stored in D_A. In contrast, for some cases, we can argue that all the information in D_A must lie within $\hat{w}(D_A)$, the domain of dependence of $w(D_A)$, for anything outside this bulk region will causally interact with the complement of D_A, $D_{\bar{A}}$. This could lead us to naively expect that $\hat{w}(D_A)$ imposes an upper bound on $R(D_A)$, however, one can construct explicit examples for which this might not be true, as we will see below.

Say that we let the region D_A cover the entire boundary, i.e.: $D_A = \mathbf{B}$, an observer within D_A will have access to a full Cauchy surface and, consequently, information about the entire past and future of the boundary theory. Since we are considering a field theory with a well defined gravity

[36]Where $w(D_A)$ is defined in the exact same way as $w(A)$ if we exchange A by D_A.
[37]See [33] for a thorough discussion.

dual, information about the past and future of the boundary should extend to information about the past and future of the bulk theory as well. In other words, an observer in **B** that has access to all possible boundary physical observables should be able to fully reconstruct the dual bulk metric[38].

If we restrict the access of this observer to knowledge of the entanglement entropy for any arbitrary region within **B**, we can ask how much of the bulk he or she can probe and, better yet, infer the geometry of [31, 33, 139]. If the bulk theory has a horizon, say a spherically symmetric black hole at the origin, it was shown in [71] that, while no extremal surface of any co-dimension (or causal lines, for that matter) can probe inside the horizon, given a fixed boundary region, co-dimension 2 surfaces probe the bulk deeper than higher co-dimension surfaces or causal lines. Now, if instead of a black hole at the origin we consider a boson star for example, we can ask the same question again: how much of the bulk spacetime can a boundary observer probe with extremal surfaces only? Note that now the entire bulk is causally connected to the boundary, so we know that $z(\mathbf{B}) \supset \mathcal{M}$, therefore, if $w(D_{\mathbf{B}})$ fails to fully cover the bulk, we will have an explicit example for which $z \supset w$ while $w \not\supseteq z$.

Given the above discussion, our goal is to search within the space of solutions of charged boson stars in asymptotically AdS spacetime found in section 2, for configurations for which we observe overlapping of extremal surfaces leading to a hollow $w(D_A)$, therefore addressing the question of whether $z(D_A) \supset w(D_A)$ while $w(D_A) \not\supseteq z(D_A)$ is feasible[39].

Our setup is both static and asymptotically globally AdS, therefore our boundary is a sphere (equation 4.29). We will look for surfaces that extend in all polar angles, so, to our applications, it suffice to describe them as curves $\theta(r)$, with anchor points $\theta(\infty) = \pm\theta_0$ corresponding to the azimuthal boundary coordinates of the start and end points (see figures 3.3, 3.4 and 3.5).

To determine whether the entangling surfaces reach the deepest regions in the bulk we will analyze the behaviour of $r_{\min}(\theta_n(r))$ for multiple surfaces with distinct boundary anchor points $\theta_n(\infty) = \pm\theta_n$, that is, the minimum value of r reached by a given entangling surface $\theta_n(r)$ with fixed boundary

[38] This is demonstrably true for the case of empty AdS [56, 57, 61, 79]. Some interesting recent discussion highlights the necessity of including non local boundary operator in the boundary observer's toolbox [23]

[39] Note that failure to find solutions obeying $z(D_A) \supset w(D_A)$ while $w(D_A) \not\supseteq z(D_A)$ does not indicate this particular phenomena is not possible, in the same way that the mere mathematical existence of such configurations is not enough to undermine the candidacy of $w(D_A)$ to the position of $R(D_A)$ for these could not be physically preferred.

anchor points θ_n.

We know that $\pm\theta(\infty)_{r_{\min}}$ (the anchor points of a surface that has $r_{\min}$ as its deepest point) covers all values of θ as we vary $r_{\min}$ from zero to infinity, as a result, for every $0 < r_0 < \infty$ there is at least one extremal surface that obeys $r_{\min}(\theta(r)) = r_0$ (figure 3.6).

However, the situation is much different if we focus on surfaces anchored at the same boundary points. In this case we expect that only one minimal area surface can be anchored at each given θ_i (figure 3.6a). While this is true in general (with the exception of $\theta = \pi/2$), this need not be the case if we consider extremal rather than minimal area surfaces (figure 3.6b), therefore we should not be alarmed if for certain boundary anchor points we find that there are multiple distinct extremum surfaces anchored to it, in fact, we are most interested in determining when such a phenomena happens. To do so we will numerically investigate conditions under which there exist multiple extremal surfaces anchored at the same boundary point that do not share the same deepest point in the bulk.

Given the above discussion it is tempting to cast the question of extracting bulk information from the boundary in the context of Morse theory. As discussed above, the existence of degenerate extremal surfaces led to an inconsistency regarding the amount of bulk information accessible to a boundary observer, in particular we argued for the possibility of regions in the bulk inaccessible to extremal surfaces. Similarly, the existence of conjugate points can be shown (for some specific riemannian manifolds) to obstruct the construction of a Morse function. Therefore, by connecting the two, we are led to believe that the existence of degenerate extremal surfaces may preclude us from inferring the geometry (or probing the topology) at least in some bulk region near such surfaces.

Numerical treatment of extremal surfaces

In order to apply the numerical results we found in sections 2 and 3 we need an equation describing extremal surfaces anchored to spheres on the boundary of the spacetime with metric 4.29. Such equation can be found by minimizing the area of these surfaces given by the integral of the induced metric on the surface in question. In the case of a surface anchored to a sphere with the background metric given by equation 4.29, the integral over

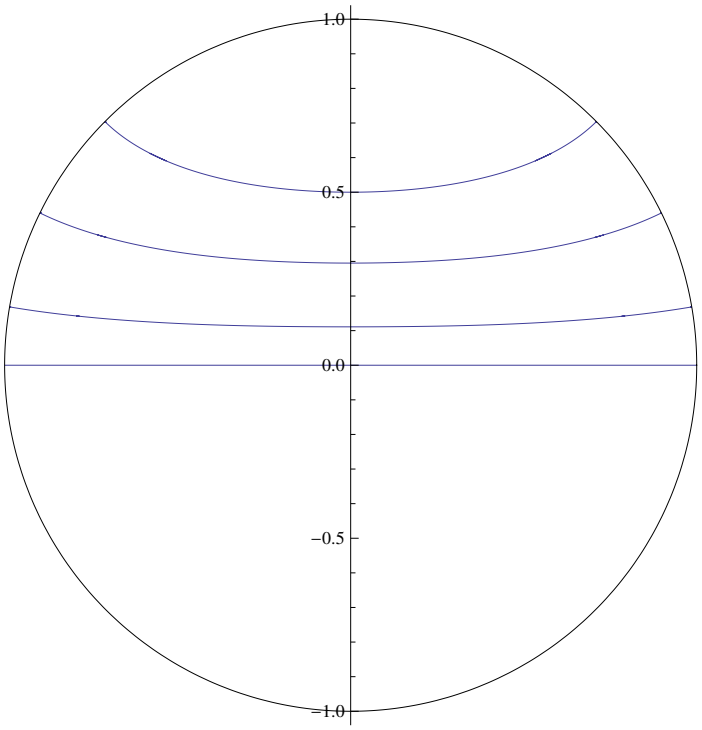

Figure 3.3: A plot of the Penrose diagram of a time slice of multiple extremal surfaces on a four dimensional, asymptotically AdS, charged boson boson star background in global coordinates for $m^2 = 0$, $q = 0.1$, and $\psi(0) = 0.2$. From top to bottom we have $\theta = \pm 0.251\pi, \pm 0.355\pi, \pm 0.446\pi, \pm 0.5\pi$. In this particular case the central density of the scalar field is below the threshold ψ_h, therefore there are no degenerate extremal surfaces (see figure 3.6), in other words, we observe a solid $w(D_A)$.

the induced metric is simply

$$A = \mathrm{Vol}(S^{D-3}) \int dr \, (\sin\theta(r))^{D-3} \, r^{D-3} \sqrt{\frac{1}{g(r)} + r^2 \left(\frac{d\theta}{dr}\right)^2}, \quad [40] \tag{3.26}$$

[40] The area obtained from equation 3.26 is infinite, however it can be regularized by taking the difference $A - A_0$, where A_0 is just equation 3.26 calculated on a fixed background metric g_0 with the appropriate function $\theta_{g_0}(r)$ and the same boundary conditions, i.e.: same boundary anchor points. In this chapter, while computing numerical values for the area of extremal surfaces was not our goal, as discussed below we did do it as a consistency check of some of the statements made in [33]. When doing so we set the reference metric to be that of pure AdS in global coordinates, that is $g_0(r) = 1 + r^2$, found θ_{g_0} by solving

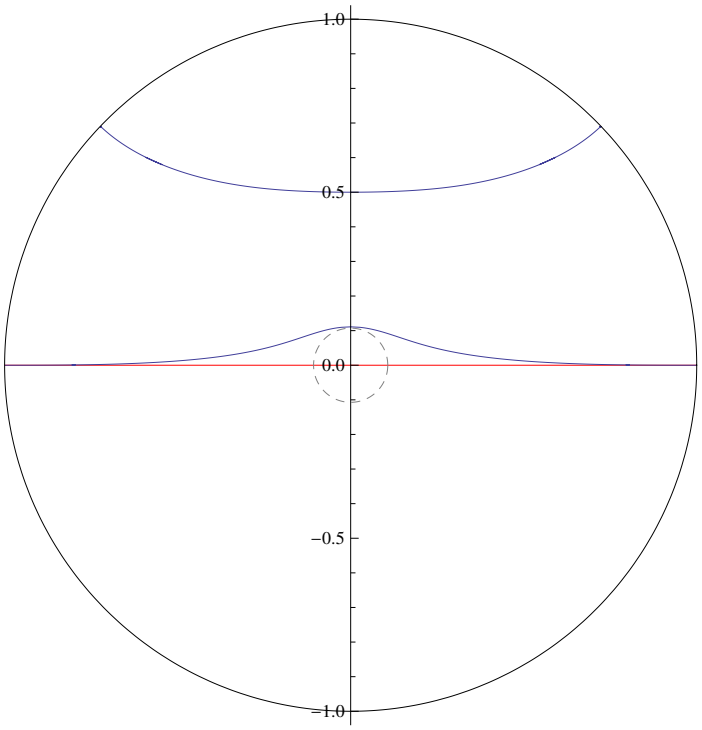

Figure 3.4: Again, a plot of the Penrose diagram of a time slice of multiple extremal surfaces on a four dimensional, asymptotically AdS, charged boson boson star background in global coordinates for $m^2 = 0$, $q = 0.1$, and $\psi(0) = 1.2$. However, in this example, the scalar central density is above the threshold ψ_h and we observe the existence of degenerate extremal surfaces for a range of boundary anchor points θ (see figure 3.6). In particular, for anchor points $\theta = \pm\pi/2$ there are three solutions two of which (blue line) lie on top of each other, have minimal area and do not penetrate the dashed small circle, while the third (red line) corresponds to a non minimal area extremal surface. As discussed in this chapter, no minimal area surface penetrates the deepest bulk points within the small dashed circle.

from which follows, by an extremization procedure, that a minimal area surface described by the curve $\theta(r)$ must obey the following second order differential equation

equation 3.27 (which greatly simplifies in this case), and computed the area difference.

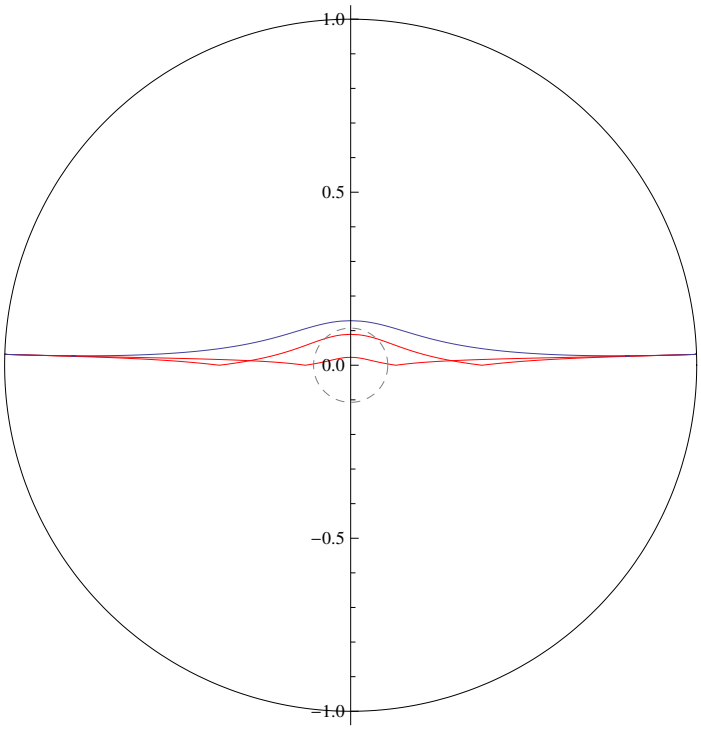

Figure 3.5: A similar plot as figures 3.3 and 3.4 highlighting the behaviour of all three extremal surfaces anchored at the same boundary points $\theta = \pm 0.49\pi$. Although two of the solutions (red lines) penetrate the dashed circle, these are not the minimal area and therefore are not part of the $w(D_A)$ set.

$$-\frac{r^{D-1}\theta'(r)\sin^{D-3}(\theta(r))\left(-\frac{g'(r)}{g(r)^2}+2r^2\theta'(r)\theta''(r)+2r\theta'(r)^2\right)}{2\left(\frac{1}{g(r)}+r^2\theta'(r)^2\right)^{3/2}}+$$
$$\frac{(D-1)r^{D-2}\theta'(r)\sin^{D-3}(\theta(r))}{\sqrt{\frac{1}{g(r)}+r^2\theta'(r)^2}}+\frac{(D-3)r^{D-1}\theta'(r)^2\cos(\theta(r))\sin^{D-4}(\theta(r))}{\sqrt{\frac{1}{g(r)}+r^2\theta'(r)^2}}$$
$$-(D-3)r^{D-3}\cos(\theta(r))\sin^{D-4}(\theta(r))\sqrt{\frac{1}{g(r)}+r^2\theta'(r)^2}+\frac{r^{D-1}\theta''(r)\sin^{D-3}(\theta(r))}{\sqrt{\frac{1}{g(r)}+r^2\theta'(r)^2}}=0. \tag{3.27}$$

Using the numerical solutions we found in section 2, in particular the function $g(r)$ in equation 4.29, we are able to solve equation 3.27 numerically and fully determine the function $\theta(r)$ in any spacetime dimension D. Our goal is to find solutions that asymptote to our desired boundary anchor points, ie.: $\theta(\infty) = \pm\theta_0$. To do so we solved equation 3.27 subjected to the boundary conditions

$$\theta(r_0) = 0, \quad \text{and} \quad \theta'(r_0) = \infty,^{41} \tag{3.28}$$

and used r_0 as a shooting parameter to meet the condition $\theta(\infty) = \theta_0$. By setting $\theta(r_0) = 10^{-6}$ and $\theta'(r_0) = 10^3$, we increased r_0 starting from 10^{-10} and were able to tune $\theta(\infty) = \theta_0$ to an accuracy of 10^{-5}. Once a solution was found we kept increasing r_0 until another solution was found or our code could no longer solve the equations. We later mirrored the solutions to generate the negative θ side of the curve, rotated it, and changed coordinates to Penrose coordinates in order to generate figures 3.3, 3.4 and 3.5.

The above described method allow us to acquire quantitative information regarding the behaviour of extremal surfaces in charged, asymptotically AdS boson star backgrounds. However, as we should expect, the solutions we find, even for fixed boundary conditions, are not unique, in fact, our goal is to investigate the conditions for the existence of degenerate solutions (multiple solutions for fixed boundary points).

From now on we shall refer to a particular solution of equation 3.27, $\theta(r)$, as an extremal surface, moreover, since we are only considering surfaces anchored at spheres, $\pm\theta(\infty)$ is enough to characterize the boundary anchor points of the extremal surface determined by $\theta(r)$.

To investigate the possibility of the existence of degenerate extremal surfaces, we use our numerical method to search for different solutions $\theta_i(r)$ for which $\theta_i(\infty) = \theta_0, \quad \forall i$, while $r_{\min}(\theta_i(r)) \neq r_{\min}(\theta_{i'}(r))$ for at least one i'. In other words, we look for extremal surfaces anchored at the same boundary points that do not share a common deepest bulk point $r_{\min}(\theta_i(r))$ (figures 3.4 and 3.5).

The existence of such multiplicity of extremal surfaces with common boundary anchor points will in general preclude most of them from having minimal area and, as argued in [33], can be used to show that no family of minimal area surfaces can cover the bulk in its entirety. Nevertheless, as a consistency check, we computed numerically the regularized area for surfaces anchored at various boundary points and confirmed that, indeed,

[41] Note how this condition follows from the spherical symmetry of the space-time in consideration.

when more than one solution exists (with the same $\theta(\infty)$), the one with the bigger $r_{\min}$ has the smallest area.

Therefore, our strategy to determine whether our charged boson star solutions display such hollow phases is to look for an extremal surface $\theta_h(r)$ that obeys $\theta_h(\infty) = \pi/2$ while having $r_{\min}(\theta_h) \neq 0$ (figure 3.4) since, from the spacetime symmetry, we know that there exist one extremal surface for which $\theta(\infty) = \pi/2$ with $r_{\min}(\theta) = 0$.

As a warming up exercise we fix the value of the parameters m^2 and q and, as we vary the central density of the scalar field ψ_0, we observe the system to transition between solid and hollow phases as seen in figure 3.6. Note how on figure 3.6a there is only one solution extending into the bulk and reaching a specific $r_{\min}$ for each θ, whereas on figure 3.6b there is more than one value of $r_{\min}$ for a given boundary anchor point (a fixed θ_0) near the $r = 0$ region.

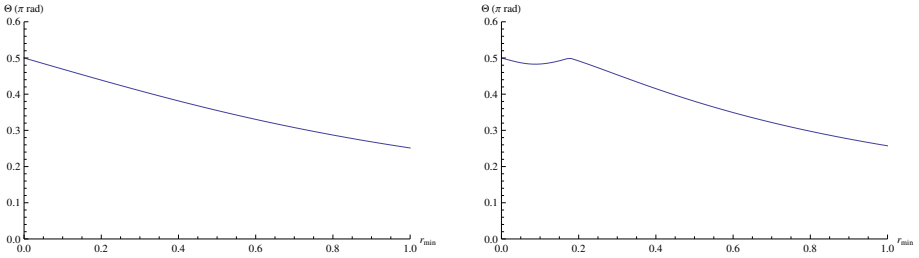

(a) $\psi(0) = 0.2$ (b) $\psi(0) = 1.2$

Figure 3.6: A comparison of two different central densities for the plot of $r_{\min}(\theta(r))$ in four dimensions, both cases with $m^2 = 0$ and $q = 0.1$. It is clear how for anchor points roughly between $0.17\pi < \theta < \pi/2$ there exist three distinct extremal surfaces with different values of $r_{\min}$, however, only one of them has minimal area. See figures 3.3, 3.4 and 3.5 for specific examples.

Our goal for the next section is to determine the precise value ψ_h of $\psi(0)$ for which this transition occur as a function of the parameters m^2 and q and, in the four dimensional case, compare it to ψ_c, the central density threshold between stable and unstable configurations.

3.5 Phase diagrams

In this section continue to apply the numerical solutions and quantities found in sections 2 and 3 to explore in further detail the conditions for which we observe solid and hollow phases. Since we are dealing with a one parameter

family of solutions and have two free theory parameters, we should be able to construct a three dimensional phase diagram and find a two dimensional surface separating solid and hollow phases. To numerically accomplish this task we start by fixing q while varying m^2. For each value of m^2 and q we look for the lowest value of $\psi(0)$ for which we observe multiple values of $r_{\min}(\theta_0)$ for the same, fixed, θ_0 and find a line separating the two regions, we then repeat this process for multiple different values of q.

As seen in figures 3.7 and 3.8, we observe a similar behaviour for both three and four dimensional cases. Is is clear that the threshold value of $\psi(0)$ decreases as we increase either m^2 or q, and a maximum, finite value is attained as the scalar mass approaches the BF bound and the charge goes to zero.

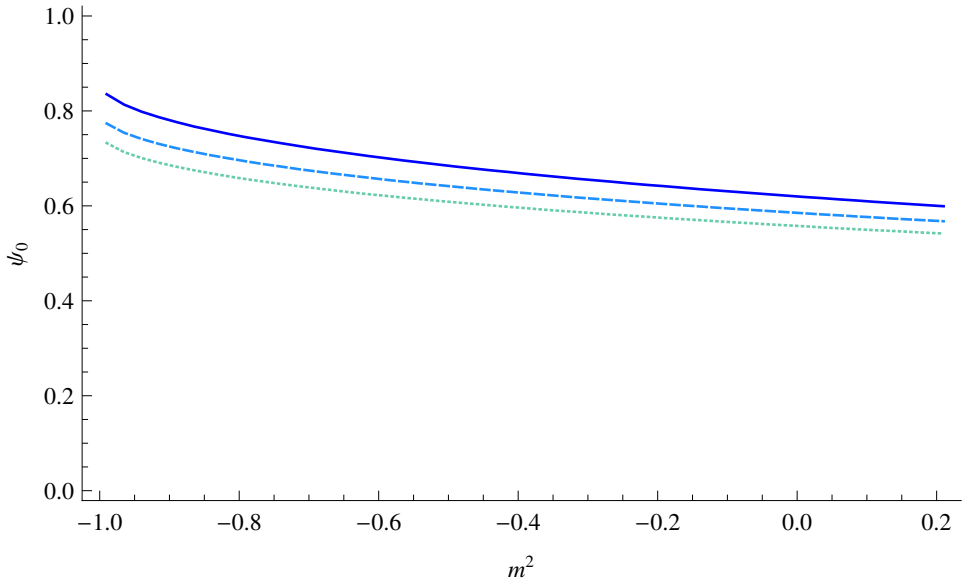

Figure 3.7: Critical scalar field central density separating solid and hollow configurations for $D = 3$ dimensions with $q = 0.1$ in blue, $q = 0.2$ in light blue (dashed) and $q = 0.3$ in green (dotted). In all cases a central density value below the line correspond to solid solutions, while above it lies the hollow regime.

As discussed earlier in this chapter, four dimensional boson stars are known to be unstable when the central scalar density rises above a critical value ψ_c in numerous different setups. Since we just established the existence of ψ_h, the threshold between solid and hollow configurations, we want to

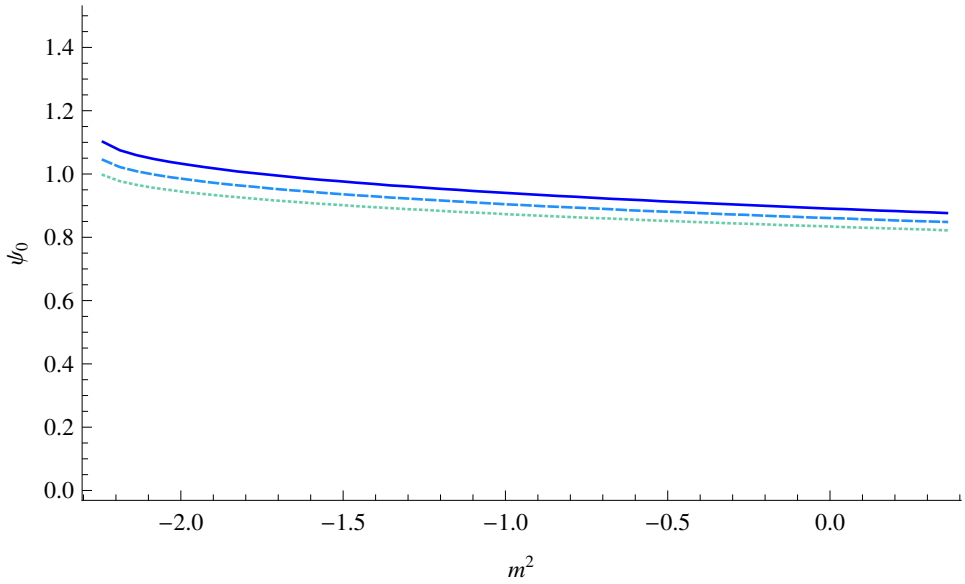

Figure 3.8: Critical scalar field central density separating solid and hollow configurations for $D = 4$ dimensions with $q = 0.1$ in blue, $q = 0.2$ in light blue (dashed) and $q = 0.3$ in green (dotted). In all cases a central density value below the line correspond to solid solutions, while above it lies the hollow regime.

compare it to ψ_c so we can determine whether the hollow solutions we find are in fact physically permitted.

Stability of AdS charged boson stars and hollowed phases.

The stability of boson stars has been a subject of intensive study in the past decades, while focus has been given to boson stars in flat spaces, similar results exist in AdS space. Despite subtle changes between the flat, curved, self interacting or charged cases, it is well known that four dimensional boson stars reach a maximum mass value for a finite central density ψ_c and are unstable past this point. The nature of the instability and how it depends on the various variations of the model, while important on their own, are not within the scope of this study, for us it suffices to know that the value of $\psi(0) = \psi_c$ for which the stars mass as a function of scalar central density, $M(\psi(0))$, is maximum represents the threshold between stable and unstable regimes and that this seems to be universal across different types of boson

stars[42].

In order to numerically determine ψ_c we fix q and m^2 and search for the highest value of the star mass M as a function of $\psi(0)$. Similarly to the phase diagrams above (figures 3.7 and 3.8), we find, for each value of q, a line dividing stable and unstable regimes in the m^2 vs. ψ_0 plane. We observe that, within the range of parameters we studied, we always have $\psi_c < \psi_h$ (as seen in figures 3.9 and 3.10), indicating that the hollow solutions we found, while being perfectly fine in a mathematical sense, do not correspond to a physically preferred phase and suffer from dynamical instabilities.

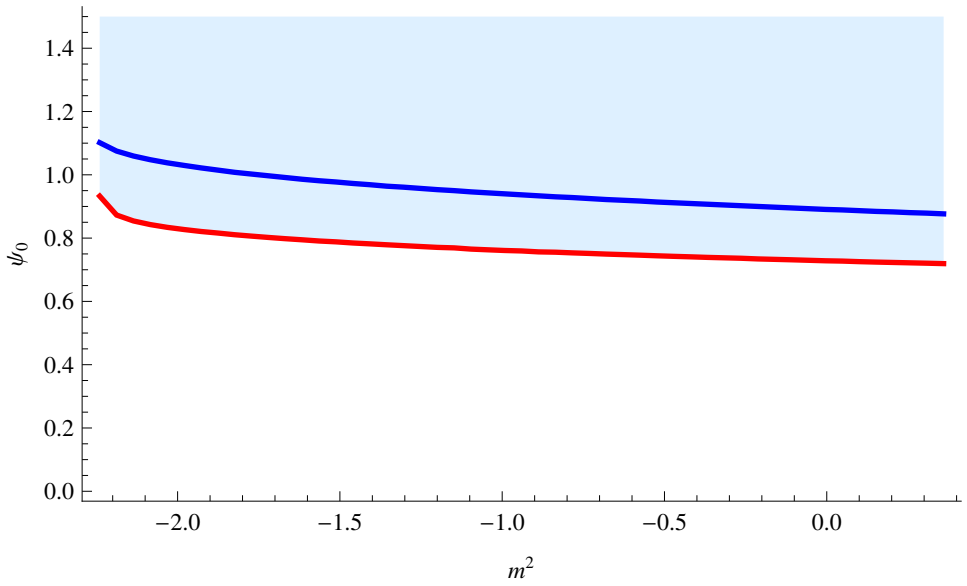

Figure 3.9: A phase diagram displaying both transitions found in $D = 4$ dimensions (stable $\rightarrow$ unstable and solid $\rightarrow$ hollow) with $q = 0.1$. The red line (below) is the stability threshold, a value of ψ_0 above it (the light blue region) renders a dynamically unstable configuration. The blue line (above), once again, represents the transition between solid and hollow configurations. It is clear from this figure how, in the range studied, only solid configurations are physically allowed.

[42]For the interested reader we direct you the reviews [124] and [90] and the work [12] for a lengthy discussion on boson star instabilities and more.

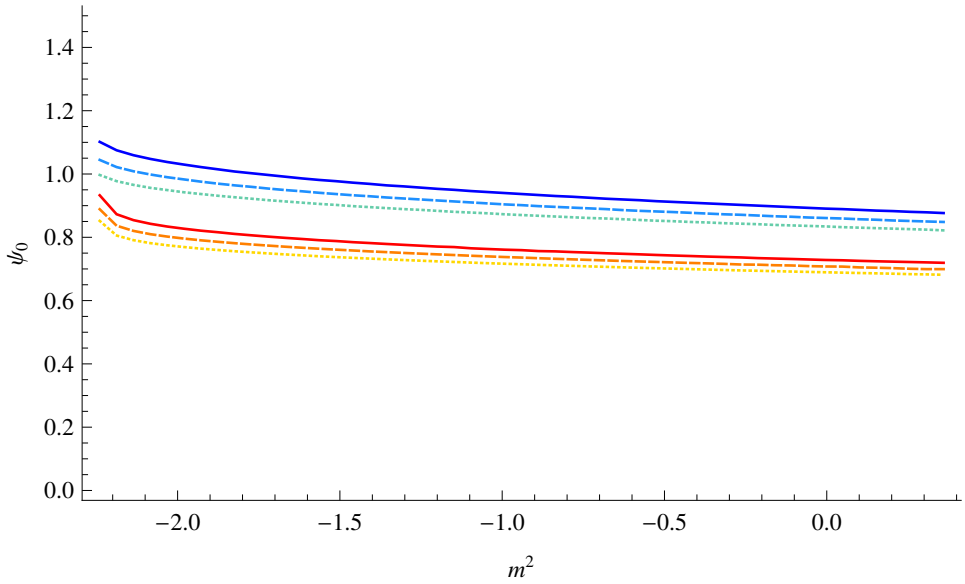

Figure 3.10: A phase diagram comparing the central densities ψ_c and ψ_h as a function of m^2 for different values of q. The dotted lines are for $q = 0.3$, the dashed lines for $q = 0.2$, while the solid lines for $q = 0.1$. The warm coloured lines (below) correspond to transition between stable and unstable configurations, while the cold coloured lines (above) transition between solid and hollow phases. As we lower the charge q both ψ_c and ψ_h increase, however their difference remains roughly unchanged, highlighting how hollow solutions are unstable for all range of parameters investigated.

3.6 Final comments

In this chapter we numerically investigated the behaviour of extremal, codimension 2, spacelike surfaces in charged, asymptotically AdS, boson star backgrounds. Our main goal was to establish the conditions for which families of minimal area spacelike surfaces anchored on the boundary fail to fully cover the bulk of the spacetime. As discussed in the Introduction, this study was motivated by recent ideas regarding a possible connection between the holographic description of entaglement entropy and the gravity dual of a reduced density matrix as discussed in [33].

We observed that the relation between the star's mass as well the the star's charge and the central density of the scalar field in four dimensions behave much like what is known for both neutral boson stars in AdS and

charged boson stars in flat space. Notably, the existence of a maximum mass for a finite $\psi(0) = \psi_c$ strongly hints towards the presence of a stability threshold and can be used to infer the physical feasibility of the hollow solutions we were so interested in. In three dimensions we found results akin to what is known in the literature for other types of boson stars, in particular, we observed a behaviour similar as the one found in [12] for $2+1$ dimensional neutral boson stars in asymptotically AdS spacetime.

Our analysis of the behaviour of extremal surfaces with fixed boundary points led us to the conclusion that, both in three and four dimensions, for fixed m^2 and q there is a maximum value for the central density of the scalar field ψ_h for which the minimal area surfaces reach every point in the bulk space (figures 3.7 and 3.8). Therefore one should expect that charged boson stars with a high enough $\psi(0)$ could provide a clear obstacle in the way of $w(D_A)$ being a universal candidate for $R(D_A)$. However we saw that, at least in four dimensions, there is good evidence indicating that solutions with $\psi(0) \geq \psi_h$ are unstable (figure 3.9). Extrapolating well known results in the literature for both boson stars with and without gauge fields in flat space, and boson stars without gauge field in AdS space, we find that for given m^2 and q there is a threshold central density value ψ_c for which the solutions cease to be stable if $\psi(0) > \psi_c$. Remarkably, in the four dimension case in question, we found that for every pair of m^2 and q, $\psi_c < \psi_h$, i.e.: solutions for which $w(D_B)$ fail to cover the entire bulk and, in particular, $z(D_A) \supset w(D_A)$ while $w(D_A) \not\supseteq z(D_A)$, are physically unstable. Unfortunately, to the extent of this author's knowledge, much less in known about the stability of three dimensional boson stars, therefore precluding us from saying anything about the stability of both regimes we found.

We believe the results found in this work support some of the ideas discussed in [33] and further explored in [23, 31, 139]. The unstable character of hollowed solutions strengthens the proposal of $w(D_A)$ as a good candidate for $R(D_A)$ and complements other recent works on the subject. We also believe that a deeper understanding of extremal surfaces on charged boson stars backgrounds can serve as a fruitful test ground for numerous holographic ideas including, but not restricted to, the holographic entanglement entropy, the holographic dual of a density matrix, zero temperature quantum phase transitions [69], etc.

Chapter 4

Rindler Quantum Gravity

4.1 Introduction and summary

According to the AdS/CFT correspondence [1, 92], asymptotically globally AdS spacetimes in certain quantum theories of gravity have an exact description as states of a conformal field theory on S^d. In this chapter, we show (see Section 4.2) that the same asymptotically AdS spacetimes may be described alternatively as entangled states of a pair of CFTs on hyperbolic space. This description in terms of hyperbolic space CFTs is precisely analogous to the description of Minkowski space field theory states in terms of entangled states of the field theory on two complementary Rindler wedges. In particular, if we focus on one of the H^d CFTs, the degrees of freedom live in a density matrix, and this density matrix describes physics in a wedge of the dual spacetime accessible to an accelerated observer, as shown in Figure 4.1.

The description of pure AdS in terms of the hyperbolic space theories is the specific entangled state[43]

$$|0_{global}\rangle = \frac{1}{Z}\sum_i e^{-\pi R_H E_i}|E_i^L\rangle \otimes |E_i^R\rangle \ , \tag{4.1}$$

where R_H is the curvature length scale of the hyperbolic space and $|E_i\rangle$ are energy eigenstates of the hyperbolic space CFTs. For this state, each hyperbolic space CFT is described by a thermal density matrix with temperature $(2\pi R_H)^{-1}$, similar to the Rindler description of the Minkowski space vacuum.[44] State (4.1) has precisely the same form as the state of a pair of CFTs on S^d that corresponds to the maximally extended eternal AdS-Schwarzschild black hole [75, 93]. This is no coincidence: thermal states of the H^d CFT correspond to asymptotically AdS black holes with boundary

[43] Here, and throughout this chapter, we use $\sum$ to denote both discrete and continuous sums over states.

[44] The fact that the reduced density matrix associated with the boundary of a single wedge of pure AdS maps to a thermal density matrix for the CFT in hyperbolic space was demonstrated recently in [29], which formed part of the inspiration for this work.

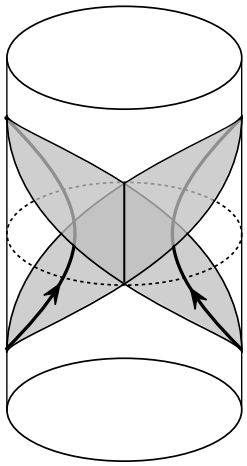

Figure 4.1: A pair of accelerating observers in pure global AdS. The spacetime region accessible to each is a wedge whose boundary geometry can be chosen as $H^d \times R$. Each wedge has a dual description as a thermal state of a CFT on this $H^d \times R$ boundary geometry. The full spacetime is described by an entangled state of the two H^d CFTs.

geometry $H^d \times R$ [41] and the choice of temperature $T = (2\pi R_H)^{-1}$ is special in that it corresponds to a "topological" black hole that is locally pure AdS.

If a Rindler wedge of pure AdS is described by a thermal density matrix, it is interesting to ask about the spacetime interpretation of the "microstates" contributing to this ensemble, i.e. the microstates of the topological black hole. We argue (see Sections 4.3 and 4.4) that typical pure states of the hyperbolic space CFT are dual to spacetimes that are almost indistinguishable from a Rindler wedge of pure AdS away from the horizon, but have the horizon replaced by some type of singularity where a geometrical description of the spacetime ceases to exist.[45] The description in equation (4.1) of pure AdS may then be given a spacetime interpretation as in Figure 4.2: a quantum superposition of disconnected singular wedges yields the connected global AdS spacetime.[46] This description suggests strongly

[45] This similar to the "fuzzball" proposal of Mathur for black hole states; see [96] for a review.

[46] This provides another explicit example of the idea [135–137] that connected spacetimes emerge by entangling degrees of freedom in the non-perturbative description. Based on these observations, Mathur has argued [97, 99] that asymptotically flat spacetime could be understood as a quantum superposition of fuzzball geometries associated with Rindler

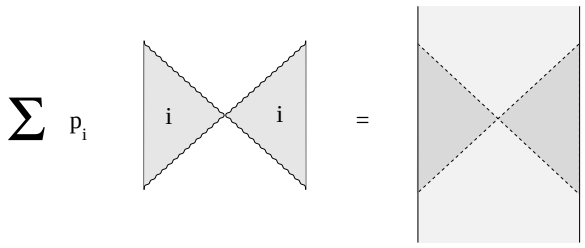

Figure 4.2: Quantum superposition of microstate geometries yielding pure AdS spacetime. Each choice of complementary Rindler wedges leads to a different decomposition of AdS into a superposition of disconnected spacetimes.

that the physics of AdS space outside the wedges (lightly shaded region in Figure 4.2) is encoded in the information about how the two H^d CFTs are entangled with each other.

The role of the microstate geometries is rather different for pure AdS as compared with an ordinary black hole. For black holes formed from collapse, the physical state is a pure state, one of the microstates of the black hole, and the black hole geometry may be understood as giving a coarse-grained description of the physics. For pure AdS, the microstates have little to do with the physical spacetime. For these microstates, spacetime ends where the Rindler horizon would have been, while in the physical spacetime, the Rindler wedge is smoothly connected to a larger spacetime. The latter property is linked to the fact that the hyperbolic space CFT degrees of freedom are highly entangled with some other degrees of freedom. Thus, in describing pure AdS, it is crucial that the degrees of freedom of the hyperbolic space CFT are entangled with the other degrees of freedom, i.e. that they are genuinely described by a density matrix.

To highlight the importance of this entanglement, we consider in Section 4.5 a concrete realization of the "disentangling experiment" discussed in [135–137]. Varying the temperature parameter in the state (4.1) away from $\beta = 2\pi R_H$ changes the degree of entanglement between the two hyperbolic space CFTs (or the two halves of the sphere in the original picture) in a particular way. In this case, we can describe exactly what happens to the geometry: for any temperature T, the corresponding global geometry is the maximally extended hyperbolic space black hole with that temperature. From these explicit geometries, we can look specifically at what happens

microstates. Our AdS discussion here provides a concrete realization of Mathur's suggestions.

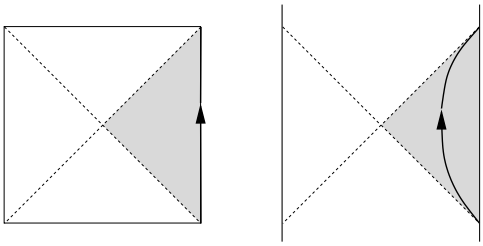

Figure 4.3: Static observer in de Sitter space (left) and accelerated observer in AdS. Both have access to only a portion of the full spacetime, bounded (on one side in the AdS case) by a horizon with a thermal character.

to a spatial slice of the spacetime as we vary the temperature. As the entanglement decreases, we find that the asymptotic regions corresponding to the two halves of the sphere become further apart and that the area of surfaces separating the two sides decreases, as argued on general grounds in [135–137].

Lessons for cosmological spacetimes

The physics of accelerated observers in AdS spacetimes shares many qualitative features with the physics of observers in cosmological spacetimes with accelerated expansion. In Figure 4.3 (right), we have depicted an AdS observer with constant acceleration. The worldline for this observer starts and ends on the AdS boundary. This observer can communicate with (send light signals to and receive light signals back from) only a portion of the full global AdS spacetime shown by the shaded region in the figure. We see that this shaded region has a very similar character to the static patch accessible to a geodesic observer in de Sitter spacetime, shown on the left in Figure 4.3. Both regions are bounded in the bulk spacetime by a horizon. Both observers see geodesic objects accelerating away from them towards the horizon. Finally, both horizons have a thermal character, emitting Unruh/Hawking radiation characteristic of some particular temperature.

These similarities give hope that some of the observations in this chapter may be helpful in understanding how to generalize AdS/CFT to provide a non-perturbative description of quantum gravity in cosmological settings. In this context, it is interesting that we have given a precise description (via a density matrix for a subset of degrees of freedom) of patches accessible to particular observers in a complete model of quantum gravity. Like static patches in de Sitter space, these patches are bounded by observer-dependent

horizons with an associated observer-dependent horizon area. In the de Sitter case, this observer-dependence obfuscates the proper interpretation of the entropy associated with this horizon area. In our present example, the interpretation of the observer-dependent entropy is clear: a single spacetime can be represented in many different ways as an entangled state of two subsets of degrees of freedom. Different choices of the subsets correspond to different patches (or different observers), and the the entropy associated to the horizon area in a patch measures the entanglement between the subsets. Alternatively, the entropy can be viewed as a count of microstates: the density matrix describing the subset of degrees of freedom associated with a single patch can be viewed as an ensemble of pure states, and each of these has a dual interpretation as a microstate geometry that is similar to the patch away from the horizon. It seems possible that all of these comments might apply equally well to de Sitter space or other cosmological spacetimes.[47] Some additional discussion on generalizing AdS/CFT to cosmological spacetimes is found in Section 4.6.

4.2 A Rindler description of asymptotically global AdS spacetimes

In the study of quantum fields on curved spacetime (or "semiclassical" quantum gravity), much of the physics of field theory on black hole backgrounds or on spacetimes with cosmological horizons can be understood by considering field theory on Rindler space, related to the physics experienced by accelerating observers in Minkowski space. It is interesting then to ask whether it is possible to describe precisely the physics accessible to an accelerated observer in a fully quantum mechanical description of gravity. In this section, we shall see that for asymptotically globally AdS spacetimes described by states of a CFT on S^d, there is an alternate dual description that is precisely analogous to the Rindler description of field theory on Minkowski space.

4.2.1 Asymptotically AdS spacetimes as entangled states of two hyperbolic space CFTs

Consider an asymptotically globally AdS spacetime dual to a pure state $|\Psi_{S^d}\rangle$ of some CFT on $S^d \times R_t$. For any point P on the boundary cylinder, we can consider the region D_P consisting of all points on the boundary which

[47] Our discussion here is similar to recent comments of Mathur in [98].

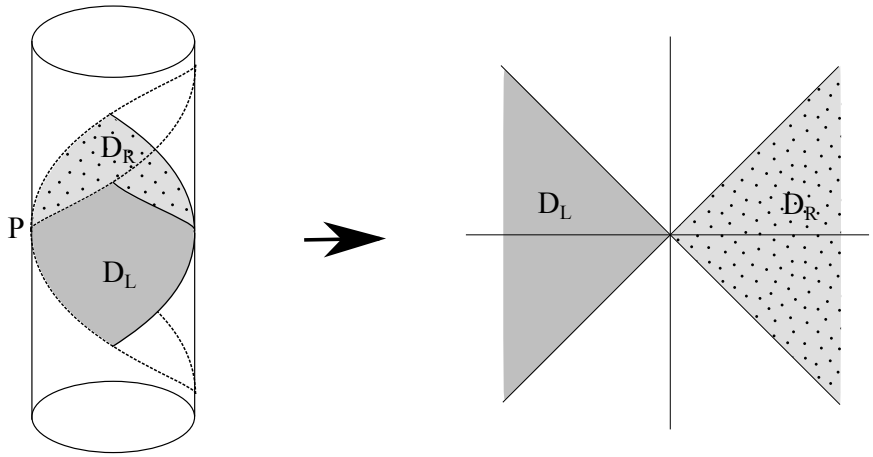

Figure 4.4: Conformal map from the boundary of a Poincare patch to Minkowski space. Region D_L (solid) maps to one Rindler wedge of Minkowski space, while the dotted region, D_R, maps to the other wedge. The Poincare patch boundary D_P is the region bounded by dashed lines.

are not timelike separated from P; for pure AdS, this forms the boundary of a Poincare patch. By a conformal transformation (reviewed in the appendix), the region D_P can be mapped to Minkowski space; associated to this, we have a map from states of the S^d CFT to states of the CFT on Minkowski space.[48]

Now, consider two complementary Rindler wedges of Minkowski space, regions $R = \{x^1 \geq 0, |t| < x^1\}$ and $L = \{x^1 \leq 0, |t| < |x^1|\}$ for some choice of coordinates. Under the map from D_P, these regions are the images of two complementary "diamond-shaped" regions,[49] as shown in Figure 4.4. Any state of the CFT on Minkowski space can be represented as an entangled state of the quantum field theories on the separate Rindler wedges R and L. For example, the Minkowski space vacuum is described in terms of field

[48]Since the region D_P includes a complete spatial slice of the boundary cylinder (a boundary Cauchy surface) knowing the state of the fields on D_P is the same information as knowing the fields on the entire boundary cylinder; thus, the map $|\Psi_{S^d}\rangle \to |\Psi_{R^d}\rangle$ is an isomorphism. Care must be taken in choosing the appropriate boundary conditions for the fields on Minkowski space.

[49]Each of these regions is the intersection of the interior of the future light cone of some point p_i with the interior of the past light-cone of a point p_f in the future of p_i. Alternatively, the regions are domain of dependence of a ball-shaped subset of some spatial slice of the boundary cylinder.

theories on the complementary Rindler wedges by the entangled state

$$|0_M\rangle = \frac{1}{Z}\sum_i e^{-\frac{\beta E_i}{2}}|E_i^L\rangle \otimes |E_i^R\rangle \ . \tag{4.2}$$

where $|E_i^L\rangle$ and $|E_i^R\rangle$ are corresponding eigenstates of the Rindler Hamiltonians on the two wedges (boost generators in the full Minkowski space).

By another conformal transformation (reviewed in the appendix) the Rindler wedges R and L can each be mapped to $H^d \times$ time, where H^d is the d-dimensional hyperbolic space with metric

$$ds^2 = du^2 + R_H^2 \sinh^2\frac{u}{R_H}\, d\Omega_{d-1}^2 \ . \tag{4.3}$$

Thus, the entangled state of the field theory on two Rindler wedges maps to an entangled state of the pair of CFTs on hyperbolic space. Under the conformal transformations to $H^d \times R_t$, the Rindler Hamiltonian in each wedge maps to the Hamiltonian generating time translations in $H^d \times R_t$. Thus, the state (4.2) describing pure global AdS spacetime maps to the state

$$|0\rangle_{S^d} = \frac{1}{Z}\sum_i e^{-\pi R_H E_i}|E_i^L\rangle_{H^d} \otimes |E_i^R\rangle_{H^d} \ . \tag{4.4}$$

of the pair of CFTs on $H^d \times R$. Here, one finds that the temperature parameter β takes on the specific value $2\pi R_H$.

In the CFT on S^d, the state corresponding to pure global AdS spacetime is clearly quite special: it is the energy eigenstate of the CFT Hamiltonian with the lowest possible energy. In the alternate description, the state (4.4) is not in any sense a minimum energy state for the Hamiltonian of either H^d CFT. However, states of the form (4.4) have the maximum amount of entanglement entropy for a given energy expectation value.[50]

We will see below that states of the $H^d \times H^d$ CFT without entanglement correspond to states of the S^d CFT with a singular stress-energy at the lightlike boundaries of the two regions that map to the two hyperbolic spaces. By the AdS/CFT dictionary, singularities in the stress-energy tensor can be associated with deformations of the metric which violate the asymptotically AdS boundary conditions. Thus, while we can associate a state of the $H^d \times H^d$ CFT to any asymptotically globally AdS spacetime (for a theory dual to a CFT on S^d), general states of the $H^d \times H^d$ CFT correspond to a more general class of spacetimes.

[50] This is true for the state (4.4) at any temperature, but within this set of states, the one with $T = (2\pi R_H)^{-1}$ is the only one with asymptotically global AdS asymptotics, as we will see explicitly in Section 4.4.

4.2.2 The description of a single Rindler wedge

So far, we have shown that any state of a CFT on $S^d \times R_t$ can be represented as an entangled state of a pair of hyperbolic space CFTs. This gives an alternate description of asymptotically global AdS spacetimes. We will now see that the information contained in the individual hyperbolic space CFTs corresponds (roughly) to the information accessible to a pair of complementary accelerating observers in the bulk. Thus, we can think of the hyperbolic space picture as giving a Rindler description of asymptotically global AdS spacetimes.

Consider first the case of pure global AdS, described in the hyperbolic space CFT picture as the entangled state (4.4). In this state, the reduced density matrix for each individual CFT is the thermal density matrix corresponding to temperature $1/(2\pi R_H)$.[51] Generally, thermal states of a CFT on hyperbolic space are dual to asymptotically locally AdS black hole solutions with boundary geometry H^d, discussed in detail in [41] and reviewed in Section 4.5 below.[52] However, for the particular temperature $1/(2\pi R_H)$, such a black hole is locally pure AdS. For such a black hole, the region outside the horizon corresponds exactly with a "Rindler wedge" of pure AdS, the region accessible to an accelerating observer whose worldline starts and ends at the past and future tips of the diamond-shaped region that maps to hyperbolic space, as shown in Figure 6.15.[53]

We will now argue that the density matrix for the single H^d CFT generally does not carry any information about the region beyond this wedge. We recall that the two copies of $H^d \times R_t$ are related by conformal transformations to two complementary diamonds (which we refer to as D_R and D_L) on the cylindrical boundary of global AdS. For the full CFT on S^d, there are many pure states that give rise to precisely the same density matrix for the region D_R. For these states, the fields in the complementary region D_L generally differ, and such differences can affect any point in the bulk in the causal past or causal future of D_L, as we see in Figure 6.15. Thus, there are many states of the full field theory for which the density matrix for D_R is the same but the physics in the region $J^+(D_L) \cup J^-(D_L)$ differs. We con-

[51] This has been derived directly in [29].

[52] There is no analog of the Hawking-Page transition here, though we have a qualitative change in the causal structure of the maximally extended solutions at $T = 1/(2\pi R_H)$. For temperatures below $(2\pi R_H)^{-1}$ the black holes have a causal structure similar to Reissner-Nordstrom AdS black holes while for temperatures higher than $(2\pi R_H)^{-1}$ the causal structure is similar to Schwarzschild AdS black holes.

[53] Here, an "accessible" point is one for which the observer can send a light signal to and receive a light signal back from that point.

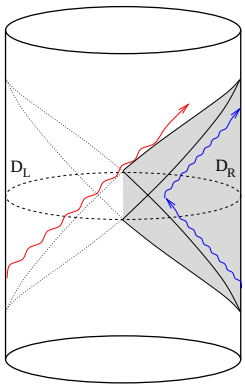

Figure 4.5: Wedges of pure AdS spacetime. Field theory observables in D_R (the shaded part of the boundary cylinder) probe the bulk region $J^+(D_R) \cap J^-(D_R)$ (the shaded region of the bulk). Any point in this region can receive a light signal (blue line) from and send a light signal to D_R. Physics outside this region can be altered by changes on the boundary that do not affect the state of the fields in D_R. One trajectory along which such changes propagate is shown in red.

clude that the density matrix associated with the region D_R (equivalently, the density matrix for the corresponding H^d CFT) knows only about the complement of $J^+(D_L) \cup J^-(D_L)$. But for pure AdS, this is exactly the region $J^+(D_R) \cap J^-(D_R)$ outside the horizon of the hyperbolic black hole with temperature $1/(2\pi R_H)$.

To summarize, the density matrices for the two hyperbolic space CFTs describe the physics in two complementary Rindler wedges of pure AdS. The individual density matrices generally do not have information about the spacetime regions beyond the respective Rindler horizons. The additional information that comes from knowing the full state as compared with knowing the two density matrices is the information about how the degrees of freedom in the two CFTs are entangled with each other. Thus, we can say that the physics in the region outside the two Rindler wedges is described by the entanglement between the two hyperbolic space CFTs.[54]

In this section, we have focused on the case of pure global AdS spacetime. More general asymptotically AdS spacetimes correspond to other entangled

[54]The arguments in this section apply equally well to Schwarzschild-AdS spacetimes dual to an entangled state of two S^d CFTs. They suggest that a single S^d CFT in a thermal density matrix knows only about the region outside the horizon of the black hole. Knowing anything about physics behind the horizon requires knowledge of both CFTs.

states of the two hyperbolic space CFTs. The question of what region of these spacetimes is associated with the density matrix for a single hyperbolic space CFT (and more generally, what region of the spacetime dual to a state $|\Psi\rangle$ of a CFT on M can be reconstructed from the density matrix for any spatial subset of degrees of freedom of the CFT) was considered by the present authors recently in [32] (and by others in [24, 72]). There, we argued that the identification of the wedges $J^+(D_R) \cap J^-(D_R)$ and $J^+(D_L) \cap J^-(D_L)$ as the duals of the density matrices associated with D_R and D_L is somewhat specific to pure AdS. For more general spacetimes (with matter), the causal wedges $J^+(D_R) \cap J^-(D_R)$ and $J^+(D_L) \cap J^-(D_L)$ do not intersect in the bulk, but the density matrices associated with D_R and D_L carry information about larger wedges $w(D_R)$ and $w(D_L)$ that generally do intersect.

4.3 The microstates of a Rindler wedge of AdS

The state (4.4) that describes pure AdS in the $H^d \times H^d$ picture has exactly the same form as the states of a CFT on $S^d \times S^d$ that describe maximally extended Schwarzschild-AdS black hole spacetimes [75, 93]. Specifically, in both cases the degrees of freedom of the two CFTs are entangled such that each "factor" theory is in a thermal state. The basic reason for this similarity is that (as we have seen) pure global AdS itself can be understood as a particular type of black hole.

We have argued that the thermal density matrix for a single CFT is dual to the region outside the horizon of the black hole. As usual, the (suitably regularized) area of the black hole horizon can be identified with the (regularized) entropy of the density matrix. For the full theory with a second CFT on H^d, this entropy would naturally be viewed as an entanglement entropy, measuring the extent to which the degrees of freedom are entangled with each other. But in discussions of black hole physics, such an entropy is more commonly viewed as a thermodynamic entropy counting microstates contributing to the ensemble described by the density matrix. Since the "black hole" in our case is a patch of pure AdS spacetime, it may seem odd to talk about its microstates. However, the thermal density matrix for the H^d CFT can certainly be viewed as an ensemble of pure states and AdS/CFT suggests that these pure states should have some dual gravity interpretation. The goal of this section is to understand better these microstate geometries.

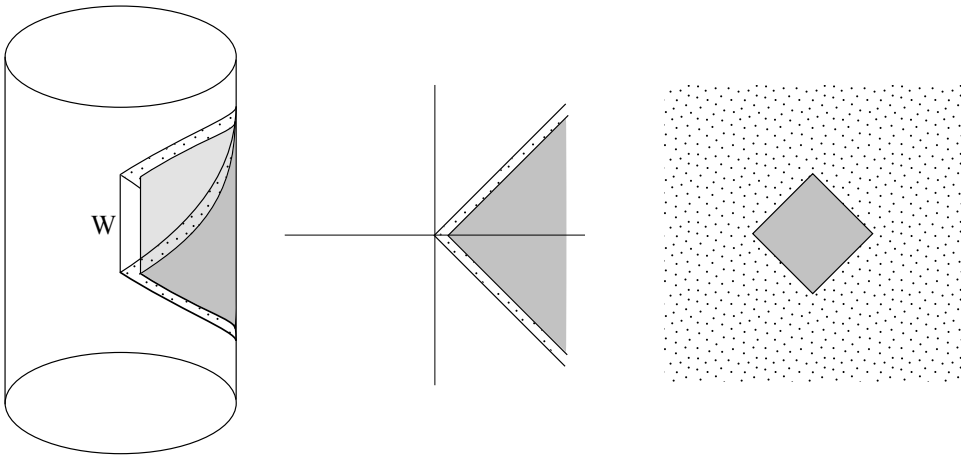

Figure 4.6: Subregion D_ϵ (shaded) of boundary D of a Rindler wedge of AdS. The complement of D_ϵ in D is shown dotted. (a) Regions D and D_ϵ on the boundary of AdS. The corresponding bulk regions are also shown. W is a surface in the bulk whose area computes the entanglement entropy of the fields in D. (b) D_ϵ is mapped to portion of a Rindler wedge. (c) D_ϵ is mapped to a finite portion of the infinite hyperbolic plane.

Interpreting the hyperbolic black hole microstates

Recall that the H^d CFT can be viewed as the theory on a Rindler wedge of a Minkowski space forming the boundary of a Poincare patch. Pure AdS corresponds to the Minkowski space vacuum and, as usual, the description of the fields on one Rindler wedge is via a thermal state. In this picture, the microstates are pure energy eigenstates of the Rindler space field theory, most of which are typical states in the ensemble described by the density matrix. For such typical states, we expect that almost any macroscopic observable will be nearly identical to the corresponding observable in the thermal state. Field theory observables (e.g. correlation functions, Wilson loops, entanglement entropies) tell us about the geometry of the dual space-time, which suggests that the gravity dual of one of these typical microstates should be almost identical to the gravity dual of the thermal state itself. Let us try to understand this in more detail.

Microstate geometries look like the Rindler wedge of pure AdS away from the horizon

Consider a domain of dependence region D_ϵ in the boundary spacetime,[55] which is slightly smaller than the boundary D of our Rindler wedge (see Figure 4.6). In the map from D to hyperbolic space times time, the region D_ϵ maps to a finite region of $H^d \times R$. Thus, we can think of the degrees of freedom in D_ϵ as forming a small subset of the full set of degrees of freedom in the hyperbolic space field theory. For a typical microstate in some thermodynamic ensemble, the reduced density matrix for a small subset of degrees of freedom should be nearly the same as the reduced density matrix that arises from the thermal state itself [52, 114]. In fact, given the exact reduced density matrix $\rho_{D_\epsilon}(T)$ arising from the thermal state of the hyperbolic space CFT, there should be many pure states of the full theory for which the reduced density matrix on D_ϵ is exactly $\rho_{D_\epsilon}(T)$. The reason is that for any density matrix $\rho = \sum p_i |A_i\rangle\langle A_i|$ we can always choose a pure state $|\Psi\rangle = \sum p_i |A_i\rangle \otimes |B_i\rangle$ in a theory with a sufficiently large number of added degrees of freedom such that the reduced density matrix for the smaller system is exactly ρ. Here, we certainly have enough degrees of freedom, since there is an infinite volume of hyperbolic space outside the finite region that is the image of D_ϵ under the conformal transformation from D to $H^d \times R$.[56] Thus, restricting to any subregion D_ϵ of D, there is no way in general that we can distinguish a pure microstate on D from the mixed state on D dual to pure AdS. According to [24, 32, 72], this means that the bulk region associated with the boundary D_ϵ will be the same as for pure AdS.[57]

[55] The "domain of dependence" of a spatial region A is the set of all points p such that every inextensible causal curve through p passes through A. The boundary D of a Rindler wedge of pure AdS is the domain of dependence of a ball-shaped subset of a spherical constant-time slice of the boundary cylinder (e.g. a hemisphere of the $t = 0$ sphere). The region D_ϵ can be taken as the domain of dependence of a slightly smaller ball.

[56] Note, however, that if a UV cutoff is imposed on the original field theory on S^d, there will be a limit to how large the region D_ϵ can be such that we can still choose a pure state on D to exactly reproduce the density matrix ρ_{D_ϵ} arising from the vacuum of the S^d CFT.

[57] For a general microstate, the density matrix ρ_{D_ϵ} will not necessarily be exactly the same as the one arising from the thermal state, but typically it will be almost identical. The corresponding bulk region should then be almost indistinguishable from pure AdS.

Rindler horizon replaced by something singular in microstate geometries

Let us now consider what happens at the boundary of the region D. After a conformal transformation that takes the region D to a Rindler wedge of Minkowski space, this boundary becomes the Rindler horizon. For any pure state of quantum field theory on Rindler space (considered together with a pure state of the quantum field theory on the complementary Rindler wedge such that we have some state of the full Minkowski space field theory), we expect that the stress-energy tensor is singular on the Rindler horizon. This was shown for the state $|0_L\rangle \otimes |0_R\rangle$ of a free scalar field theory in [112] and we demonstrate it more generally for any product state $|\Psi_L\rangle \otimes |\Psi_R\rangle$ in Section 4.4. We also show in Section 4.5.3 that the state $|0_L\rangle \otimes |0_R\rangle$ gives a singular stress-energy tensor on the Rindler horizon for any conformal field theory. We expect this conclusion to extend to any product state.[58] Thus, while the field theory observables for a pure state on D can be arbitrarily close to the vacuum observables away from the Rindler horizon, the behavior at this horizon (i.e. the boundary of D) is drastically different.

What is the bulk interpretation of this? We have seen above that the bulk region of the microstate spacetime associated with any smaller region D_ϵ will be almost indistinguishable from a wedge of pure AdS. On the other hand, as D_ϵ grows to become the full region D, drastic differences appear, with various observables diverging as we hit the boundary of D. This suggests that the bulk spacetime dual to a typical microstate of the H^d CFT in the $T = (2\pi R_H)^{-1}$ thermal ensemble differs significantly from the Rindler wedge of pure AdS at the horizon. These differences can only occur at the horizon of the Rindler wedge region, since we have seen that any smaller wedge should be almost indistinguishable from AdS. This suggests that the dual of a microstate of the $T = (2\pi R_H)^{-1}$ hyperbolic black hole should look like a Rindler wedge of AdS, but with the bulk horizon replaced by some type of singularity, probably of a non-geometric character.

More evidence for such singular behavior comes from considering the behavior of entanglement observables in the field theory and their proposed gravity dual description. We recall that according to the proposal of Ryu and Takayanagi [118] (and the covariant generalization [73]), the von Neumann entropy of the density matrix associated with some spatial region A of a

[58] This is consistent with a result from algebraic quantum field theory that finite subregions of a quantum field theory do not admit pure states [28, 46]. This implies that starting from a product state in e.g. a lattice regularized theory, and taking a continuum limit must lead to some singular behavior at the interface between the regions.

quantum field theory with weakly curved holographic dual is equal to the area of an extremal surface W in the dual spacetime such that the boundary of W is the same as the boundary of A (as in figure 4.6). For a microstate of the H^d CFT, we expect that the von Neumann entropy associated with a smaller region D_ϵ should be very similar to that for the same region in the thermal state. On the other hand, for the entire region D, the von Neumann entropy for the thermal state dual to a wedge of pure AdS is equal to the area of the Rindler horizon, while the von Neumann entropy of a pure microstate is zero. For the microstate, this implies either that the surface W has zero area, or that the Ryu-Takayanagi formula no longer applies (e.g. because the relevant region of spacetime no longer has a weakly curved geometrical description). In either case, it appears that the metric on the boundary of the Rindler wedge is replaced by something singular (or non-geometric) when we pass from the black hole geometry (i.e. the wedge of pure AdS) to the microstate geometry.

Connections to previous work

Our observations here illustrate and elaborate on an observation in [135–137] about the emergence of spacetime in AdS/CFT. There, it was pointed out, based on the example of the eternal AdS black hole, that a classically connected spacetime can arise from quantum superpositions of spacetimes with two disconnected components. This phenomenon is apparent in the present setup: we have argued that typical microstates in the H^d CFT thermal ensemble correspond to spacetimes similar to a Rindler wedge of AdS, but with the horizon replaced by something singular or non-geometrical. In the state (4.4) describing pure AdS, we have a superposition of states $|E_i^L\rangle \otimes |E_i^R\rangle$, each of which can be interpreted as a disconnected pair of these microstate spacetimes. The quantum superposition (4.4) represents pure global AdS spacetime, giving rise to the picture in Figure 4.2. Compared to the earlier observations [135–137], a new feature is that (for this particular case) the microstate geometries contributing to the superposition are almost identical to pure AdS in their interior, but end rather abruptly at the place where the horizon would be in the connected version of the spacetime. Also, since there are many possible choices for complementary Rindler wedges in AdS, this example highlights the fact that there are many ways to decompose a given spacetime into a superposition of disconnected spacetimes.

Our conclusions about the geometry of Rindler microstates are similar to the "fuzzball" proposal of Mathur in that black hole microstates are geometries for which the horizon of the black hole has been replaced by

something else. In our case, the "something else" may simply be some kind of lightlike singularity at which spacetime ends.[59] Mathur has specifically proposed [97, 99] (based on a flat space limit of the observations in [136] about eternal AdS black holes) that a Rindler wedge of asymptotically flat space should have fuzzball microstates, and that empty space can be represented as a quantum superposition of disconnected geometries consisting of a pair of these Rindler fuzzballs. Our results confirm Mathur's suggestions in detail for the closely related case of empty AdS space. In this case, we have been able to give an explicit description of the Rindler-space theories (the hyperbolic space CFTs) and a (somewhat indirect) description of the fuzzball-geometries (the gravity duals of specific microstates of these hyperbolic CFTs).

4.4 Rindler space results

In this section, we consider a free massless scalar field theory on 1+1-dimensional Minkowski space and its alternative description based on the fields in a pair of complementary Rindler wedges. We prove that if a state factorizes into left and right components, i.e. if it is not entangled, its energy-momentum diverges on the Rindler horizon. This result suggests that "AdS microstates" discussed in the previous section are singular on the horizon of the AdS Rindler wedge. Interestingly, a divergent stress-energy on the boundary violates the AdS asymptotics, so the microstates cannot even be said to be asymptotically AdS! In the next section we complement this calculation with evidence that a state without entanglement represents a spacetime whose two parts have pinched off and disconnected from one another.

Consider a scalar field ϕ in two-dimensional Minkowski spacetime. We would like to divide this spacetime into a left and a right Rindler wedge. Defining $U = t - z$ and $V = t + z$, the right Rindler wedge is given by $U < 0 < V$. Because the dynamics of the left- and right-moving modes is independent and identical, we focus below on the right-moving sector, whose dynamics is independent of V.

[59] Note however, that some of the arguments we have used here are specific to the hyperbolic space CFT. In a similar discussion with H^d replaced by S^d, we could argue in a similar way that the eternal black hole geometry behind the horizon has no relevance for black hole microstate spacetimes, but not that the microstates spacetimes are exactly the same as the black hole but with an abrupt end where the horizon would be.

A complete set of right-moving Rindler modes is

$$\phi_{\lambda,R}(U) = \Theta(-U)\frac{1}{\sqrt{4\pi\lambda}}(-aU)^{i\lambda/a} , \tag{4.5}$$

$$\phi_{\lambda,L}(U) = \Theta(U)\frac{1}{\sqrt{4\pi\lambda}}(aU)^{-i\lambda/a} , \tag{4.6}$$

in terms of which, the field ϕ has an expansion:

$$\phi(U) = \int_0^\infty d\lambda \ \left(b_{\lambda,R}\phi_{\lambda,R} + b^\dagger_{\lambda,R}\phi^*_{\lambda,R}\right) \ + \ \int_0^\infty d\lambda \ \left(b_{\lambda,L}\phi_{\lambda,L} + b^\dagger_{\lambda,L}\phi^*_{\lambda,L}\right) . \tag{4.7}$$

The relationship between the Minkowski vacuum and the Rindler vacuum can be written as

$$|0,\mathrm{Mink}\rangle = \mathcal{U}|0,L\rangle|0,R\rangle , \tag{4.8}$$
$$\text{where } \ \mathcal{U} = \prod_{\lambda>0}\exp\left(-\arctan(e^{-\pi\lambda/a})(b^\dagger_{\lambda,R}b^\dagger_{\lambda,L} - b_{\lambda,R}b_{\lambda,L})\right) .$$

For definiteness, we focus attention on the UU-component of the stress-energy tensor. Taking the expectation value of the stress-energy tensor in the Minkowski vacuum as our reference point, we find that the stress-energy in the Rindler vacuum is

$$\begin{aligned} T^{RL}_{UU}(U) &= \langle 0,L|\langle 0,R|(\partial_U\phi(U))^2|0,L\rangle|0,R\rangle \ - \ \langle 0,\mathrm{Mink}|(\partial_U\phi(U))^2|0,\mathrm{Mink}\rangle \\ &= -2\int_0^\infty d\lambda \ \left[\beta_\lambda^2\left(|\partial_U\phi_{\lambda,R}|^2 + |\partial_U\phi_{\lambda,L}|^2\right) \ + \ 2\alpha_\lambda\beta_\lambda \mathrm{Re}\left(\partial_U\phi_{\lambda,L}\partial_U\phi_{\lambda,R}\right)\right] , \end{aligned} \tag{4.9}$$

where $\alpha_\lambda = e^{\pi\lambda/a}\beta_\lambda = (1-e^{-2\pi\lambda/2})^{-1/2}$ are the Rindler coordinates Bogoliubov coefficients.

At nonzero U, only the first term in equation (4.9) is non-zero. Using equations (4.5,4.6), we get that $T^{RL}_{UU}(U\neq 0) = -1/(48\pi U^2)$. To study the stress energy tensor at $U=0$, we follow the approach in [112], and regularize the operator by replacing the modes $\phi_{\lambda,R/L}$ in equation (4.9) with $\phi^\epsilon_{\lambda,R/L}$ given by

$$\phi^\epsilon_{\lambda,R}(U) = \frac{1}{\sqrt{4\pi\lambda}}\frac{(a(U-i\epsilon))^{i\lambda/a} - (a(U+i\epsilon))^{i\lambda/a}}{e^{\pi\lambda/a} - e^{-\pi\lambda/a}} , \tag{4.10}$$

$$\phi^\epsilon_{\lambda,L}(U) = \frac{1}{\sqrt{4\pi\lambda}}\frac{e^{\pi\lambda/2}\left(a(U-i\epsilon)\right)^{-i\lambda/a} - e^{-\pi\lambda/2}\left(a(U+i\epsilon)\right)^{-i\lambda/a}}{e^{\pi\lambda/a} - e^{-\pi\lambda/a}} \tag{4.11}$$

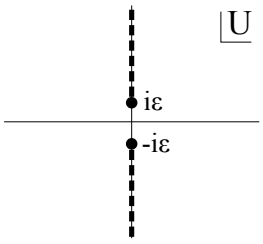

Figure 4.7: Position of cuts in the U-plane for formulas (4.10) and (4.11).

These expressions are valid and finite on the entire real line when we place the cuts as shown Figure 4.7. Such placement of cuts implies, for example, that for $U < 0$,

$$(a(U-i\epsilon))^{i\lambda/a} = ((e^{-i\pi})(-a(U-i\epsilon)))^{i\lambda/a} = e^{\pi\lambda/a}\,(-a(U-i\epsilon))^{i\lambda/a}\ . \quad (4.12)$$

This ensures that $\phi^{\epsilon}_{\lambda,R/L}$ approach $\phi_{\lambda,R/L}$ for $\epsilon \to 0$. We can now show that $\int_{-\infty}^{\infty} dU\ T^{RL}_{UU}$ is positive and diverges for small ϵ like ϵ^{-1}. Thus, the Rindler vacuum has a divergent stress-energy tensor on the boundary at $U = 0$.

We now demonstrate that it is not possible to cancel this singularity in the stress-energy tensor at the horizon in a general separable state:[60]

$$|\Psi\rangle = \sum_{k=1}^{\infty}\sum_{n_i=1}^{\infty}\int\left(\prod_{i=1}^{k}d\lambda_i\right)f_{(n_1,\ldots,n_k)}(\lambda_1,\ldots,\lambda_k)\left(\prod_{i=1}^{k}(b^{\dagger}_{\lambda_i,L})^{n_i}\right)|0\rangle_L \quad (4.14)$$
$$\otimes\sum_{k=1}^{\infty}\sum_{n_i=1}^{\infty}\int\left(\prod_{i=1}^{k}d\lambda_i\right)g_{(n_1,\ldots,n_k)}(\lambda_1,\ldots,\lambda_k)\left(\prod_{i=1}^{k}(b^{\dagger}_{\lambda_i,R})^{n_i}\right)|0\rangle_R\ .$$

The expectation value of the stress-energy tensor in this state is equal to that of the Rindler vacuum plus the additional contribution

$$\begin{aligned} T^{\Psi}_{UU} &= \langle\Psi|(\partial_U\phi(U))^2|\Psi\rangle \ - \ \langle 0,L|\langle 0,R|(\partial_U\phi(U))^2|0,L\rangle|0,R\rangle \\ &= \langle\Psi|:(\partial_U\phi(U))^2:|\Psi\rangle\ , \end{aligned} \quad (4.15)$$

[60] This state is more general than a tensor product of Fock space states of the left/right Rindler wedges, which takes the form

$$\sum_{n=1}^{\infty}\int\left(\prod_{i=1}^{n}d\lambda_i\right)f_n(\lambda_1,\ldots,\lambda_n)\left(\prod_{i=1}^{n}b^{\dagger}_{\lambda_i,L/R}\right)|0\rangle_{L/R}\ . \quad (4.13)$$

However, the typical states contributing to a finite temperature ensemble at infinite volume are of this more general form.

where :: indicates normal ordering of Rindler raising and lowering operators. Then

$$T^{\Psi}_{UU} = \int_0^\infty d\sigma_1 \int_0^\infty d\sigma_2 \quad \Big[\quad \langle\Psi|b_{\sigma_1,L} b_{\sigma_2,L}|\Psi\rangle \, \partial_U \phi_{\sigma_1,L} \partial_U \phi_{\sigma_2,L} \; + \; \text{c.c.} \tag{4.16}$$

$$+ \; 2 \, \langle\Psi|b^\dagger_{\sigma_1,L} b_{\sigma_2,L}|\Psi\rangle \, \partial_U \phi^*_{\sigma_1,L} \partial_U \phi_{\sigma_2,L} \tag{4.17}$$

$$+ \; \langle\Psi|b_{\sigma_1,R} b_{\sigma_2,R}|\Psi\rangle \, \partial_U \phi_{\sigma_1,R} \partial_U \phi_{\sigma_2,R} \; + \; \text{c.c.} \tag{4.18}$$

$$+ \; 2 \, \langle\Psi|b^\dagger_{\sigma_1,R} b_{\sigma_2,R}|\Psi\rangle \, \partial_U \phi^*_{\sigma_1,R} \partial_U \phi_{\sigma_2,R} \tag{4.19}$$

$$+ \; 2 \, \langle\Psi|b_{\sigma_1,L} b_{\sigma_2,R}|\Psi\rangle \, \partial_U \phi_{\sigma_1,L} \partial_U \phi_{\sigma_2,R} \; + \; \text{c.c.} \tag{4.20}$$

$$+ \; 2 \, \langle\Psi|b^\dagger_{\sigma_1,L} b_{\sigma_2,R}|\Psi\rangle \, \partial_U \phi^*_{\sigma_1,L} \partial_U \phi_{\sigma_2,R} \; + \; \text{c.c.} \Big] \tag{4.21}$$

Terms (4.17) and (4.19) are non-negative everywhere, for example

$$\int_0^\infty d\sigma_1 \int_0^\infty d\sigma_2 \langle\Psi|b^\dagger_{\sigma_1,L} b_{\sigma_2,L}|\Psi\rangle \partial_U \phi^*_{\sigma_1,L} \partial_U \phi_{\sigma_2,L} \; = \; \left| \int_0^\infty d\sigma \; \partial_U \phi_{\sigma,L} \; b_{\sigma,L}|\Psi\rangle \right|^2 \tag{4.22}$$

and therefore their contribution to the stress-energy tensor cannot cancel the Rindler vacuum singularity at $U = 0$, which is also positive.

For terms (4.16), (4.18) and (4.20), consider the behavior of the regularized stress-energy tensor near $U = 0$, $\int_{-\delta}^{\delta} dU T^{\Psi}_{UU}$ for small δ. For concreteness, we focus on the term (4.16), the argument for the other terms being similar. Under the substitution $U = \epsilon x$, we see that as $\epsilon \to 0$

$$\int_{-\delta}^{\delta} dU \; \partial_U \phi_{\sigma_1,L} \partial_U \phi_{\sigma_2,L} \; \to \; \epsilon^{-1-i\sigma_1-i\sigma_2} \times \text{ (smooth function of } \sigma_1 \text{ and } \sigma_2) \; . \tag{4.23}$$

Due to the rapidly oscillating factor $\epsilon^{-i\sigma_1-i\sigma_2}$, integrating over σ_1 and σ_2 in equation (4.16) will give $\lim_{\epsilon\to 0} \epsilon \int_{-\delta}^{\delta} dU T^{\Psi}_{UU} = 0$. The locus where the oscillations cancel, $\sigma_1 + \sigma_2 = 0$, lies outside the region of integration $\sigma_1 > 0, \sigma_2 > 0$, so even if $\langle\Psi|b_{\sigma_1,L} b_{\sigma_2,L}|\Psi\rangle$ were to contribute a delta function $\delta(\sigma_1 - \sigma_2)$ to the integrand, the integral would remain zero.

The remaining term, (4.21), could give a non-zero contribution, if $\langle\Psi|b^\dagger_{\sigma_1,R} b_{\sigma_2,L}|\Psi\rangle$ contributed $\delta(\sigma_1 - \sigma_2)$, as the rapidly oscillating term takes the form $\epsilon^{\pm i(\sigma_1-\sigma_2)}$. However, the separable form of our state $|\Psi\rangle$ does not allow for such a delta-function term in $\langle\Psi|b^\dagger_{\sigma_1,R} b_{\sigma_2,L}|\Psi\rangle$.

Thus any separable state has a divergent stress-energy tensor on the boundary at $U = 0$. To cancel the singularity in the stress-energy tensor on the boundary, we need an entangled state. As an example, consider the

Minkowski vacuum written in the following suggestive and convenient form

$$|\text{Mink}\rangle = \prod_{\lambda>0}\left[\frac{1}{\sqrt{Z_\lambda}}\sum_{n=0}^{\infty} e^{-\pi n\lambda/a}\frac{(b^\dagger_{\lambda,R})^n}{\sqrt{n!}}\frac{(b^\dagger_{\lambda,L})^n}{\sqrt{n!}}\right]|0,R\rangle|0,L\rangle \ , \tag{4.24}$$

such that each wedge is in a thermal density matrix with the Rindler temperature $T = a/2\pi$. In this state, $\langle\text{Mink}|b_{\sigma_1,R}b_{\sigma_2,L}|\text{Mink}\rangle = \delta(\sigma_1-\sigma_2)e^{-\pi\sigma_1/a}/(1-e^{-2\pi\sigma_1/a}) = \delta(\sigma_1-\sigma_2)\,\beta_{\sigma_1}\alpha_{\sigma_1}$. Since $T^{|\text{Mink}\rangle}_{UU} = -T^{RL}_{UU}$, this delta-function contribution must cancel the divergence at $U = 0$ precisely.

We have demonstrated than the singularity in the stress-energy tensor at $U = 0$ can only be cancelled in a state with entanglement between the right and the left Rindler wedge. Our discussion in Section 4.3 indicates that it should be possible to cancel the Rindler vacuum stress-energy tensor in the interior of a Rindler wedge by adding Rindler quanta to the Rindler vacuum. To complete our discussion, we will now show that we can achieve this to any desired accuracy with only a single quantum. Consider:

$$|\Psi_1\rangle = \int d\lambda f(\lambda) b^\dagger_{\lambda,L}|0\rangle_L|0\rangle_R \ , \tag{4.25}$$

where

$$f(\lambda) = \frac{e^{-(\lambda-\lambda_0)^2/(2\Delta^2)}}{\sqrt{2\pi}\Delta} \ . \tag{4.26}$$

At nonzero U we get (approximately, with Δ small enough)

$$T^{\Psi_1}_{UU} = 2\left|\int d\lambda f(\lambda)\partial_U\phi_{L,\lambda}\right|^2 = \frac{\lambda_0}{2\pi a^2U^2}e^{-\Delta^2(\ln(aU))^2/a^2} \ . \tag{4.27}$$

For (aU) in the interval $[e^{-a/\Delta}, e^{a/\Delta}]$, $T^{\Psi_1}_{UU}$ is approximately $\frac{\lambda_0}{2\pi a^2U^2}$. By adjusting Δ and λ appropriately, we can therefore construct a state with arbitrarily small total stress-energy tensor $T^{\Psi_1}_{UU} + T^{RL}_{UU}$ inside the shaded region in Figure 4.6(b).

4.5 Effects of disentangling on geometry

We have seen that entanglement is crucial for the description of pure AdS space in terms of a pair of hyperbolic space CFTs. To further highlight this, we consider in this section the effects on the bulk geometry of changing the amount of entanglement between the degrees of freedom in the two theories, which correspond to the two halves of the sphere in the original picture. This

provides an explicit example of the "disentangling experiment" proposed in [136].

As we have seen, the "Rindler" description of pure global AdS space is given by the state

$$|0_M\rangle = \frac{1}{Z}\sum_i e^{-\frac{\beta E_i}{2}}|E_i^L\rangle \otimes |E_i^R\rangle \tag{4.28}$$

with temperature chosen as $\beta = 2\pi R_H$. In this state, the degrees of freedom in the two hyperbolic space CFTs are entangled with each other. The claim in [136] was that if we change the state so that this entanglement is decreased, the dual spacetime should pinch off in the sense that the area of the bulk minimal surface separating the two halves should decrease and the distance between points in the two asymptotic regions should increase.

In the present context, we can decrease (or increase) the entanglement between the two sides by lowering (or raising) the temperature in the state (4.28).[61] In this case, each separate CFT on H^d will be in a thermal state, corresponding in the bulk to an asymptotically AdS black hole (brane) with boundary geometry H^d. These black holes were described and interpreted in the AdS/CFT context in [41]. The full state (4.28) corresponds to the maximally extended version of these black holes with two asymptotic regions. By studying the geometry of a spatial slice of these black hole spacetimes as a function of β, we will see that the qualitative expectations in [136] are precisely realized in this explicit example.

4.5.1 Review of the hyperbolic black holes

In $d+2$ spacetime dimensions, the hyperbolic black hole geometry for temperature T is described by the metric

$$ds^2 = -f(r)dt^2 + \frac{dr^2}{f(r)} + \frac{r^2}{l^2}(dH^d)^2 \tag{4.29}$$

with

$$f(r) = \frac{r^2}{l^2} - \frac{\mu}{r^{d-1}} - 1\ . \tag{4.30}$$

[61] The entanglement can be quantified by the entanglement entropy $S = -\mathrm{tr}\,(\,)\,\rho_R \ln \rho_R$. This entropy is divergent, but can be regulated by introducing an ultraviolet cutoff in the theory. In this case, the difference between the entanglement entropy for two different states of the theory (considering the same pair of complementary spacetime regions) should be finite and regulator independent as the cutoff is removed.

This has temperature

$$\beta = \frac{4\pi l^2 r_+}{d r_+^2 - l^2(d-1)}\,, \tag{4.31}$$

where r_+ is the horizon radius defined by $f(r_+) = 0$. The case $\mu = 0$ corresponds to the "topological black hole" that is a patch of pure AdS space. Both positive and negative values of μ are allowed, with the constraint that

$$\mu > \mu_{ext} = -\frac{2}{d-1}\left(\frac{d-1}{d+1}\right)^{\frac{d+1}{2}} l^{d-1}\,. \tag{4.32}$$

These coordinates cover the region exterior to the horizon, but the spacetime can be extended in the usual way to include a second asymptotic region (or more in the case $\mu < 0$). The causal structure is similar to the Schwarzschild-AdS black hole for $\mu > 0$ and to the Reissner-Nordstrom AdS black hole for $\mu < 0$.

4.5.2 Geometrical effects of changing the temperature / entanglement

We would now like to compare the geometries for different values of μ (which controls the temperature/entanglement). Note that the boundary geometry is fixed; for all values of μ the metric takes the asymptotic form:

$$ds^2 = -\frac{r^2}{l^2}dt^2 + \frac{l^2}{r^2}dr^2 + \frac{r^2}{l^2}(dH^d)^2 \tag{4.33}$$

Thus, we can match the various spacetimes asymptotically by identifying points with the same t, r, and H^d coordinates in the region of large r.

Distance across the spacetime

First, we ask how the distance across the spacetime from one asymptotic region to the opposite one depends on μ. Of course, the distance is infinite, but its deviation from the $\mu = 0$ case of pure AdS is finite and well defined. To compute this, we can choose some cutoff distance R. Then the distance across the spacetime on the $t = 0$ slice (corresponding to the $\tau = 0$ slice in global coordinates) at the origin of the hyperbolic space is

$$2\int_{r_+}^{R} \frac{dr}{\sqrt{f(r)}}\,. \tag{4.34}$$

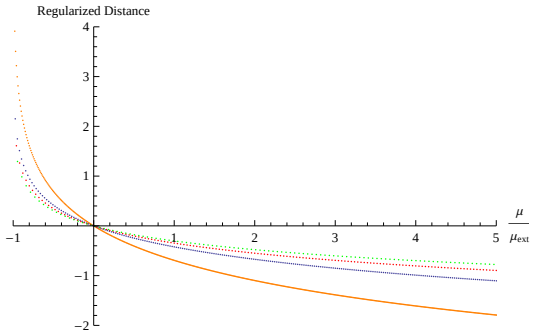

Figure 4.8: Numerical integration of regularized distance for d=1, 2, 3, 4 (orange, blue, red, green, respectively).

Subtracting off the result for $\mu = 0$ (with the same cutoff R) and taking the limit as $R \to \infty$ gives

$$L(\mu) - L(0) = 2\int_{r_+(\mu)}^{\infty} dr \left\{ \frac{1}{\sqrt{\frac{r^2}{l^2} - \frac{\mu}{r^{d-1}} - 1}} - \frac{1}{\sqrt{\frac{r^2}{l^2} - 1}} \right\} - 2\int_{l}^{r_+(\mu)} \left\{ \frac{dr}{\sqrt{\frac{r^2}{l^2} - 1}} \right\} \tag{4.35}$$

This is finite, since the integrand in the first integral behaves as $1/r^{d+1}$ for large r. For $d = 1$, we have explicitly that

$$\Delta L = -l \ln(1 + \mu). \tag{4.36}$$

Thus, the two sides of the spacetime get further apart as the entanglement between the corresponding degrees of freedom decreases. The same conclusion holds for other values of d as indicated by a numerical evaluation of equation (4.35) (see Figure 4.8). These results are consistent with the general expectations in [136].

Areas of minimal surfaces

We can similarly look at the areas (i.e. d-dimensional volumes) of minimal surfaces in the spacetime. We first consider the surface $r = r_+$ that divides the spacetime in half and forms the horizon of the hyperbolic black hole. The area of this is infinite, but we can look at the area per unit field theory volume as a function of μ. This is proportional to r_+^d, where r_+ is related to μ by $\mu = r_+^{d-1}(r^2/l^2 - 1)$ (monotonic for $\mu > \mu_{ext}$). Thus, the area of the surface separating the two halves of the space increases monotonically as we increase the entanglement (e.g. for $d = 1$, we get Area $\propto \sqrt{\mu + 1}$).

We can also look at the areas of other $t = 0$ spacelike surfaces that approach smaller spherical regions of the boundary. These extremize the action

$$A = \mathrm{Vol}(S^{d-1}) \int dr\, r^{d-1} \sinh^{d-1} u(r) \sqrt{\frac{1}{\frac{r^2}{l^2} - \frac{\mu}{r^{d-1}} - 1} + r^2 \left(\frac{du}{dr}\right)^2}\,. \tag{4.37}$$

For $d = 1$, the action simplifies to

$$L = \int dr \sqrt{\frac{l^2}{r^2 - l^2(1+\mu)} + r^2 \left(\frac{du}{dr}\right)^2}\,. \tag{4.38}$$

In this case, the path $u(r)$ must satisfy

$$\frac{d}{dr}\left\{ \frac{r^2 \frac{du}{dr}}{\sqrt{\frac{l^2}{r^2 - l^2(1+\mu)} + r^2 \left(\frac{du}{dr}\right)^2}} \right\} = 0 \tag{4.39}$$

Assuming $dr/du = 0$ at some $r = r_{min}$, we have

$$\frac{du}{dr} = \frac{1}{r} \frac{l}{\sqrt{r^2 - l^2(1+\mu)}} \frac{r_{min}}{\sqrt{r^2 - r_{min}^2}} \tag{4.40}$$

Setting the origin of hyperbolic space $u = 0$ at this r_{min}, we find that the asymptotic value of u (which we call u_0) as $r \to \infty$ is:

$$u_0 = \frac{\ln \frac{r_{min} + l\sqrt{1+\mu}}{r_{min} - l\sqrt{1+\mu}}}{2\sqrt{1+\mu}} \tag{4.41}$$

Inverting the relationship, we obtain:

$$r_{min} = l\sqrt{1+\mu}\, \coth\left(u_0 \sqrt{1+\mu}\right) \tag{4.42}$$

From expression (4.38), the length of such a curve in the region $r < R$ of spacetime is:

$$\begin{aligned} l(\mu, R) &= 2l \int_{r_{min}}^{R} \frac{dr}{\sqrt{r^2 - l^2(1+\mu)}} \frac{r}{\sqrt{r^2 - r_{min}^2}} \\ &= 2l \ln \frac{\sqrt{R^2 - r_{min}^2} + \sqrt{R^2 - l^2(1+\mu)}}{\sqrt{r_{min}^2 - l^2(1+\mu)}} \end{aligned} \tag{4.43}$$

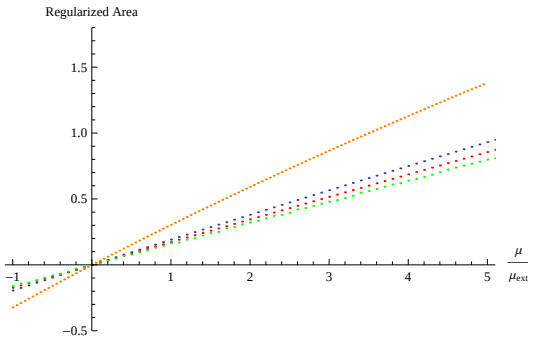

Figure 4.9: Numerical integration of regularized distance with $u_0 = 1$ for d=1, 2, 3, 4 (orange, blue, red, green, respectively).

We can again subtract off the value for $\mu = 0$ and take the limit as $R \to \infty$ to obtain the finite result:

$$l(\mu) - l(0) = 2l \ln \frac{\sinh(u_0\sqrt{1+\mu})}{\sinh(u_0)\sqrt{1+\mu}} \,. \tag{4.44}$$

We see that the area separating the two regions decreases as we lower the temperature (hence decreasing the entanglement entropy). The higher-dimensional versions can be tackled numerically, and we see that essentially the same pattern is repeated for all cases (Figure 4.9). These results, together with the distance across spacetime, provides a realization of the ideas in [136], that is, as entanglement entropy decreases, the two wedges of spacetime pinch off from each other.

4.5.3 CFT on S^d interpretation of the H^d states at different temperatures

At temperature $T = (2\pi R_H)^{-1}$, the state (4.28) maps back to the vacuum state of the S^d CFT, so the energy density is constant on the sphere (equal to the Casimir energy density). For other temperatures, the energy density is spatially constant and time-independent in the hyperbolic space picture, but not in the S^d description. In this section, we determine explicitly the stress-energy tensor on S^d for the state corresponding to (4.28) at an arbitrary temperature.

For the states corresponding to hyperbolic black holes at various temperatures, the stress-energy tensor in the dual CFT on hyperbolic space with metric

$$ds^2 = -dT^2 + R^2(du^2 + \sinh^2 u \, d\Omega_{d-1}^2) \tag{4.45}$$

is given by [41]

$$\langle T^{\mu}{}_{\nu}\rangle = \frac{1}{16\pi G l}\left(\epsilon_d + \frac{\mu}{l^{d-1}}\right)\,\mathrm{diag}(-d,1,\ldots,1), \tag{4.46}$$

where

$$\epsilon_d = \frac{2(d!!)^2}{(d+1)!d} \tag{4.47}$$

for odd d and zero for even d. For these states, we can map back to states of the CFT on S^d. In this case, we have the metric on the region D is conformally related to the hyperbolic space metric:

$$g^{sphere}_{\mu\nu} = e^{2\phi} g^{hyp}_{\mu\nu} \tag{4.48}$$

Hence, we conclude that [22]

$$(\langle T_{sphere}{}^{\alpha}{}_{\beta}\rangle_{\mu} - \langle T_{sphere}{}^{\alpha}{}_{\beta}\rangle_{\mu=0}) = e^{-(d+1)\phi}(\langle T_{hyp}{}^{\alpha}{}_{\beta}\rangle_{\mu} - \langle T_{hyp}{}^{\alpha}{}_{\beta}\rangle_{\mu=0})\,, \tag{4.49}$$

where the $\mu = 0$ state corresponds to the vacuum of the field theory on the sphere.

Starting from the metric (4.45) for hyperbolic space times time, the change of coordinates

$$\tan(\tau/R) = \frac{\sinh(T/R)}{\cosh u} \tag{4.50}$$

$$\tan\theta = \frac{\sinh u}{\cosh(T/R)} \tag{4.51}$$

gives

$$ds^2 = e^{2\phi}\big(-d\tau^2 + R^2(d\theta^2 + \sin^2\theta\, d\Omega^2_{d-1})\big) \tag{4.52}$$

with

$$e^{2\phi} = \frac{\cos^2(\tau/R) + \sin^2\theta}{\cos^2(\tau/R) - \sin^2\theta}\,. \tag{4.53}$$

In these coordinates, the stress tensor is

$$\langle T^{\mu}{}_{\nu}\rangle = \frac{1}{16\pi G l}\left(\epsilon_d + \frac{\mu}{l^{d-1}}\right)\big(\mathrm{diag}(1,1,\ldots,1) - (d+1)\,\mathbf{M}\big)\,, \tag{4.54}$$

where

$$\mathbf{M} = \begin{pmatrix} \frac{1}{1-\tan^2\theta\,\tan^2(\tau/R)} & \frac{\sin\theta\,\sin(\tau/R)\cos\theta\,\cos(\tau/R)}{1-\sin^2\theta-\sin^2(\tau/R)} & \\ -\frac{\sin\theta\,\sin(\tau/R)\cos\theta\,\cos(\tau/R)}{1-\sin^2\theta-\sin^2(\tau/R)} & \frac{1}{1-\cot^2\theta\,\cot^2(\tau/R)} & \\ & & \mathbf{0} \end{pmatrix} \tag{4.55}$$

Using (4.49), we find that the stress tensor for the corresponding state of the CFT on the domain of dependence of the half-sphere (i.e. the region D) with metric

$$ds^2 = -d\tau^2 + R^2\big(d\theta^2 + \sin^2\theta\, d\Omega_{d-1}^2\big) \tag{4.56}$$

is

$$\langle T_{sphere}{}^{\alpha}{}_{\beta}(\mu)\rangle - \langle T_{sphere}{}^{\alpha}{}_{\beta}\rangle_{vac} = \frac{\mu}{16\pi G l^d}\left(\frac{\cos^2(\tau/R)+\sin^2\theta}{\cos^2(\tau/R)-\sin^2\theta}\right)^{(d+1)/2}\big(\mathbf{1}-(d+1)\mathbf{M}\big)\,. \tag{4.57}$$

As an example, the energy density (minus the Casimir energy) is given by

$$T^{00} - T^{00}_{vac} = \frac{\mu}{16\pi G l^d}\left(\frac{\cos^2(\tau/R)+\sin^2\theta}{\cos^2(\tau/R)-\sin^2\theta}\right)^{(d+1)/2}\left(\frac{d+1}{1-\tan^2\theta\,\tan^2(\tau/R)}-1\right) \tag{4.58}$$

This diverges on the lightlike boundary of the causal development region of the half-sphere, $\tau/R = \pm(\pi/2-\theta)$. At $\tau = 0$ the energy density

$$T^{00} - T^{00}_{vac} = \frac{d\mu}{16\pi G l^d}\left(\frac{1+\sin^2\theta}{1-\sin^2\theta}\right)^{(d+1)/2} \tag{4.59}$$

diverges at the equator $\theta = \pi/2$ and this singularity propagates forward and backward in time along the light sheets. We note also that for $\mu < 0$ the $\tau = 0$ energy density is negative away from the equator.[62] However, since the total energy on the sphere must be higher than for the vacuum state of the CFT, there must be a singular positive contribution to the energy density at the equator such that the total energy on the sphere (relative to the vacuum energy) is positive.

While we have focused in this section on some CFT with a gravity dual, the stress-energy tensor for an arbitrary conformal field theory at finite temperature on $H^d \times R$ is determined by homogeneity and conformal invariance (tracelessness) to be

$$\langle T^{\mu}{}_{\nu}\rangle = f(2\pi R_H T)\,\mathrm{diag}(-d, 1, \ldots, 1), \tag{4.60}$$

[62] The negative energy density here is a well-known possibility, which illustrates how the weak and null energy conditions may be violated. The negative energy should be thought of as a Casimir-type vacuum energy. Certain inequalities restrict the extent of such negative energy densities. They can be used to prove averaged versions of the energy conditions in certain situations (see e.g. [45]).

proportional to (4.46) that was our starting point. Thus, the result (4.57) holds in general, with the replacement

$$\frac{\mu}{16\pi G l^d} \to f(2\pi R_H T) - f(1) \ . \tag{4.61}$$

In particular, except for the special temperature $T = (2\pi R_H)^{-1}$ that corresponds to the vacuum state on S^d, the stress energy tensor is singular at the boundary of the domain of dependence of the half-sphere.

4.6 Comments on generalization to cosmological spacetimes

In the introduction, we recalled various qualitative similarities between Rindler patches of AdS and patches accessible to observers in cosmological spacetimes. Based on these similarities, it seems plausible that the description of physics inside a cosmological horizon should be in terms of a density matrix for some degrees of freedom. However, both the details of the patch geometry and the local spacetime dynamics are different in cosmological examples. In this section, we offer a few comments on how the holographic description might be modified in going from the case of accelerated observers in AdS to the case of observers in cosmological spacetimes[63].

A characteristic feature of asymptotically AdS spacetimes not present in the cosmological examples is the AdS boundary. The patches accessible to an observer in de Sitter space or other homogeneous spacetimes with accelerated expansion are bounded by the cosmological horizon and have finite spatial volume. In the AdS case, all the patches we have described have infinite spatial volume since they include a boundary region. We know that the boundary region is tied to the UV degrees of freedom in the field theory. Thus, we might guess that patches of AdS without the boundary region are described by a reduced density matrix for a subset of field theory degrees of freedom that excludes the UV degrees of freedom; such density matrices have been considered recently in [15]. For a CFT on S^d, excluding the UV degrees of freedom (e.g. spherical harmonic modes of the fields with angular momenta above a certain cutoff) leaves us with a finite number of degrees of freedom, those of a large N matrix model with a finite number of matrices. Thus, a description for finite volume patches might be via mixed states for a large N matrix model, where these matrix model degrees of freedom are entangled with (and perhaps interacting with) other degrees of freedom

[63] For some other approaches to this question, see [6, 16, 48, 51, 128].

associated with the rest of the spacetime.[64] A very similar conclusion was reached by Susskind in [130] for independent reasons.

At a more detailed level, in order to describe local bulk physics characteristic of a spacetime with positive, rather than negative cosmological constant, we should expect that the Hamiltonian associated with time evolution in some patch should be different from one describing patches of AdS. Short of providing a specific suggestion here, we only observe that for a particular geodesic trajectory in AdS, flat, and de Sitter space, other geodesic trajectories respectively accelerate towards, move away at constant velocity, or accelerate away from this trajectory. In the context of matrix models, these behaviors can be put in "by hand" at the classical level by choosing positive, zero, or negative mass-squared terms for bosonic degrees of freedom. Thus, a completely speculative suggestion would be that the type of matrix model whose mixed states would describe physics in a patch of a spacetime with accelerated expansion might involve negative mass squared terms for the bosonic matrices.[65] We caution, however, that quantum effects typically dominate the effective potential in a matrix model; only for very special theories, typically with significant cancellations in the effective potential due to supersymmetry, do we expect any kind of dual spacetime picture to emerge. For an alternate (and more in-depth) discussion on how to modify CFT physics in order to describe de Sitter or FRW (rather than AdS) dynamics, see [38, 39].

[64] We are not suggesting that arbitrarily small or localized patches of spacetime can be associated with some particular degrees of freedom, only that certain patches may be associated with certain mixed states of a model with a finite number of degrees of freedom.

[65] A slightly more concrete motivation of this suggestion is as follows. Starting from the $\mathcal{N} = 4$ SYM theory on S^3, a particular way to truncate to the IR degrees of freedom is to keep only the lowest spherical harmonic modes. This can be done in a way that preserves maximal supersymmetry, and the result is the Plane Wave Matrix Model, which has positive mass for all bosonic degrees of freedom. The density matrix for this model that arises starting from the vacuum of $\mathcal{N} = 4$ SYM and tracing out the rest of the degrees of freedom should describe a patch of pure AdS. For flat spacetime, the most concrete proposals for dual descriptions involve limits of models for which the bosonic potential has many flat directions (e.g. the BFSS matrix model). It is from these flat directions (preserved at the quantum level) that the asymptotic flatness of the dual spacetime is supposed to emerge. Thus, our naive suggestion is realized in specific models for the AdS and flat cases.

Part II

Applications of AdS/CFT

Chapter 5

Holographic Fluids and Metric Perturbations

5.1 Introduction

In the AdS / CFT correspondence the energy momentum tensor of the boundary field theory corresponds to the metric tensor of the bulk theory. In practise, this means that the expectation value of the field theory energy momentum tensor is given by the fall off of the bulk metric field; equivalently, $\langle T_{\mu\nu} \rangle$, together with the boundary metric, comprise a full set of boundary conditions for the bulk metric field.

Since the metric field is closely connected to the boundary stress tensor, we immediately wonder about what sorts of metrics are dual to certain generic types of stress tensors. Furthermore, we should expect that by constraining the types of field theories we want to consider e.g.:, by restricting to those that are solutions of some arbitrary set of equations, we would be left with a much smaller set of bulk duals. In particular, we can consider a minimalistic approach and impose only the conservation equations $T^{\mu}{}_{\mu} = 0$ and $\partial_{\mu} T^{\mu\nu} = 0$ on the boundary theory and investigate what sorts of constraints will arise on the bulk geometry. This has been a topic of intense study in the past few years and many results exist. Notably, it is known that the gravity dual of a field theory with an energy momentum tensor that obeys the hydrodynamics equations and has well defined temperature and velocity fields must be non pathological: however, if any of these conditions is relaxed, it is not known what should be expected.

In this chapter we will use the gauge / gravity duality and fluid / gravity correspondence to look in detail at how small perturbations of the boundary field theory stress tensor are reflected in the bulk metric. To accomplish this we will add small perturbations to a well known black brane solution dual to a relativistic fluid at finite temperature. These metrics perturbations will naturally generate corrections to the boundary energy momentum tensor which, in turn, will be constrained by the conservation equations. Therefore,

the perturbations considered will be constrained to those that render the boundary stress tensor traceless and divergenceless to first order. Once the most general perturbation of this kind is written we will see how to use Einstein's Equations to first order in the perturbation parameter to find both analytical and numerical metric corrections.

5.2 Fluid / gravity correspondence

The above mentioned perturbative approach, when applied to perturbations in the long wavelength limit, leads to the well known fluid / gravity correspondence. Certain gravity solutions known as black branes can be generalized to describe the behaviour of plasmas for which both temperature and velocity fields are a function of space-time coordinates. These generalized black branes are not solutions of Einstein's equations, but can be corrected in a perturbative fashion, order by order, such that the corrected metric does, indeed solve Eintein's equations up to the desired order [21, 134].

What distinguishes these fluid / gravity correspondence models from a completely generic perturbation is the long wavelength approximation, in such limit the conservation equations lead directly to the well known relativistic hydrodynamic equations, including higher derivatives corrections. Equivalently, the energy momentum tensor of the dual field theory [14] is precisely that of a relativistic, conformal fluid with temperature T and proper velocity u^μ, with the higher derivative corrections introducing less than perfect characteristic such as viscosity, compressibility and so on [126]. It is, therefore, qualitatively written as

$$T^{\mu\nu} \propto T^d \left(\eta^{\mu\nu} + (d-1)u^\mu u^\nu\right) + \mathcal{O}\left(\partial u\right).$$

Before we can move to a broader discussion, in the remainder of this section we will see the fluid / correspondence in more detail.

5.2.1 Long wavelength limit

Often, under the right conditions, the macroscopic behaviour of a many particle system is remarkably different than its microscopic behaviour. While the true number of degrees of freedom thermodynamical systems have is usually of order 10^{23} or larger, the macroscopic system may be described by a handful of physical quantities. Although we do not fully understand the transition between the IR and UV behaviour, we know certain conditions

the systems must obey in order for such a macroscopic description to be available.

Clearly, if a system of many particles changes too fast (say, the average kinetic energy of particles within a certain finite region) it may be hard, or even impossible to assign a meaningful macroscopic physical quantity (in the current example, temperature) that characterizes the whole system or (macroscopic) parts of it. Therefore, it is natural to expect that, while variations of the tentative macroscopic quantities are allowed, these should be characterized by a length scale large enough so that the quantity can still be well defined, in other words, they should vary slowly. The precise meaning of slowly varying is dependent on the system in question, below we discuss an appropriate definition for our current problem.

In the case of fluids, our intuition tell us that not only temperature, but also the fluid's velocity, are the basic quantities necessary to macroscopically describe its behaviour. Again, both temperature and velocities are allowed to change, in other words, we expect them to be functions of both position and time, nevertheless, in order to properly define these two quantities we will require that they are slowly varying. Formally speaking, we can only employ the fluid approximation for a system in which the scale at which the temperature varies is small compared to the temperature it self, and similarly for the velocity field, i.e.:

$$\frac{\partial T}{T} \ll 1, \quad \text{and} \quad \frac{\partial u}{u} \ll 1, \tag{5.1}$$

equivalently, if L is the typical length at which the temperature is varying, than we must impose $LT \gg 1$.

For any many-particle system for which temperature and velocity fields can be defined (obeying the above conditions), we can make use of the fluid approximation to describe it. This is not only true for relativistic field theories, but, as we will see, can also be used to study holographic field theories and boosted black branes [21, 134].

5.2.2 The Fefferman-Graham expansion

From the AdS/CFT dictionary we know that the bulk metric field is connected to the energy momentum tensor of the boundary theory. More precisely, the expectation value of the boundary field theory energy momentum tensor is given by a particular term of the fall off of the bulk metric. At this point we can wonder about whether this is finite or physically meaningful at all, since the energy momentum tensor is a notoriously problematic quantity

in conventional field theory. In the context of AdS/CFT, the procedure of calculating it [14] includes a normalization step[66] usually taking the empty AdS space as the zero value for the field theory stress tensor and computing the difference.

Quantitatively, the relation between bulk metric and boundary energy momentum tensor is made evident when the bulk metric is written in the Fefferman-Graham gauge,

$$ds^2 = \frac{l^2}{z^2}\left(dz^2 + g_{\mu\nu}(x,z)dx^\mu dx^\nu\right), \tag{5.2}$$

where l is the AdS radius and the AdS boundary is at $z = 0$. When written in this form, we can expand the metric $g_{\mu\nu}$ in series around $z = 0$,

$$g(x,z) = g_{(0)}(x) + z^2 g_{(2)}(x) + \cdots + z^d g_{(d)}(x) + h_{(d)}(x) z^d \log z^2 + \mathcal{O}\left(z^d + 1\right), \tag{5.3}$$

and immediately read off the boundary field theory's energy momentum tensor from the z^d coefficient [34]

$$\langle T_{\mu\nu}\rangle = \frac{d}{16\pi G_N} g_{(d)\mu\nu} + X_{\mu\nu}[g_n], \tag{5.4}$$

where $X_{\mu\nu}[g_n]$ is related to the conformal anomalies of the boundary CFT. In what follows we will restrict our discussions to a four dimensional bulk gravity theory (1 + 2d boundary CFT), for which the term $X_{\mu\nu}[g_n]$ is zero.

5.2.3 Fluid / gravity correspondence

Since its first appearance [21] the fluid / gravity correspondence has come a long way, and not only our understanding of it has increased dramatically, but also the number of examples and models multiplied considerably. In its original form, this correspondence was a parallel between generalized boosted black branes subjected to small corrections and field theories with fluid-like energy momentum tensors with higher derivative corrections.

From the AdS/CFT dictionary we know that black branes (black holes with a flat horizon) in four dimensional anti de Sitter space with metric

$$ds^2 = 2dvdr - r^2 f(br)dv^2 + r^2 d\vec{x}^2, \tag{5.5}$$

where

$$f(r) = 1 - \frac{1}{r^3}, \quad b = \frac{3}{4\pi T},$$

[66] Equivalently, the addition of a counter term to the gravity action.

with T the temperature of the black brane and $v = t + \int \frac{dr}{r^2 f(r)}$ a ingoing null coordinate, are dual to a strongly coupled plasma at finite temperature T. This metric can be generalized by a Lorentz transformation and still remain a solution of Einstein's equations. Written again in Eddington-Finkelstein coordinates, the boosted black brane metric with proper velocity

$$u^0 = \frac{1}{\sqrt{1-\vec{\beta}^2}}, \quad u^i = \frac{\beta^i}{\sqrt{1-\vec{\beta}^2}} \tag{5.6}$$

is

$$ds^2 = -2u_\mu dx^\mu dr - r^2 f(br)\, u_\mu u_\nu dx^\mu dx^\nu + r^2 P_{\mu\nu} dx^\mu dx^\nu, \tag{5.7}$$

where $P_{\mu\nu} = \eta_{\mu\nu} + u_\mu u_\nu$ is the projection operator to directions orthogonal to u_μ.

The above metric can be further generalized to a position dependent version ($u_\mu \to u_\mu(x)$, and $T \to T(x)$ in equation 5.7) that, while not an exact solution of Einstein's equations, can be corrected in such a way to become a solution up to a certain perturbation other (again, in the long wave length limit). Schematically we have

$$g^{(0)}(x) \to g^{(0)}(x) + \epsilon g^{(1)}(x) + \epsilon^2 g^{(2)}(x) + \cdots,$$

such that

$$EE(g^{(0)}) = 0 + \mathcal{O}(\epsilon), \tag{5.8}$$

$$EE(g^{(0)} + \epsilon g^{(1)}) = 0 + \mathcal{O}\left(\epsilon^2\right), \tag{5.9}$$

$$\cdots$$

where $g^{(0)}(x)$ is the position dependent version of 5.7, $g^{(i)}$ is the most general covariant correction that can be added to the ansatz 5.7 that obeys the symmetries of the problem and EE stands for Einstein's equations applied to the metric in question.

When imposed on these generalized black brane solutions, the conservation equations lead precisely to the hydrodynamic equations for the boundary theory together with higher derivative corrections. With AdS/CFT techniques [14] the energy momentum tensor for the boundary theory can be found to be

$$T^{\mu\nu} = \frac{1}{2}\left(\frac{4\pi T}{3}\right)^3 (\eta^{\mu\nu} + 3u^\mu u^\nu) + \mathcal{O}(\partial u), \tag{5.10}$$

which is precisely what we would expect for a relativistic perfect fluid with higher derivatives corrections.

5.3 Conservation equations and the stress energy tensor

We can try to generalize the discussion above and go beyond the long wavelength limit. We saw how under the right assumptions the conservation equations led directly to the relativistic hydrodynamics equations. Nevertheless, we expect any physical system to obey such general physical laws, so it is interesting to ask what sort of general behaviours about a system can we infer by imposing the conservation equations only.

The above question is even more interesting in the context of holographic field theories since it immediately extends to a gravitational systems as well. Therefore, we should expect that by investigating this question we can also gain knowledge of a gravitational system reacts to small perturbations and how the metric fall off must behave if this system is to obey the conservation equations.

5.3.1 A simple example

We wish to study the metric dual to the most general boundary stress tensor and, in particular, what conditions guarantee its regularity and what kind of information from each side can we extract if we know either the energy momentum tensor of the boundary dual theory, or the bulk metric.

Since the boundary stress tensor is determined by the fall off of the bulk metric, we should be able to infer information about the bulk metric from the kind of boundary energy momentum tensor it induces; conversely, we should also be able to predict certain characteristics of the dual field theory energy momentum tensor by looking at the bulk metric.

To illustrate this discussion let us consider a simple example of a field theory in $(1+2)$ dimensions with a constant and diagonal — regularized — energy momentum tensor

$$T_{\mu\nu} = \begin{pmatrix} a+b & 0 & 0 \\ 0 & a & 0 \\ 0 & 0 & b \end{pmatrix}, \tag{5.11}$$

with a and b constants. When $b = a$ this is simply a stationary relativistic fluid at finite temperature dual to a black brane with metric given by equation 5.5 and temperature

$$T = \frac{3}{4\pi} (2a)^{\frac{1}{3}} .$$

The conservation equations imposed on this boundary stress tensor lead trivially to

$$T^{\mu}{}_{\mu} = 0, \quad \text{and} \quad \nabla_{\mu} T^{\mu}{}_{\nu} = 0. \tag{5.12}$$

Therefore, as far as the conservation equations go, the theory in question is perfectly acceptable, however, its holographic dual says otherwise. In order to see this we must first find the appropriate dual metric that has the correct asymptotic fall off. Given the simple nature of this particular ansatz we are able to find a fully non linear solution which not only tell us the whole story but also servers as a bench mark for perturbations around similar metrics.

By writing down a generic metric in the GF form and using the symmetries of the problem to simplify the ansatz, we are able to find that the metric dual to a CFT with equation (5.11) as stress tensor is given by

$$ds^2 = \frac{1}{z^2}(dz^2 - A(z)B(z)^{-a-b}dt^2 + A(z)B(z)^a dx^2 + A(z)B(z)^b dy^2), \tag{5.13}$$

with

$$A(z) = \left(1 - \frac{a^2+ab+b^2}{48} z^6\right)^{\frac{2}{3}}, \tag{5.14}$$

and

$$B(z) = \left(\frac{1 + \sqrt{\frac{a^2+ab+b^2}{48}} z^3}{1 - \sqrt{\frac{a^2+ab+b^2}{48}} z^3}\right)^{\frac{2}{3}\sqrt{\frac{3}{a^2+ab+b^2}}}. \tag{5.15}$$

Notice that this metric has a horizon at $z = \left(\frac{48}{a^2+ab+b^2}\right)^{\frac{1}{6}}$.

When $a = b$ this horizon is regular and the metric is smooth across it, in particular, the square of the Riemann tensor, $R^a{}_{bcd}$, is finite at the horizon. However, if $a \neq b$ this is no longer the case, the horizon is now singular, not only the metric components become pathological, but also the square of the Riemman tensor diverges at the former horizon surface[67]; in other words, the bulk metric has a naked singularity at $z = \left(\frac{48}{a^2+ab+b^2}\right)^{\frac{1}{6}}$ for a constant, diagonal and anisotropic $T_{\mu\nu}$, despite it being a solution of the hydrodynamics equations.

This result indicates that the conservation equations alone can not be the whole story when searching for CFT states with well behaved gravity duals

[67] The full expression for the square of the Riemann tensor, while perfectly calculable, is far too long and adds little to the present discussion. Below we will return to this problem in a perturbative fashion which is enough to illustrate the divergence of $(R^a{}_{bcd})^2$.

(even in the case of energy momentum tensors as simple as the one above); it is clear from this example that they fail to exclude the existence of naked singularities. In addition we also see that highly non trivial information about the geometry is encoded in the boundary CFT state. It is known that relativistic fluids with a definite four velocity and temperature are dual to non pathological space times — black branes — however we were able to show how these conditions can not be relaxed too indiscriminately.

Since the ultimate goal should be to analyze more generic types of boundary stress tensors, which can only be done perturbativelly, it is interesting to study the above result in the perturbative regime as well, in this way we are able to identify what sorts of phenomena are available at first, second, or higher orders in the perturbation parameter. This is easily done just by setting $b = a + \epsilon$, where ϵ is a small parameter.

By expanding the metric components is powers of ϵ we find

$$A(z)B(z)^a = A(z)B(z)^a|_{\epsilon=0} + \epsilon F_x(z) + O\left(\epsilon^2\right), \tag{5.16}$$

where

$$F_x(z) = \frac{\left(az^3-4\right)\left(\frac{4}{4-az^3}-\frac{1}{2}\right)^{2/3}\left(\left(az^3+4\right)\log\left(\frac{8}{4-az^3}-1\right)-2az^3\right)}{12a\sqrt[3]{16-a^2z^6}},$$

and

$$A(z)B(z)^b = A(z)B(z)^a|_{\epsilon=0} - \epsilon F_y(z) + O\left(\epsilon^2\right), \tag{5.17}$$

where

$$F_y(z) = \frac{\left(az^3-4\right)\left(\frac{4}{4-az^3}-\frac{1}{2}\right)^{2/3}\left(\left(az^3+4\right)\log\left(\frac{8}{4-az^3}-1\right)+2az^3\right)}{12a\sqrt[3]{16-a^2z^6}},$$

which clearly showcases hints of pathological behaviour already at first order. The expansion of the square of Riemann tensor, however, gives

$$\begin{aligned} R^a{}_{bcd}R_a{}^{bcd} \quad = \quad & \frac{24\left(a^4z^{12}+16a^3z^9+224a^2z^6+256az^3+256\right)}{\left(az^3+4\right)^4} - \\ & \frac{3072\left(az^6\left(az^3-4\right)\right)}{\left(az^3+4\right)^5}\epsilon + \frac{2048z^6}{\left(az^3-4\right)^4\left(az^3+4\right)^6}F_R(z)\epsilon^2 \\ & +\mathcal{O}\left(\epsilon^3\right), \end{aligned} \tag{5.18}$$

where

$$F_R(z) = a^6z^{18} - 16a^5z^{15} + 320a^4z^{12} - 960a^3z^9 + 4480a^2z^6 - 2048\left(az^3-1\right),$$

from which we can conclude that the curvature divergence at the horizon can only be seen at second or higher orders in the perturbation expansion, which indicates that while a second order analysis is necessary to better characterize the geometry of space time, many of its aspects can be inferred from first order only.

5.3.2 Generalization

Now that we understand better the simplest case of a energy momentum tensor that solves hydrodynamics equations and has a non well behaved dual, we could in principle try to generalize it. Ideally we would like to study a completely generic perturbation around the black brane geometry

$$g_{\mu\nu}(z,x) = g^{BB}_{\mu\nu}(z,x) + \epsilon h_{\mu\nu}(z,x). \tag{5.19}$$

Such perturbation is naturally connected to a deformation of the boundary stress tensor

$$T_{\mu\nu} = T^{BB}_{\mu\nu} + \epsilon \delta T_{\mu\nu}. \tag{5.20}$$

To quantitatively address the above equations we can solve Einstein's Equation perturbatively using (5.19) as our ansatz while imposing (5.20) (together with the conservation equations) as a boundary condition on the solutions.

With a solution in hand we can look at the behaviour of the metric function $h_{\mu\nu}(z,x)$ near the horizon and compare it to the exact case discussed above, this would allow us to determine whether a particular boundary stress tensor leads to a bulk naked singularity, the blow up or vanishing of metric components, and etc.

In practice, the procedure outlined above cannot be applied to a completely generic situation. What we could do, however, is focus on certain simpler ansatz, such as $\mathrm{e}^{ikx} h_{\mu\nu}(z)$ and try to determine conditions for well behaved bulk geometries dual to these configurations. Many different approaches could be used to explore this question further, and a thorough analysis of this ansatz will be left for future work.

5.4 Discussion

In this chapter we discussed how to use the gauge / gravity duality and fluid / gravity correspondence to look in detail at how small perturbations of the boundary field theory stress energy tensor are reflected on the bulk metric.

When the perturbations are in the long wavelength limit we know from the literature that the conservation equations lead to the well known relativistic hydrodynamics equations, and the energy momentum tensor of the field theory is that of a relativistic conformal fluid with higher order corrections.

However, we were interested in knowing how far we could go if the long wavelength limit was given up. In other words, what sort of information and constraints on both the field theory as well as the gravity bulk arise from imposing the conservation equations on a generic space-time or field theory with a given generic energy momentum tensor.

What we saw was that, even for a very simple example, some interesting, non trivial, behaviours could arise. In particular, we looked in detail at a field theory with a constant and traceless energy momentum tensor (equation (5.11)). For this system we were able to find an exact solution for the bulk metric (equation (5.13)) that asymptotes to the desired stress energy tensor, this allowed us to explore this example closely and investigate how the relation between the constants a and b was reflected on the bulk geometry.

What we saw was that when $a \neq b$, even perturbatively, the bulk geometry was plagued with a naked singularity. When considering $a = b + \epsilon$, with $\epsilon \ll 1$ we saw that the naked singularity only made itself evident at second order in ϵ (when the Riemann tensor divergence appeared), despite the metric tensor itself showcasing signs of pathological behaviour already at first order.

We finished by glancing over how the simple case considered could be generalized. Unfortunately fully generalizing this approach is not viable, however some special cases may be within reach of numerical methods. From our discussion above we believe that in the case of a perturbative analysis, looking at the metric components at first order may provide strong evidence for the existence or not, of space-time pathologies.

Chapter 6

Density versus Chemical Potential in Holographic Field Theories

6.1 Introduction

The AdS/CFT correspondence [53, 92, 140], which conjectures the equivalence of a gravity theory in $d+1$ dimensions and a gauge theory in d dimensions, has become a valuable tool for the study of strongly coupled field theories. Using the correspondence, many questions about quantum field theories may be phrased in the context of a gravity theory; in the limit of strong coupling, certain previously intractable field theory calculations are mapped to relatively simple classical gravity computations.

Holography and finite density

One difficult regime of strongly coupled field theory that gauge / gravity duality is particularly suited to study is that of finite charge density. Here, lattice techniques fail due to the 'sign problem': at finite chemical potential, the Euclidean action becomes complex which results in a highly oscillatory path integral. We can avoid this difficulty by mapping the problem to a gravity dual using the AdS/CFT dictionary. According to the dictionary, in order to have a global $U(1)$ symmetry in the field theory, one needs to include a $U(1)$ gauge field in the gravity bulk. The charge density and chemical potential are encoded in the asymptotic behaviour of the gauge field. At strong coupling in the field theory, the bulk theory is well described by classical gravity, and one may solve the classical equations of motion on the gravity side to study the field theory at finite density.

Given this relatively simple access to finite density configurations, we might hope that some physically realistic strongly interacting systems may be approximately described by a holographic dual. In this case, qualitative features of the holographic theory would carry over to the exact theory. It

would be useful to characterize the types of finite density field theories that have a dual formulation and admit this type of study.

In this chapter, we seek to answer this question from the perspective of the holographic theory. Specializing to holographic probes, in which fields are considered as small fluctuations on fixed gravitational backgrounds, we study systems with the minimal structure of a conserved charge and find the $\rho - \mu$ relations that are possible in the field theory duals. We attack this problem by first deriving constraints on the relationship based on general grounds before studying several specific examples of holographic field theories.

Summary of results

In our study, we observe that, at large densities, the field theory dual to a substantial class of gravity models can be described by a power law relation of the form[68]

$$\rho = c\mu^{\alpha}. \tag{6.1}$$

Firstly, we look to understand the constraints on the the $\rho - \mu$ relationship from the point of view of the field theory, using local stability and causality. Usually, results here depend on the particular form of the free energy. In all cases with $\rho - \mu$ behaviour (6.1), local thermodynamic stability places the condition $\alpha > 0$ on the exponent. In general, for a theory at low temperature, we may write the particular free energy expansion $f \propto -\mu^{\alpha+1} - a\mu^{\beta}T^{\gamma}$, with $\gamma > 0$ and $a > 0$, with corresponding charge density $\rho \propto (\alpha+1)\mu^{\alpha} + a\beta\mu^{\beta-1}T^{\gamma}$. Combined, local stability and causality demand that $\alpha \geq 1$ and $\gamma > 1$.

Next, we consider Born-Infeld and Maxwell actions for the gauge field in a generic background. Under mild assumptions, in both cases, the power α is constrained. For the Born-Infeld action, the condition

$$\alpha > 1 \qquad \text{(Born-Infeld action)} \tag{6.2}$$

arises,[69] while, for the Maxwell action, the power law coefficient is fixed to

$$\alpha = 1. \qquad \text{(Maxwell action)} \tag{6.3}$$

[68] Here and throughout, α refers to the power in this form of $\rho - \mu$ relationship.

[69] Naively, we could construct systems for which $\alpha \leq 1$, however, in these situations, the contribution of the constant charge density to the total energy diverges, consequently we can not say that there is a power law relation. This divergence signals a breakdown of the probe approximation rendering these systems outside the scope of this chapter. Notice that $\alpha > 1$ is consistent with the bound derived from stability and causality.

Interestingly, these conditions are in agreement with those derived from field theory considerations, giving rise to the same range of possible values of α. In summary, all power law relationships consistent with stability and causality can be realized in simple probe gauge field setups by varying the background metric.

To see which values of α arise for backgrounds corresponding to specific models, we explore a variety of $3+1$ Poincaré-invariant holographic field theories dual to Dp-Dq brane systems and 'bottom-up' models with gauge and scalar fields. The former have been used, for example, in studies of holographic systems with fundamental matter [86, 95, 105, 120, 138], producing many features of QCD, including confinement,[70] chiral symmetry breaking, and thermal phase transitions [2, 13, 20, 87]. Bottom-up, phenomenological models have been studied in various model-building applications including superconductors[71] [58–60, 64, 66, 67] and superfluids [10, 18, 62].

In the Dp-Dq systems, table 6.1, a variety of powers α in the range $1 < \alpha \leq 3$ are realized, respecting the $\alpha > 1$ constraint. Note that these results only involve the Born-Infeld action and neglect couplings of the brane to other background spacetime fields.

	Probe brane								
	$d=4$						$d=5$		
Background branes	D9	D8	D7	D6	D5	D4	D8	D7	D6
D3	3		3		3				
D4		5/2		2		3/2	3		5/2
D5			2					2	
D6				3/2					

Table 6.1: The power α in the relationship $\rho \propto \mu^\alpha$ at large ρ for $3+1$ dimensional field theories dual to the given brane background with the indicated probe brane, with $d-1$ shared spacelike directions. For $d=5$ the theory is considered to have a small periodic spacelike direction while for background Dp branes with $p > 3$, the background is compactified to $3+1$ dimensions.

In the phenomenological probe models, table 6.2, in all cases except one (the probe gauge field in the black hole background), the dominant power

[70] It was recently pointed out that the usual identification of the black D4 brane as the strong coupling continuation of the deconfined phase in the field theory is not valid [94].

[71] A top-down realization of a gauge / gravity superconductor has been found in [7].

α is determined by conformal invariance, since we consider asymptotically AdS backgrounds.[72] Since μ and T are the only dimensionful parameters, the density must take the form $\rho = \mu^{d-1}h(T/\mu)$, where the underlying space has d spacetime dimensions. At large μ and fixed T, we can expand h to see that μ^{d-1} dominates the $\rho - \mu$ relationship. In systems with one small periodic spacelike direction, the dominant power α is larger than the corresponding theory without a periodic direction since, at large densities, on the scale of the distance between charges, the theory is effectively higher dimensional.[73] Our study of bottom-up models also includes an analysis of the gravity models in the full backreacted regime. As seen in table 6.2, the power law α in these cases is also determined by the same conformal invariance argument.

In these bottom-up models we are more interested in the detailed behaviour at intermediate values of μ. It is found that, in general, when the scalar field condenses in the bulk, the corresponding field theory is in a denser state than that without the scalar field. As well, the field theory dual to the gauge field and scalar field in the soliton background is in a denser state than that dual to the same fields in the black hole background. In the systems with a scalar field, at large μ, the $\rho-\mu$ relationship is well fit by the form $\rho = c(q, m^2)\mu^\alpha$,[74] where q and m^2 are the charge and mass-squared of the scalar field. While the power α is fixed by the conformal invariance, we find that the scaling coefficient $c(q, m^2)$ increases with increasing q or decreasing m^2.

[72] Different power laws can arise for holographic theories on different backgrounds, such as Lifshitz spacetimes. However, these will not be considered here.

[73] The phase transition that holographic theories with a periodic direction undergo as the density increases was studied in [81].

[74] In the probe cases we can scale q to 1, leaving $c = c(m^2)$.

Regime	Background	Fields	$d=4$	$d=5$
probe	black hole	ϕ	1	1
		ϕ, ψ	3	4
	soliton	ϕ, ψ		4
backreacted	black hole	ϕ	3	4
		ϕ, ψ	3	4
	soliton	ϕ, ψ		4

Table 6.2: The power α in the relationship $\rho \propto \mu^\alpha$ at large ρ for $3+1$ dimensional field theories dual to the given gravitational background with the stated fields considered in either the probe or backreacted limits. ϕ is the time component of the gauge field, ψ is a charged scalar field, and d is the number of spacetime dimensions. For $d=5$ the theory is considered to have a small periodic spacelike direction.

Organization

In section 6.2, we discuss some possible general examples of finite density field theories and attempt to establish bounds on the $\rho - \mu$ relationship by imposing thermodynamical constraints on these systems. In section 6.3 we briefly introduce holographic chemical potential and find, for Maxwell and Born-Infeld types of action, under mild assumptions, to what extent they reproduce the relationship found in 6.2. In section 6.4 we investigate the probe limit of both top-down and bottom-up theories; first we study Dp-Dq systems, then we move to gauge and scalar fields in both black hole and soliton (with one extra periodic dimension) backgrounds. Section 6.5 extends the analysis of the bottom-up models to include the backreaction of the fields on the metric.

Relation to previous work

Some of the results presented in this chapter have appeared previously in the literature. Finite density studies for probe brane systems have appeared for the Sakai-Sugimoto model [20, 63, 84, 116], the D3-D7 system [9, 42, 43, 86, 105], and the D4-D6 system [100]. The bottom-up models we consider are naturally studied at finite chemical potential (see, for example, [58] for the black hole case and [68] for the soliton dual to a $2+1$ dimensional field theory) due to the presence of the gauge field.

Our work focusses on the $\rho - \mu$ relation at large chemical potential over

a broad class of theories that are dual to 3+1 dimensional field theories. We find, on very general grounds, constraints on the $\rho-\mu$ relation in holographic models constructed from Maxwell and Born-Infeld actions. Additionally, we use thermodynamical considerations to constrain the $\rho-\mu$ relation from the field theory point of view and find that these constraints are in agreement with those derived holographically. Further, we extend the analysis in the above references to the large density regime and include additional examples, collecting the results of a large range of models.

6.2 CFT thermodynamics

In this section, by appealing to local thermodynamic stability and causality in the field theory, we attempt to establish generic constraints satisfied by the coefficient α from a purely field theory stand point. The results found here will lay ground for our intuition when approaching this problem from the holographic side.

Generic system at large chemical potential

In order to study the density and chemical potential from the field theory perspective, we begin with a general ansatz for the free energy of a hypothetical system. In the large density limit, we expect that the chemical potential will dominate the expression, so we may write[75]

$$f \propto -\mu^{\alpha+1} - a\mu^{\beta}T^{\gamma} + \ldots, \tag{6.4}$$

where the dots denote corrections higher order in T/μ. For a positive, imposing a positive entropy density $s = -(\partial f/\partial T)|_{\mu} > 0$ implies $\gamma > 0$, consistent with the second term being subleading in the low temperature expansion.

Considering the field theory as a thermodynamical system and imposing local stability demands that [36][76]

$$\chi = \left(\frac{\partial \rho}{\partial \mu}\right)_T > 0, \tag{6.5}$$

and

$$C_\rho = T\left(\frac{\partial s}{\partial T}\right)_\rho = -T\left[\frac{\partial^2 f}{\partial T^2} - \left(\frac{\partial^2 f}{\partial T \partial \mu}\right)^2 \frac{1}{\frac{\partial^2 f}{\partial \mu^2}}\right] > 0. \tag{6.6}$$

[75] Recall $\rho = -(\partial f/\partial \mu)_T$ so that, again, $\rho \propto \mu^{\alpha}$.

[76] χ is the charge susceptibility and C_ρ is the specific heat at constant volume.

Applying these to (6.4) in the $T/\mu \to 0$ limit gives the constraints $\alpha > 0$ and $\gamma > 1$.

Examining the speed of sound v_s of our system also allows us to establish a constraint. To ensure causality, we impose

$$0 \leq v_s \leq 1, \tag{6.7}$$

with the speed of sound given by [62]

$$v_s^2 = -\frac{\left[\left(\frac{\partial^2 f}{\partial T^2}\right)\rho^2 + \left(\frac{\partial^2 f}{\partial \mu^2}\right)s^2 - 2\left(\frac{\partial^2 f}{\partial T \partial \mu}\right)\rho s\right]}{(sT+\rho\mu)\left[\left(\frac{\partial^2 f}{\partial T^2}\right)\left(\frac{\partial^2 f}{\partial \mu^2}\right) - \left(\frac{\partial^2 f}{\partial T \partial \mu}\right)^2\right]}, \tag{6.8}$$

where ρ and s are the charge and entropy densities. For $\gamma > 1$, this implies the stronger bound of $\alpha \geq 1$. This is the same bound as derived in section 6.3 from consideration of the bulk dual of field theories. It is interesting that it arises from very general circumstances in both cases.

Zero temperature

In the zero temperature limit of ansatz (6.4) only the first term survives, so that $f \propto -\mu^{\alpha+1}$. In this case, the only condition for local stability is given by equation (6.5), which trivially leads to $\rho \propto \mu^\alpha$ with $\alpha > 0$. Computing the speed of sound and enforcing causality leads again to $\alpha \geq 1$.

General conformal theory

For a conformal field theory in d spacetime dimensions, the most general free energy density is

$$f = -\mu^d g\left(\frac{T}{\mu}\right), \tag{6.9}$$

where $g(x)$ is an arbitrary dimensionless function. Local stability depends on the details of the function g, and a general statement is not possible at this point. To ensure causality, we compute equation (6.8), finding the speed of propagation to be

$$v_s^2 = \frac{1}{d-1}, \tag{6.10}$$

from which it follows directly that a conformal theory obeys requirement (6.7) only in dimension $d \geq 2$. This result is trivial, as sound waves are not possible if there are no spacelike dimensions to propagate in.

Free fermions

As an example, we will compute the $\rho - \mu$ relationship for a system of free fermions. In the grand canonical ensemble, the partition function for spin 1/2 particles of charge q in a 3 dimensional box and subjected to a large chemical potential is

$$\mathcal{Z}(\mu, T) = \prod_{\vec{n}} (1 + e^{-\beta(E_{\vec{n}} - \mu q)}), \tag{6.11}$$

where the product is over available momentum levels. The partition function for antiparticles follows with the replacement $q \to -q$ so we include antiparticles by considering the total partition function $\tilde{\mathcal{Z}}(\mu, T) = \mathcal{Z}(\mu, T)\mathcal{Z}(-\mu, T)$. Passing to the continuum limit, approximating the fermions as massless, and setting $q = 1$, the resultant charge density is

$$\rho = \frac{\mu^3}{3\pi^2} + \frac{\mu T^2}{3}. \tag{6.12}$$

The dominant power in this case is the same as is expected in a generic conformal field theory.

6.3 General holographic field theories at finite density

It was shown in the previous section how local stability and causality lead to $\alpha \geq 1$. In this section, under mild assumptions, we investigate the Born-Infeld and Maxwell actions in the large μ regime and observe to what extent they fall under the general results from section 6.2.

6.3.1 Finite density

To find constraints on the $\rho - \mu$ relation in holographic field theories, we begin by studying very general systems with the minimal structure of a conserved charge. The holographic dictionary gives that a conserved charge in the field theory is dual to a massless $U(1)$ gauge field A in the bulk [103]. If the gauge field is a function only of the radial coordinate r, the chemical potential and the charge density are encoded in the behaviour of A as

$$\mu = A_t(\infty) \tag{6.13}$$

and

$$\rho = -\frac{\partial S_E}{\partial A_t(\infty)}, \tag{6.14}$$

where S_E is the Euclidean action evaluated on the saddle-point and the derivative is taken holding other sources fixed. As discussed in [86], an equivalent expression for the charge density is[77]

$$\rho = \left(\frac{1}{d-2}\right) \frac{\partial \mathcal{L}}{\partial(\partial_r A_t)}, \tag{6.15}$$

where the normalization of ρ has been chosen for later convenience. After writing down the gravitational lagrangian, our prescription for computing the charge density at a given chemical potential is to solve the equations of motion with a fixed boundary condition for the gauge field, equation (6.13), before reading off the density using equation (6.15).

6.3.2 Gauge field actions

To include a gauge field in our AdS/CFT construction, we simply include it in the bulk action. Two gauge field lagrangians that have appeared in holographic studies are the Maxwell and the Born-Infeld lagrangians. Typically, the Maxwell action is used in bottom-up holographic models while the Born-Infeld action appears in the study of brane dynamics. Below, in section 6.4 we will consider holographic models using both types of lagrangians. However, much insight can be gained by investigating these actions under generic conditions. Therefore, in this section, we study general versions of these two lagrangians, at fixed temperature and large chemical potential, in the probe approximation.[78] Interpreting our results using (6.13) and (6.15), we will develop some constraints for the $\rho - \mu$ relationship in holographic theories described by these actions.

The Maxwell action

Consider a gauge field described by the Maxwell action $\int \sqrt{-g}F^2$ in a general background of the form

$$ds^2 = g^{FT}_{\mu\nu}(r)dx^\mu dx^\nu + g_{rr}(r)dr^2. \tag{6.16}$$

If we assume homogeneity in the field theory directions and consider a purely electrical gauge field (keeping only its time-component), the lagrangian is

[77] Generically, A_t is a cyclic variable, so that the conjugate momentum is conserved, and we may evaluate this expression at any r.

[78] In the probe approximation, we assume there is no backreaction on the gravity metric. This is enforced in this case by studying the gauge field lagrangian on a fixed background geometry.

simply

$$\mathcal{L} = g(r) \left(\partial_r A_t\right)^2 , \tag{6.17}$$

for some function $g(r)$. From this we find

$$\rho = \left(\frac{2}{d-2}\right) g(r) \partial_r A_t . \tag{6.18}$$

In the systems considered below, the spacetime either has a horizon or smoothly cuts off at some radius $r_{\min}$. The value of the gauge field at this point is a boundary condition for the problem. Below, $A_t(r_{\min})$ is either zero or a constant, neither of which affect the $\rho - \mu$ behaviour; we take $A_t(r_{\min}) = 0$ here. Integrating (6.18), we find

$$\mu = \rho \left(\frac{d-2}{2}\right) \int_{r_{\min}}^{\infty} \frac{dr}{g(r)} . \tag{6.19}$$

Provided the integral is finite, we have

$$\rho \propto \mu . \tag{6.20}$$

Thus, for any holographic field theory with the gauge field described only by the Maxwell lagrangian in a fixed metric we have $\alpha = 1$.

The Born-Infeld action

The Born-Infeld action is the non-linear generalization of Maxwell electrodynamics and is the appropriate language in which to describe the dynamics of gauge fields living on branes. Assuming homogeneity in the field theory directions, so that the gauge potential varies only with the radial direction, these systems are governed by an action of the generic form[79]

$$\mathcal{L} = \sqrt{g(r) - h(r)(\partial_r A_t)^2}, \tag{6.21}$$

where again, we take A_t to be the only non-zero part of the gauge field. The charge density is given by the constant of motion

$$\rho = \left(\frac{1}{d-2}\right) \frac{h(r)\partial_r A_t(r)}{\sqrt{g(r) - h(r)(\partial_r A_t)^2}} . \tag{6.22}$$

[79] $g(r)$ and $h(r)$ are arbitrary functions; $g(r)$ is not related to the previous discussion.

Here, we assume that the gauge field is sourced by a charged black hole horizon at r_+.[80] Euclidean regularity of the potential A_t fixes its value at the horizon as $A_t(r_+) = 0$ [86]. Then, we can integrate to find

$$\mu = \int_{r_+}^{\infty} dr \sqrt{\frac{g(r)}{h(r)}} \frac{(d-2)\rho}{\sqrt{h(r) + (d-2)^2\rho^2}}. \tag{6.23}$$

To extract the large ρ behaviour, we split the integral at $\Lambda \gg 1$. For $\rho \gg \Lambda$, the integral from r_+ to Λ approaches a constant, while the functions in the integral from Λ to ∞ can be approximated by their large r forms, which will be denoted with a ∞ subscript. The expression for the chemical potential now becomes

$$\mu \approx \int_{r_+}^{\Lambda} dr \sqrt{\frac{g(r)}{h(r)}} + \int_{\Lambda}^{\infty} dr \sqrt{\frac{g_\infty(r)}{h_\infty(r)}} \frac{(d-2)\rho}{\sqrt{h_\infty(r) + (d-2)^2\rho^2}}. \tag{6.24}$$

The ρ dependence of μ comes from the second term. If $g_\infty(r)/h_\infty(r) \approx r^{2m}$ and $h_\infty(r) \approx r^n$, by putting $x = r/\rho^{2/n}$ we find that

$$\mu \sim \rho^{(2+2m)/n} \int_{\frac{r_+}{\rho^{2/n}}}^{\infty} dx \frac{x^m}{\sqrt{x^n + 1}}. \tag{6.25}$$

The convergence of the integral here requires that $n/(2+2m) > 1$, resulting in the relationship

$$\rho \propto \mu^\alpha \quad \text{with} \quad \alpha > 1, \tag{6.26}$$

where the power α depends on the specific bulk geometry.

6.4 Holographic probes

With the general constraints of the previous sections in hand, we move on to study particular holographic field theories in the probe approximation, to see which specific values of α are realized. Here, we study two common probe configurations that have arisen in previous holographic studies. These are extensions of the actions considered in section 6.3. First, we examine probe branes in the black brane background using the Born-Infeld action.

[80] To have a non-trivial field configuration, a source for the gauge field in the bulk is required. In the low temperature, horizon-free versions of these models, this source is given by lower dimensional branes wrapped in directions transverse to the probe branes [142].

Then, we move on to the phenomenological perspective, in which we write down an effective gravity action without appealing to the higher dimensional string theory. In this approximation, using the Maxwell action, we look at the gauge field in both the planar Schwarzschild black hole and soliton backgrounds, with and without a coupling to a scalar field.

In both cases, in the systems we consider, the only sources in the field theory are the temperature T and chemical potential μ. Below, we fix T and work at large μ (such that $\mu/T \gg 1$). In this regime, we look for a relationship $\rho \propto \mu^\alpha + \ldots$, where the dots denote terms higher order in T/μ.

6.4.1 Probe branes and the Born-Infeld action

In the systems we will consider here, the background consists of N_c D-branes; in the large N_c limit, these branes are replaced with a classical gravity metric. In this regime, fundamental matter is added by placing N_f probe branes in the geometry [82].

The brane action

Assuming that the background spacetime metric $G_{\mu\nu}$ is given, the action governing the dynamics of a single Dq probe brane is the Born-Infeld action

$$S \propto \int d^{q+1}\sigma e^{-\phi}\sqrt{-\det(g_{ab} + 2\pi\alpha' F_{ab})}. \tag{6.27}$$

Here, latin indices refer to brane coordinates and greek indices denote spacetime coordinates, while $X^\mu(\sigma^a)$ describes the brane embedding. g_{ab} is the induced metric on the probe brane given by $g_{ab} = \partial_a X^\mu \partial_b X^\nu G_{\mu\nu}$, F_{ab} is the field strength for the $U(1)$ gauge field on the brane, and ϕ is the dilaton field. Following the previous discussion, the only component of the gauge field we choose to turn on is A_t, additionally, we assume it depends only on the radial coordinate r, $A_t = A_t(r)$. Considering that the probe brane is extended in the r direction and the spacetime metric is diagonal, the lagrangian simplifies to

$$\mathcal{L} \propto e^{-\phi}\sqrt{-\det(g_{ab})\left(1 + \frac{(\partial_r A_t)^2}{g_{tt}g_{rr}}\right)}, \tag{6.28}$$

where we rescaled A_t to absorb the $2\pi\alpha'$ term. In the notation of equation (6.21), we can write

$$g(r) = -\det(g_{ab})e^{-2\phi}, \tag{6.29}$$

$$h(r) = \frac{\det(g_{ab})e^{-2\phi}}{g_{tt}g_{rr}}. \tag{6.30}$$

The background

For N_c Dp branes, at large N_c, the high temperature background is the black Dp brane metric, given by[81]

$$ds^2 = H^{-1/2}(-fdt^2 + d\vec{x}_p^2) + H^{1/2}\left(\frac{dr^2}{f} + r^2 d\Omega_{8-p}^2\right), \tag{6.31}$$

with

$$H(r) = \left(\frac{L}{r}\right)^{7-p}, \quad f(r) = 1 - \left(\frac{r_+}{r}\right)^{7-p}, \quad e^{\phi} = g_s H^{(3-p)/4}. \tag{6.32}$$

L is the characteristic length of the space, while g_s is the string coupling. This metric has a horizon at $r = r_+$.

Our probe Dq brane is fixed to share $d-1$ spacelike directions with the Dp branes. If $p > d-1$, the fundamental matter propagates on a d dimensional defect and we may consider the extra $p-(d-1)$ directions along the background brane to be compactified, giving an effective d dimensional gauge theory at low energies. Alternatively, we can build a $d-1$ dimensional gauge theory by compactifying one or more of the directions shared by the probe and background branes. Below, we will study field theories that are effectively $3+1$ dimensional using both methods.

We stipulate that the Dq probe brane wraps an S^n inside the S^{8-p} and extends along the radial direction r. These quantities are related by $q = d + n$. The induced metric on the Dq brane is

$$ds^2 = H^{-1/2}(-fdt^2 + d\vec{x}_{d-1}^2) + \left(\eta(r) + \frac{H^{1/2}}{f}\right)dr^2 + H^{1/2}r^2 d\Omega_n^2, \tag{6.33}$$

where

$$\eta(r) = \partial_r X^\mu \partial_r X^\nu G_{\mu\nu} - G_{rr}. \tag{6.34}$$

[81] More details on this solution can be found in [95].

Calculating equations (6.29) and (6.30) gives[82]

$$g(r) = r^{2n} f H^{\frac{1}{2}(p+n-d-3)} \left(\eta(r) + \frac{H^{1/2}}{f} \right), \tag{6.35}$$

$$h(r) = r^{2n} H^{\frac{1}{2}(p+n-d-2)}, \tag{6.36}$$

from which (6.23) gives the chemical potential

$$\mu = \int_{r_+}^{\infty} dr \frac{(d-2)\rho}{\sqrt{r^{2n}\left(\frac{L}{r}\right)^{(\frac{7-p}{2})(p+n-d-2)} + (d-2)^2\rho^2}} \sqrt{\frac{f\eta(r)}{H^{1/2}} + 1}. \tag{6.37}$$

Now, $\eta(r)$ will be some combination of $(\partial_r \chi_i)^2$, where the χ_i denote the directions of transverse brane fluctuations. By writing down the equations of motion we can observe that $\partial_r \chi_i = 0$ is a solution, in which case the probe brane goes straight into the black hole along the radial direction r. This describes the high temperature, deconfined regime; we set $\eta(r) = 0$ in the following.

For large ρ we find

$$\rho \propto \mu^{\frac{1}{4}[(p-7)(p-d-2)+(p-3)(q-d)]}, \tag{6.38}$$

so that for the probe brane systems,

$$\alpha = \frac{1}{4}[(p-7)(p-d-2) + (p-3)(q-d)]. \tag{6.39}$$

As above, α is constrained as $\alpha > 1$ for convergence of the integral. If $\alpha \leq 1$, the contribution of the constant charge density to the total energy diverges, signalling a breakdown of the probe approximation. At this point, we can use equations (6.38) and (6.39) to investigate what type of $\rho - \mu$ behaviours can arise from Dp-Dq brane constructions.

Example: the Sakai-Sugimoto model

The well-known Sakai-Sugimoto model [120] consists of N_f probe D8-$\overline{\text{D8}}$ branes in a background of N_c D4 branes compactified on a circle. We have $p = 4$, $q = 8$, and $d = 4$. Putting these numbers into (6.38) yields

$$\rho \propto \mu^{5/2}, \tag{6.40}$$

consistent with previous results [20, 116].

[82] We leave the constant factors of g_s from e^{ϕ} out of the lagrangian, as our goal here is just the power law dependence.

$\rho - \mu$ in $3+1$ dimensional probe brane theories

Equation (6.39) determines the dominant power law behaviour in all Dp-Dq configurations relevant to $3+1$ dimensional field theory. As discussed above, we can set the number of shared probe and background directions to be $d-1=3$ or put $d-1=4$ and demand one of the the spacelike shared directions to be periodic; see table 6.1 for the results. The power $\alpha = 3$ is an upper bound for the $3+1$ dimensional probe brane gauge theories we have considered.

Our calculation above involves only the Born-Infeld action for the probe brane and in particular neglects any possible Chern-Simons terms that appear due to the coupling between the brane and a spacetime tensor field. The Chern-Simons term is important in the D4-D4 system, for example [138].

6.4.2 Bottom-up models and the Einstein-Maxwell action

We now turn our attention to bottom-up AdS/CFT models in the probe regime. To construct a phenomenological gauge / gravity model, we begin with a theory of gravity with a cosmological constant, such that the geometry is asymptotically AdS. To study the relationship between charge density and chemical potential in the dual field theory, we demand that there must be a gauge field in the bulk. At this point, our model has the ingredients for us to compute our desired result. But, one may ask what type of extensions are possible. Motivated by superconductivity and superfluidity studies, we will consider also a charged scalar field in our gravity theory. Adding a scalar field alters the dynamics of the system, notably resulting in different phases [54, 85]. When the scalar field takes on a non-zero expectation value, this breaks the $U(1)$ gauge symmetry in the bulk and corresponds to the presence of a $U(1)$ condensate in the boundary theory.

The particular model we study is the Einstein-Maxwell system with a charged scalar field:

$$S = \int d^{d+1}x\sqrt{-g}\left\{\mathcal{R} + \frac{d(d-1)}{L^2} - \frac{1}{4}F^{\mu\nu}F_{\mu\nu} - |\partial_\mu\psi - iqA_\mu\psi|^2 - V(|\psi|)\right\} \quad (6.41)$$

Different dual field theories may be obtained by considering this action in different regimes and with different parameters. Below, we make the following ansatz for the gauge and scalar fields:

$$A = \phi(r)dt, \quad \psi = \psi(r). \quad (6.42)$$

The r component of Maxwell's equations will give that the phase of the complex field ψ is constant, so without loss of generality we take ψ real. For the remainder of the study, we choose units such that $L = 1$ and consider the potential $V(\psi) = m^2\psi^2$.

The probe limit

To get the probe approximation for the system described by (6.41), we rescale $\psi \to \psi/q$ and $A \to A/q$ before taking $q \to \infty$ while keeping the product $q\mu$ fixed (to maintain the same $A - \psi$ coupling). The gauge and scalar fields decouple from the Einstein equations and we study the fields in a fixed gravitational background.

The background is governed by the action

$$S = \int d^{d+1}x\sqrt{-g}\left\{\mathcal{R} + d(d-1)\right\}. \tag{6.43}$$

One solution here is the planar Schwarzschild-AdS black hole, given by

$$ds^2_{bh} = (-f_{bh}(r)dt^2 + r^2 dx_i dx^i) + \frac{dr^2}{f_{bh}(r)}, \tag{6.44}$$

with

$$f_{bh}(r) = r^2\left(1 - \frac{r_+^d}{r^d}\right), \tag{6.45}$$

where r_+ is the black hole horizon. Below, we consider two systems in the Schwarzschild-AdS background: the probe gauge field, and the probe gauge and scalar fields.

Computing μ and ρ

If the kinetic term for the gauge theory on the gravity side is the Maxwell lagrangian,

$$\mathcal{L} = \frac{1}{4}\sqrt{-g}F_{\mu\nu}F^{\mu\nu}, \tag{6.46}$$

then for an asymptotically AdS space the field equation for the time component of the gauge field is

$$\phi'' + \frac{d-1}{r}\phi' + \cdots = 0, \tag{6.47}$$

where $'$ denotes an r derivative and $\ldots$ denotes terms that have higher powers of $1/r$. The solution is

$$\phi(r) = \phi_1 + \frac{\phi_2}{r^{d-2}} + \ldots . \tag{6.48}$$

Recalling that $\phi(\infty) = \mu$ determines that $\phi_1 = \mu$, while we can plug (6.48) into (6.46) and compute, using (6.15), that $\phi_2 = \rho$. We have that

$$\phi(r) = \mu - \frac{\rho}{r^{d-2}} + \ldots , \tag{6.49}$$

so that in practice, below, we just have to read off the coefficients of the leading and next to leading power of $1/r$ to find the chemical potential and the charge density.

The scalar field

Solving the scalar field equation at large r in an asymptotically AdS space results in the behaviour

$$\psi = \frac{\psi_1}{r^{\lambda_-}} + \frac{\psi_2}{r^{\lambda_+}} + \ldots , \tag{6.50}$$

where

$$\lambda_\pm = \frac{1}{2}\left\{ d \pm \sqrt{d^2 + 4m^2} \right\}. \tag{6.51}$$

For m^2 near the Breitenlohner-Freedman (BF) bound [25, 26], in the range $-(d-1)^2/4 \geq m^2 \geq -d^2/4$, the choice of either $\psi_1 = 0$ or $\psi_2 = 0$ results in a normalizable solution [85]. For $m^2 > -(d-1)^2/4$, ψ_1 is a non-normalizable mode and ψ_2 is a normalizable mode. For the cases with the scalar field, we define our field theory by taking $\psi_1 = 0$, so that we never introduce a source for the operator dual to the scalar field.

The probe gauge field

Here, we study the probe gauge field, without the scalar field, in the Schwarzschild-AdS background (6.44). The equation of motion for ϕ is

$$\phi'' + \frac{d-1}{r}\phi' = 0. \tag{6.52}$$

Regularity at the horizon demands that $\phi(r_+) = 0$ and the AdS/CFT dictionary gives $\phi(\infty) = \mu$, leading to

$$\phi(r) = \mu \left(1 - \frac{r_+^{d-2}}{r^{d-2}} \right). \tag{6.53}$$

Then, applying (6.49), we have

$$\rho = \mu r_+^{d-2}. \tag{6.54}$$

The horizon r_+ depends only on the temperature, $T = r_+ d/4\pi$,[83] so this is a linear relationship between ρ and μ, in accordance with (6.20).

Adding a scalar field

We now turn on the scalar field in (6.41), and consider the dynamics in the Schwarzschild-AdS background (6.44).

The field equations become

$$\psi'' + \left(\frac{f_{bh}'}{f_{bh}} + \frac{d-1}{r}\right)\psi' + \left(\frac{q^2\phi^2}{f_{bh}^2} - \frac{m^2}{f_{bh}}\right)\psi = 0, \tag{6.55}$$

$$\phi'' + \frac{d-1}{r}\phi' - \frac{2q^2\psi^2}{f_{bh}}\phi = 0. \tag{6.56}$$

At this point, we can scale q to 1 by scaling ϕ and ψ, and so m is the only parameter here.

The coupling allows the gauge field to act as a negative mass for the scalar field. At small chemical potentials, $\psi = 0$ is the solution. As we increase μ, the effect of the gauge field on the scalar field becomes large enough such that the effective mass of the scalar field drops below the BF bound of the near horizon limit of the geometry, so that a non-zero profile for ψ is possible, and we have a phase transition to the field theory state with broken $U(1)$ symmetry. A smaller (more negative) squared mass results in a smaller critical chemical potential, at which the scalar field turns on.

Using a simple shooting method, for $d = 4$ we numerically solve equations (6.55, 6.56) and arrive at the relationship

$$\rho = c_{bh}^p(m^2)\mu^3, \tag{6.57}$$

where $c_{bh}^p(m^2)$ is a scaling constant that depends on the mass of the scalar field. The coupling to the scalar field has resulted in the larger power ($\alpha = 3$) in the scaling of ρ. A smaller squared mass corresponds to a larger value of c_{bh}^p and, for a given chemical potential, is dual to field theory with a higher charge density. In figure 6.1, we can see the existence of a denser state when the scalar field turns on as well as the relative relation between the mass of the scalar field and the charge density in the field theory.

[83] For a Euclidean metric $ds^2 = \alpha(r)d\tau^2 + \frac{dr^2}{\beta(r)}$ with periodic $\tau = it$ coordinate and $\alpha(r_+) = \beta(r_+) = 0$, regularity at the horizon demands that the temperature (the inverse period of τ) be given by $T = \sqrt{\alpha'(r_+)\beta'(r_+)}/4\pi$.

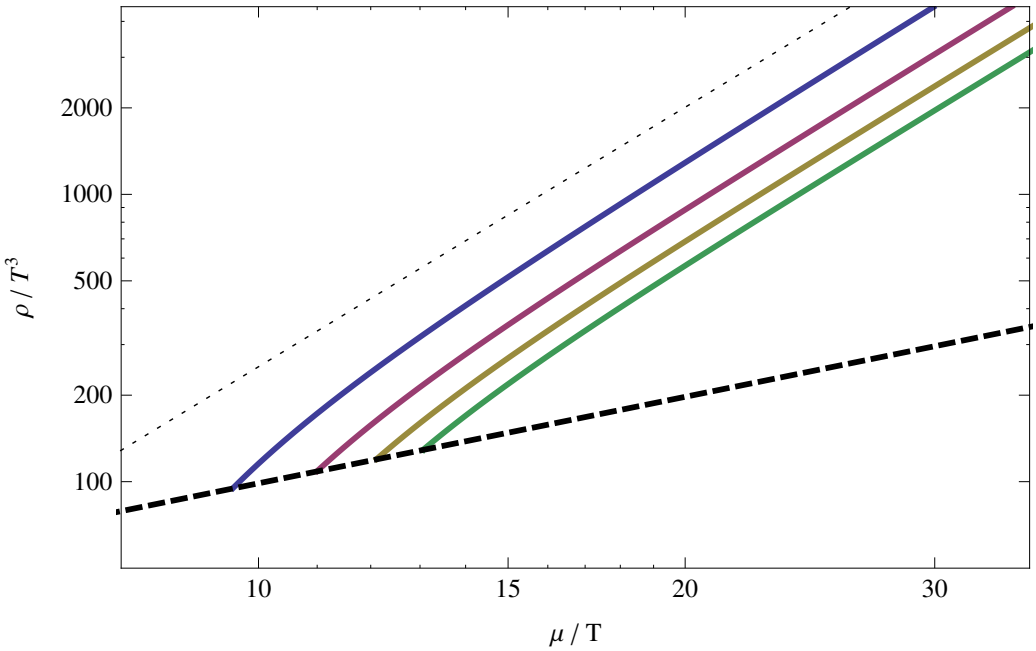

Figure 6.1: Charge density versus chemical potential for the probe gauge and scalar fields, section 6.4.2, on a log-log scale. The thick dashed line is for the system with no scalar field for which, analytically, $\rho \propto \mu$. At a critical chemical potential, depending on the mass of the scalar field, configurations with non-zero scalar field become available. The thin dotted line is a model power law $\rho \propto \mu^3$, as described in equation (6.57). From left to right, the thick solid lines are for scalar field masses $m^2 = -15/4$, $-14/4$, $-13/4$, and -3. A more negative scalar field mass results in a denser field theory state at a given chemical potential.

The soliton probe

Motivated by recent work [19, 68, 107], we now add more structure to the bulk theory in the form of an extra periodic dimension. To model a $3+1$ dimensional field theory, we set $d = 5$ and stipulate that this includes one periodic spacelike coordinate w of length $2\pi R$. At energies much less than the scale set by this length, $E \ll 1/R$, the dual field theory will be effectively $3+1$ dimensional. The extra dimension sets another scale for the field theory

and enables a richer phase structure in the system.[84]

With the extra periodic direction, there is another solution to the background described by (6.43). This is the AdS-soliton, given as the double-analytic continuation of the Schwarzschild-AdS solution (6.44):

$$ds^2_{sol} = (r^2 dx_\mu dx^\mu + f_{sol}(r) dw^2) + \frac{dr^2}{f_{sol}(r)}, \tag{6.58}$$

with

$$f_{sol} = r^2 \left(1 - \frac{r_0^5}{r^5}\right). \tag{6.59}$$

Here, r_0 is the location of the tip of the soliton. For regularity, it is fixed by the length of the w dimension as

$$r_0 = \frac{2}{5R}. \tag{6.60}$$

By computing the free energy of the systems, it can be shown that the soliton background dominates over the black hole background for small enough temperatures and chemical potentials. As the temperature or chemical potential is increased, there is a first order phase transition to the black hole, which is the holographic version of a confinement / deconfinement transition.

For zero scalar field, the soliton can be considered at any temperature and chemical potential; the period of the Euclidean time direction defines the temperature while $\phi = \mu =$ constant is a solution to the field equations. In this case, $\rho = 0$ and we do not have an interesting $\rho - \mu$ relation. Considering a non-zero scalar field provides a source for the gauge field and allows non-trivial configurations.

In the soliton background (6.58), the equations of motion are

$$\psi'' + \left(\frac{f'_{sol}}{f_{sol}} + \frac{4}{r}\right)\psi' + \left(\frac{q^2\phi^2}{r^2 f_{sol}} - \frac{m^2}{f_{sol}}\right)\psi = 0, \tag{6.61}$$

$$\phi'' + \left(\frac{f'_{sol}}{f_{sol}} + \frac{2}{r}\right)\phi' - \frac{2q^2\psi^2}{f_{sol}}\phi = 0. \tag{6.62}$$

As in the black hole case, at this point we can set $q = 1$ by scaling the fields.

[84] The phase diagram including both black hole and soliton solutions, was studied in [68] for a $2+1$ dimensional field theory in the context of holographic superconductors and in [19] for a $3+1$ dimensional field theory in the context of holographic QCD and colour superconductivity.

After numerically integrating, we have

$$\rho = c_{sol}^{p}(m^2)\mu^4. \tag{6.63}$$

Compared to the black hole case, above, we find a larger power of μ. At large densities, the average distance between charges becomes small compared to the size R of the periodic direction. In this limit, the system becomes effectively higher dimensional and so we would expect a larger power α in the $\rho - \mu$ relationship. The numerics were consistent with this result.

As can be seen in figure 6.2, a more negative mass squared results in a smaller critical chemical potential and a denser field theory state at a given chemical potential. This is as expected by comparing the structure of the equations to those in the black hole case. Further, at a given chemical potential, the soliton solution corresponds to a denser field theory state than the black hole solution with the same scalar field mass.

6.5 $\rho - \mu$ in backreacted systems

Despite our analysis in section 2 relying on the probe approximation, it is interesting to ask how much of a difference allowing for backreaction on the bottom-up models could make to the $\rho - \mu$ relation and the bounds found previously. Henceforth we generalize the bottom-up model introduced in section 6.4.2 and allow for the backreaction of the gauge and scalar field on the metric. Recall that the action is

$$S = \int d^{d+1}x\sqrt{-g}\left\{\mathcal{R} + d(d-1) - \frac{1}{4}F^{\mu\nu}F_{\mu\nu} - |\partial_\mu\psi - iqA_\mu\psi|^2 - m^2\psi^2\right\} \tag{6.64}$$

We start by studying the well-known Reissner-Nordstrom-AdS (RN-AdS) solution to the Einstein equation, in which $\psi = 0$. Later, we allow the scalar field to acquire a non-zero profile and investigate its consequences on the $\rho - \mu$ profile. We finish with the investigation of the backreacted version of the solitonic solution.

6.5.1 Charged black holes

The backreacted solution with no scalar field is the planar RN-AdS black hole, given by

$$ds^2 = (-f_{\rm RN}(r)dt^2 + r^2 dx_i dx^i) + \frac{dr^2}{f_{\rm RN}(r)}, \tag{6.65}$$

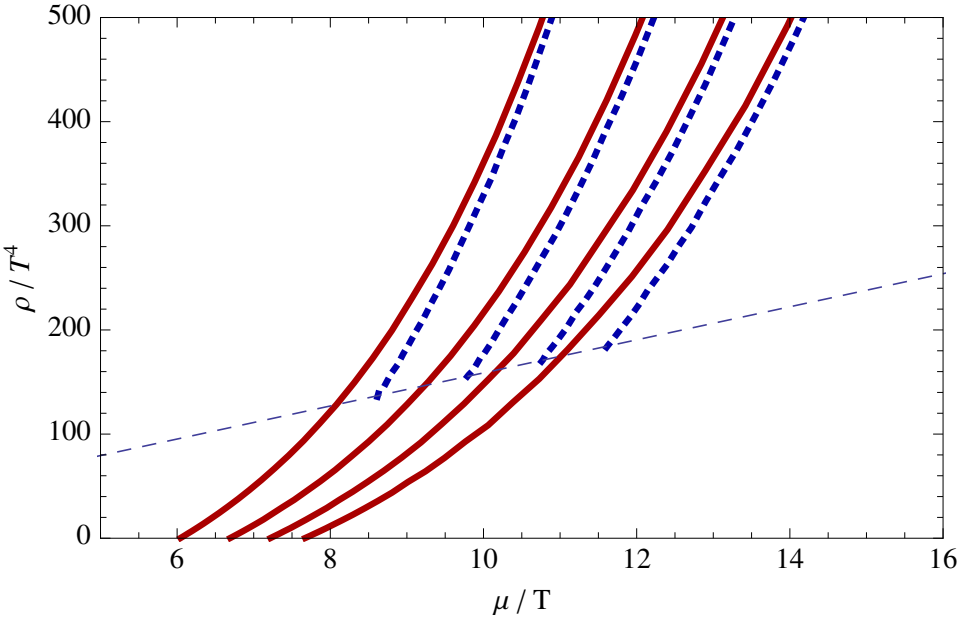

Figure 6.2: Charge density versus chemical potential for the probe gauge and scalar fields in the soliton background, section 6.4.2, and the $d = 5$ black hole background, section 6.4.2. The thin dashed line is the probe gauge field in the black hole background for which, analytically, $\rho \propto \mu$. The thick solid lines are the soliton results (from left to right, the squared mass of the scalar field is $-22/4$, -5, $-18/4$, and -4) while the thick dashed lines are the black hole results (again, from left to right, $m^2 = -22/4$, -5, $-18/4$, and -4). Each of the thick lines approaches the power law $\rho \propto \mu^4$, equation (6.63). At a given chemical potential, the soliton background gives a field theory in a denser state.

with[85]

$$f_{\rm RN}(r) = r^2 \left(1 - \left(1 + \frac{(d-2)\mu^2}{2(d-1)r_+^2} \right) \frac{r_+^d}{r^d} + \frac{(d-2)\mu^2}{2(d-1)} \frac{r_+^{2(d-2)}}{r^{2(d-1)}} \right) . \tag{6.66}$$

The gauge potential is

$$\phi(r) = \mu \left(1 - \frac{r_+^{d-2}}{r^{d-2}} \right) , \tag{6.67}$$

[85]We parametrize this solution in terms of the location of the horizon r_+ and the asymptotic value of the gauge field (the chemical potential μ) instead of the usual choices of the charge and mass of the black hole.

so that, using (6.49), we have $\rho = \mu r_+^{d-2}$. Here, the horizon r_+ can be expressed as a function of the temperature and chemical potential through the Hawking temperature

$$T = \frac{1}{4\pi}\left(dr_+ - \frac{(d-2)^2\mu^2}{2(d-1)r_+}\right). \tag{6.68}$$

Eliminating r_+ in favour of ρ and μ in (6.68), we may solve for ρ to find

$$\rho = \left(\frac{(d-2)^2}{2d(d-1)}\right)^{\frac{d-2}{2}} \mu^{d-1}\left[\left(\frac{2(d-1)}{d}\right)^{\frac{1}{2}}\frac{2\pi T}{(d-2)\mu} + \sqrt{1+\frac{8\pi^2(d-1)T^2}{d(d-2)^2\mu^2}}\right]^{d-2}. \tag{6.69}$$

Notice that the dominant power in the $\rho-\mu$ relationship is μ^{d-1}, as expected in a d dimensional conformal field theory. For $d = 4$, the particular large μ expansion is

$$\rho = \frac{1}{6}\mu^3 + \frac{\pi}{\sqrt{6}}\mu^2 T + \frac{1}{2}\pi^2\mu T^2 + \frac{1}{4}\sqrt{\frac{3}{2}}\pi^3 T^3 + \ldots. \tag{6.70}$$

6.5.2 Hairy black holes

If we turn on the scalar field, an analytic solution to the equations of motion is no longer possible and we turn to numerical calculation. We take as our metric ansatz

$$ds^2 = -g(r)e^{-\chi(r)}dt^2 + \frac{dr^2}{g(r)} + r^2(dx_i dx^i), \tag{6.71}$$

where $g(r)$ will be fixed to have a zero at r_+, giving a horizon. We arrive at the following equations of motion:

$$\psi'' + \left(\frac{g'}{g} - \frac{\chi'}{2} + \frac{d-1}{r}\right)\psi' + \frac{1}{g}\left(\frac{q^2\phi^2 e^{\chi}}{g} - m^2\right)\psi = 0, \tag{6.72}$$

$$\phi'' + \left(\frac{\chi'}{2} + \frac{d-1}{r}\right)\phi' - \frac{2q^2\psi^2}{g}\phi = 0, \tag{6.73}$$

$$\chi' + \frac{2r\psi'^2}{d-1} + \frac{2rq^2\phi^2\psi^2 e^{\chi}}{(d-1)g^2} = 0, \tag{6.74}$$

$$g' + \left(\frac{d-2}{r} - \frac{\chi'}{2}\right)g + \frac{re^{\chi}\phi'^2}{2(d-1)} + \frac{rm^2\psi^2}{d-1} - dr = 0. \tag{6.75}$$

The first two equations can be derived via the Euler-Lagrange equations for ϕ and ψ, while the final two equations are the tt and rr components of Einstein's equation.

In this system, as in the probe case, section 6.4.2, at small chemical potentials the scalar field is identically zero. As we increase the chemical potential above a critical value, the system undergoes a second order phase transition to a state with non-zero scalar field. When the scalar field condenses, the corresponding field theory is in a denser state at the same chemical potential than for the system without scalar field.

We solve the equations numerically for $d = 4$, to yield the result, in the phase with the scalar field,

$$\rho = c_{bh}(q, m^2)\mu^3. \tag{6.76}$$

As we increase the charge or decrease the mass squared of the scalar field, the critical chemical potential, at which the scalar condenses, decreases, while the scaling coefficient c_{bh} increases. The scaling coefficient $c_{bh}(q, m^2)$ is, in all cases we checked, larger than the coefficient of the μ^3 term in the AdS-Reissner-Nordstrom black hole, equation (6.70), indicating that the density scales faster with the chemical potential when the scalar field is present.

When we include metric backreaction for the black hole, the dominant power in the $\rho - \mu$ relationship is greater than the probe case when there is no scalar field and is the same as the probe case when there is a scalar field, indicating that, at least for the systems considered, the bounds found for the $\rho - \mu$ behaviour apply to the backreacted cases as well.

6.5.3 Backreacted soliton

Motivated by the form of the soliton background (6.58) we choose the metric ansatz

$$ds^2 = \frac{dr^2}{r^2 B(r)} + r^2 \left(e^{A(r)} B(r) dw^2 - e^{C(r)} dt^2 + dx_i dx^i \right), \tag{6.77}$$

where we constrain $B(r_0) = 0$ so that the tip of the soliton is at r_0. The field and Einstein equations give

$$\psi'' + \left(\frac{6}{r} + \frac{A'}{2} + \frac{B'}{B} + \frac{C'}{2} \right) \psi' + \frac{1}{r^2 B} \left(\frac{e^{-C}(q\phi)^2}{r^2} - m^2 \right) \psi = 0, \tag{6.78}$$

$$\phi'' + \left(\frac{4}{r} + \frac{A'}{2} + \frac{B'}{B} - \frac{C'}{2} \right) \phi' - \frac{2\psi^2 q^2 \phi}{r^2 B} = 0, \tag{6.79}$$

$$B'\left(\frac{4}{r}-\frac{C'}{2}\right)+B\left(\psi'^2-\frac{1}{2}A'C'+\frac{e^{-C}\phi'^2}{2r^2}+\frac{20}{r^2}\right)+ \\ +\frac{1}{r^2}\left(\frac{e^{-C}(q\phi)^2\psi^2}{r^2}+m^2\psi^2-20\right)=0, \quad (6.80)$$

$$C''+\frac{1}{2}C'^2+\left(\frac{6}{r}+\frac{A'}{2}+\frac{B'}{B}\right)C'-\left(\phi'^2+\frac{2(q\phi)^2\psi^2}{r^2B}\right)\frac{e^{-C}}{r^2}=0, \quad (6.81)$$

$$A'=\frac{2r^2C''+r^2C'^2+4rC'+4r^2\psi'^2-2e^{-C}\phi'^2}{r(8+rC')}. \quad (6.82)$$

We solve equations (6.78-6.81) numerically with asymptotically AdS boundary conditions before integrating (6.82) to find A.[86] The results are consistent with a $\rho-\mu$ relationship of the form

$$\rho=c_{sol}(q,m^2)\mu^4. \quad (6.83)$$

As in the probe case, the effective higher dimension of the space dictates the power in the relationship. The dependence of $c_{sol}(q,m^2)$ on q and m^2 is as in the backreacted black hole case, section 6.5.2. Like the black hole with scalar field, the backreacted soliton with scalar field gives the same dominant power α as the corresponding probe case.

6.6 Discussion

In this chapter we studied the $\rho-\mu$ relation for a variety of holographic field theories, and set conditions for physically consistent relationships based on local stability and causality. We observed that all of the examples considered are well modelled by a power law $\rho=c\mu^\alpha$ in the large μ regime and that none of them fail to satisfy any of the general constraints stablished in sections 6.3 and 6.2. Except for the case of a probe gauge field in the Schwarzschild-AdS black hole background, the power α in all the bottom-up models obeyed the generic dimensional argument discussed in the introduction, as can be seen in table 6.2. This resulted in a larger power for the models with an extra periodic dimension. The brane constructions, table 6.1, displayed a larger variety of power laws, with the range $1<\alpha\leq 3$, where α depended on the particular dimensions of the probe and background branes.

[86] More details on the numerical process can be found in [19].

The study of bottom-up models led to the conclusion that, in general, the presence of a non-zero profile for the scalar field in the bulk induces a larger charge density on the boundary. In most cases, this change was realized as an increase of the scaling coefficient c while the power law was kept unaltered. The only exception was the probe Einstein-Maxwell case, section 6.4.2. Here, in the absence of a scalar field, the probe Maxwell field enjoys its standard linear equations of motion, and naturally we find a linear $\rho-\mu$ relationship. With a non-zero scalar field, the power law becomes $\rho \propto \mu^{d-1}$, as expected for the underlying CFT. In systems with an extra periodic direction, the numerical results displayed in figure 6.2 support the conclusion that at a given (large enough) chemical potential, the solitonic phase is denser than the corresponding black hole phase.

Despite our attempt to survey a large variety of holographic models, we do not claim to have presented a complete report and we do not discard the possibility of finding different $\rho - \mu$ relations in other types of bottom-up and top-down models. For example, one generalization would be to include $N_f > 1$ flavour branes in the Dp-Dq systems; this has been shown to change the power α in the relation [116]. It would be interesting to extend this study to other classes of systems and to see how the results compare to those given here.

Chapter 7

Color Super Conductivity

7.1 Introduction

Background

Quantum Chromodynamics is believed to display a rich phase structure at finite temperature and chemical potential, with phase transitions associated with deconfinement, nuclear matter condensation, the breaking of (approximate) flavor symmetries (which are exact in generalizations with equal quark masses and/or massless quarks), and the onset at high density of quark matter phases displaying color superconductivity [3, 4] (for reviews see for example [5, 102, 106, 115, 127]). However, apart from the regimes of asymptotically large temperature or chemical potential, a direct analytic study of the thermodynamic properties of the theory is not possible.

Even using numerical simulations, only the physics at zero chemical potential is currently accessible, since at finite μ the Euclidean action becomes complex, and the resulting oscillatory path integral cannot reliably be simulated using standard Monte-Carlo techniques.[87] Current proposals for the phase diagram of QCD and related theories are largely based on qualitative arguments and phenomenological models. While these provide a plausible picture, it is possible that they miss important features of the physics. It would certainly be satisfying to have examples of theories similar to QCD in which the full phase diagram could be explored directly.

The holographic approach

A modern route to understanding properties of strongly coupled gauge theories, that would be otherwise inaccessible, is via the AdS/CFT correspondence, or gauge theory / gravity duality. This suggests that certain quantum field theories (usually called "holographic theories"), generally with large-rank gauge groups, are equivalent to gravitational systems. By

[87] Note however that the regime of small μ/T may be accessible numerically via a perturbative expansion.

this correspondence, calculations of physical observables in the field theory are mapped to gravitational calculations; in many cases difficult strongly-coupled quantum mechanical calculations in the field theory (such as those required to understand the thermodynamic properties of QCD) are mapped to relatively simple classical gravity calculations. Optimistically, it may then be possible to find a theory qualitatively similar to QCD for which the physics at arbitrary temperature and chemical potential can be understood exactly via simple calculations in a dual gravitational system.

By now, there are well-known examples in gauge-theory / gravity duality for which the field theory shares many of the qualitative features of QCD (see, for example [120]). Further, many of these theories have been studied at finite temperature and chemical potential, revealing phase transitions associated with deconfinement, chiral symmetry breaking, meson melting, and the condensation of nuclear matter. However, to date, most of the theories that can be studied reliably using dual gravity calculations have the restriction that the number of flavors is kept fixed in the large N_c limit. In such theories, the physics at large chemical potentials is known to be qualitatively different than in real QCD. For example, at asymptotically large chemical potential, theories with large N_c and fixed N_f are believed to exhibit an inhomogeneous "chiral density wave" behavior [35, 125], rather than the homogenous quark matter phases predicted for finite N_c and N_f. In order to find examples of holographic theories which most closely resemble real QCD at finite chemical potential, one should therefore attempt to find examples of calculable gravitational systems corresponding to theories with finite N_f/N_c. This situation presents some technical challenges, as we now review.

In the well-known examples of holographic gauge theories, the addition of flavor fields in the field theory corresponds to adding D-branes on the gravity side [82]. Quarks correspond to strings which have one endpoint on these D-branes, while mesons correspond to the quantized modes of open strings which begin and end on the branes. The configurations of these D-branes in theories with finite N_f and large N_c are determined by finding action-minimizing configurations of the branes on a fixed background geometry. On the other hand, in order to have N_f of order N_c in a large N_c theory, we need a large number of these flavor branes, and these will back-react on the spacetime geometry itself. For $N_f \sim N_c$, there are as many degrees of freedom in the flavor fields as there are in the color fields (gauge fields and adjoints), so it is natural to expect that the back-reaction will be so significant that in the final description the flavor branes themselves will be completely replaced by a modified geometry with fluxes (in the same way

that the branes whose low-energy excitations give rise to the adjoint degrees of freedom do not appear explicitly in the gravity dual description of the field theory).

There has been significant progress in understanding the back-reaction of flavor branes, with some fully-back reacted analytic solutions available (for a review see [110]), but so far, there has not been enough progress to fully explore the phase structure of a QCD-like theory with finite N_f/N_c. In particular, as far as we are aware, color superconductivity phases have not been identified previously in holographic field theories.[88]

Quark matter from the bottom up

In this chapter, we aim to come up with a holographic system describing a confining gauge theory that does exhibit a quark-matter phase with color superconductivity at large chemical potential. However, motivated by recent condensed matter applications of gauge/gravity duality (see, for example [54]), we will avoid many of the technical challenges described above by taking what is known as a "bottom up" approach. Rather than working in a specific string theoretical model which takes into account the back-reaction of flavor branes, we will make an ansatz for the ingredients necessary for such a model to describe the relevant physics. We study the simplest possible gravitational theory with this minimal set of features, with the hope that it captures the qualitative physics of interest. We will indeed find that even this simple theory exhibits many of the expected features.

Ingredients

We wish to construct a gravitational theory to provide a holographic description of a four-dimensional confining gauge theory on Minkowski space with $N_f \sim N_c$ flavors. On the gravity side, the Minkowski space will appear as the fixed boundary geometry of our spacetime, but we must have at least one extra dimension corresponding to the energy scale in the field theory. Since the field theory has a scale (the QCD or confinement scale), the asymptotic behavior of the solution must exhibit an additional scale relative to the asymptotically AdS geometries that appear in gravity duals of conformal field theories. In the simplest examples of gravity duals for confining gauge theories, this scale is provided by the size of an additional

[88] However, see [30] for a possible manifestation of the related color-flavor locking phase in a holographic system.

circular direction in the geometry.[89] Thus, we will work with a gravitational system in six dimensions whose boundary geometry is $R^{3,1} \times S^1$. We will assume that the asymptotic geometry is locally Anti-de-Sitter space, so the confining gauge theory we consider arises from a five-dimensional conformal field theory compactified on a circle. When we study the theory at finite temperature, there will be an additional circle in the asymptotic (Euclidean) geometry, the Euclidean time direction whose period is $1/T$.

The gauge theories we are interested in have at least one other conserved current, corresponding to baryon (or quark) number. By the usual AdS/CFT dictionary, this operator corresponds on the gravity side to a $U(1)$ gauge field in the bulk. The asymptotic value of the time component for this gauge field corresponds to the chemical potential in our theory, while the asymptotic value of the radial electric flux corresponds to the baryon charge density in the field theory. For a given chemical potential, the minimum action solution will have some specific value for the flux, allowing us to relate density and chemical potential.

The color superconductivity phases believed to exist at large density in QCD and related theories are usually characterized by condensates of the form $\langle\psi\psi\rangle$, bilinear in the quark fields ψ, which spontaneously break the $U(N)$ gauge symmetry, and the $U(1)_B$ global symmetry. Naively, we would want to model such operators by a bulk charged scalar field corresponding to the condensate. However, bulk fields always correspond to gauge-invariant operators, while by definition the $\psi\psi$ bilinears which break the gauge symmetry are not gauge-invariant (in fact, there is no way to make a singlet from two fundamental fields, except in the case of $SU(2)$). Additionally, the simplest gauge-invariant operators charged under $U(1)_B$ involve N ψ fields and have dimension of order N, thus our holographic dual theory should have *no* light scalar fields charged under the $U(1)_B$ gauge field.

The correct way to understand the condensation of the $\psi\psi$ bilinears is as an example of spontaneously broken gauge symmetry (as in the Higgs mechanism), rather than as a phase transition characterized by some gauge-invariant order parameter. Nevertheless, the transition to color superconductivity *can* be characterized by the discontinuous behavior of gauge-invariant operators, which are of the form $\psi\psi(\psi\psi)^\dagger$. Such operators are gauge invariant and neutral under the $U(1)_B$, and therefore should correspond to an uncharged scalar field in the bulk with dimension of order 1.[90]

[89] There are other possibilities here, as we mention briefly in the discussion section.

[90] As emphasized to us by Andreas Karch, a gauge invariant operator of the form $\mathcal{O}_4 = \psi\psi(\psi\psi)^\dagger$ can be written as a sum of terms $\mathcal{O}_\alpha\mathcal{O}_\alpha$ where each $O_\alpha \sim (\psi^\dagger\psi)_\alpha$ is gauge invariant (and α represents flavor/Lorentz indices). Thus, $\mathcal{O}_4$ is something like a

Combining everything so far, we want to study gravity in six dimensions with negative cosmological constant and boundary geometry $R^{3,1} \times S^1$ with a $U(1)$ gauge field and a neutral scalar field. The simplest action for this system is[91]

$$\int d^6x\sqrt{-g}\left\{\mathcal{R} + \frac{20}{L^2} - \frac{1}{4}F^2 - |\partial_\mu\psi|^2 - m^2|\psi|^2\right\}, \tag{7.1}$$

where we include one tunable parameter, the mass m of the scalar field, which determines the dimension of the corresponding operator in the dual field theory. More generally, we could consider other potentials for the scalar field, or a more complicated action (e.g. with a Chern-Simons term or of Born-Infeld type) for the gauge field, but we restrict here to this simplest possible model.[92]

Results

Starting with the model (7.1), we have explored the phase structure by minimizing the gravitational action for specific values of temperature (corresponding to the asymptotic size of the Euclidean S^1 direction) and chemical potential (corresponding to the asymptotic value of A_0). Our results for the phase diagrams are shown in figures 7.1,7.2,7.3. For small μ, we find a confined phase at low-temperature and a deconfined phase at high temperature, with the scalar field uncondensed in each case. However, increasing μ at zero temperature, we find (setting $L_{AdS} = 1$) for $-\frac{25}{4} \leq m^2 \leq -5$ a transition to a phase with nonzero scalar condensate (on a geometry with horizon) and finite homogeneous quark density, as expected for a color superconductivity phase. Increasing the temperature from zero, we find a transition back to the deconfined phase at a remarkably low temperature; for example, at $m^2 = -6$, the critical temperature at which superconductivity disappears is

$$T/\mu \sim .00006333\ .$$

double-trace operator. In a large N theory, factorization of correlators implies that the expectation value of $\mathcal{O}_4$ can be calculated classically from the $\mathcal{O}_\alpha$ expectation values (up to $1/N$ corrections). Thus, discontinuous behavior of $\mathcal{O}_4$ should be directly related to discontinuous behavior in the simpler gauge-invariant operators O_α (which also have no baryon charge), so it may be more appropriate to think of the scalar field in our model as being dual to one of these simpler operators.

[91] Since we will also consider the case of a charged scalar field, we have written the action using standard normalizations for a complex scalar, but we will take the scalar to be real in the uncharged case.

[92] For another approach to modeling the QCD phase diagram by an effective holographic approach, see for example [36, 55].

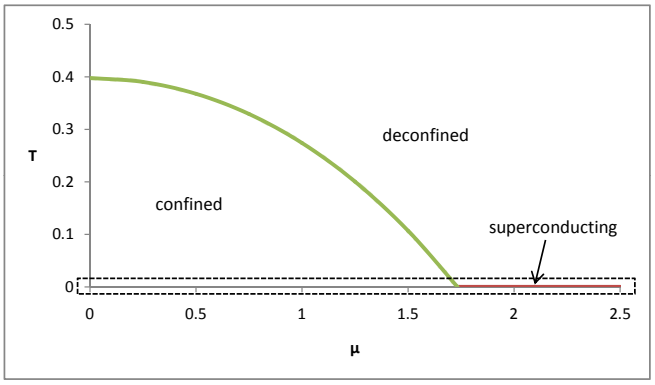

Figure 7.1: Phase diagram of our model gauge theory with $m^2 = -6$, $R = 2/5$. Region in dashed box is expanded in next figure.

The tendency for the scalar field to condense at low temperatures for the range of masses above can be understood in a simple way, as explained for example in [60, 74]. In $d+1$-dimensional anti-de Sitter space with anti-de Sitter radius L, the minimum mass for a scalar field to avoid instability is $m^2_{BF} = -d^2/(4L^2)$. The minimum action solution for large chemical potential in the absence of any scalar field is a planar Reissner-Nordstrom black hole solution with one of the isometry directions periodically identified. In the limit of zero temperature, the near horizon region of this black hole has geometry $AdS^2 \times R^4$, with the radius of the AdS^2 equal to $L_2 = L/\sqrt{20}$. Thus, in the near-horizon region, there will be an instability toward condensation of the scalar field if $m^2 < -1/(4L_2^2) = -5/L^2$. We thus have a range (setting $L = 1$) of $-25/4 \leq m^2 \leq -5$ for which the scalar field tends to condense in the near-horizon region but is stable in the asymptotic region. Numerical simulations verify that we indeed have scalar field condensation for precisely this range of masses.

While there is no guarantee that the gravitational system we study has a legitimate field theory dual, "top-down" gravitational systems corresponding to fully consistent field theories must have the same basic elements (usually with additional fields and a more complicated Lagrangian). The fact that the expected physics emerges even in our stripped-down version suggests

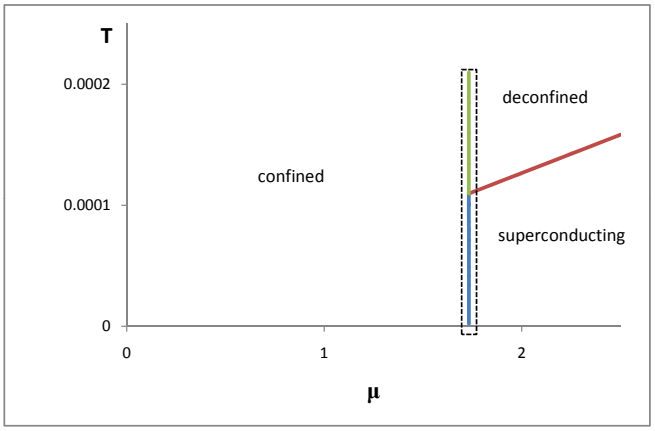

Figure 7.2: Phase diagram of our model gauge theory with $m^2 = -6$, $R = 2/5$. Region in dashed box is expanded in next figure.

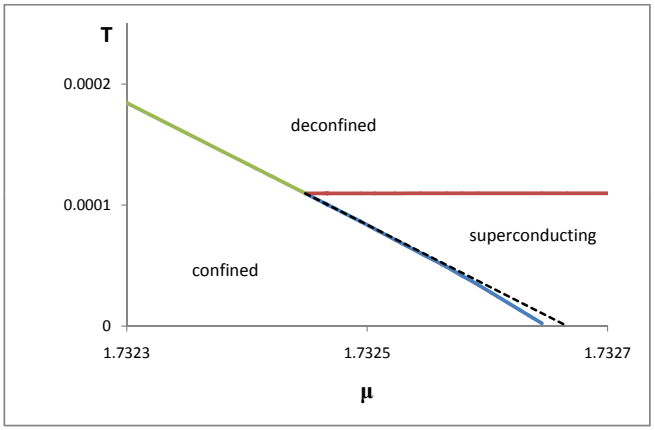

Figure 7.3: Phase diagram of our model gauge theory with $m^2 = -6$, $R = 2/5$. The dashed curve represents the phase boundary in theory without a scalar field.

that quark-matter phases will be found also in the complete models, once back-reaction effects are under control. Optimistically, qualitative features that we find in the bottom-up model (such as the extremely low transition temperature between superconducting and deconfined phases) may be present also in more complete holographic theories. In this case, our simple model may provide novel qualitative insights into fully consistent QCD-like theories.

Charged scalar

While less relevant to color superconductivity, it is also interesting to explore the physics of our model when we make the scalar field charged under the gauge field. In this case, the scalar field corresponds to a gauge-invariant operator in the field theory that is charged under the $U(1)$ associated with A, and the kinetic term for the scalar field is modified in the usual way as $\partial_\mu\psi \to \partial_\mu\psi - iqA_\mu\psi$. As we have argued above, this symmetry cannot be $U(1)_B$, but could be another flavor symmetry, such as isospin in a model with two or more flavors. The flavor superconductivity associated with meson condensation was studied previously in the holographic context (with finite N_f), for example in [7, 8, 17]. Our results are qualitatively similar to the ones obtained in those studies, and we leave more detailed comparison for future work.

In section 5 below, we determine the phase diagram for various values of q and m. The same system was studied for the 2+1 dimensional case in [68] and originally in [107] for the case of large q. The application there was to holographic insulator/superconductor systems, but the intriguing resemblance of the phase diagrams in those papers to QCD phase diagrams partially motivated the present study.

7.2 Basic setup

In this chapter, we consider holographic field theories with a conserved current J^μ, assumed to be a baryon current (or isospin current when we consider charged scalar fields) and some gauge-invariant operator $\mathcal{O}$ whose condensation indicates the onset of (color or flavor) superconductivity. We would like to explore the phase structure of the theory for finite temperature T and chemical potential μ; that is, we would like to find the phase that minimizes the Gibbs free energy density $g = e - Ts - \mu\rho$, where e, s, and ρ are the energy density, entropy density, and charge density in the field theory. We

can also ask about the values of e, s, ρ, and $\langle \mathcal{O} \rangle$ as a function of temperature and chemical potential.

As discussed in the introduction, our holographic theories are defined by a dual gravitational background which involves a metric, $U(1)$ gauge field, and scalar field, with a simple action

$$\int d^6x\sqrt{-g}\left\{\mathcal{R} + \frac{20}{L^2} - \frac{1}{4}F^2 - |\partial_\mu\psi|^2 - m^2|\psi|^2\right\} . \tag{7.2}$$

We choose coordinates (t, x, y, z) for the non-compact field theory directions, w for the compact field theory direction, and r for the radial direction. We take boundary conditions for which the asymptotic (large r) behavior of the metric is

$$ds^2 \;\rightarrow\; \left(\frac{r}{L}\right)^2 \left(-dt^2 + dx^2 + dy^2 + dz^2 + dw^2\right) + \left(\frac{L}{r}\right)^2 dr^2 ,$$

where w is taken to be periodic with period R. To study the theory at finite temperature, we take the period of $\tau = it$ in the Euclidean solution to be $1/T$.

The equations of motion constrain the gauge field to behave asymptotically as

$$A_\nu = a_\nu - \frac{j_\nu}{3r^3} + \dots .$$

Since A_ν is assumed to be the field corresponding to the conserved baryon current operator J^ν, in the field theory, the usual AdS/CFT dictionary tells us that a_ν is interpreted as the coefficient of the J^ν in the Lagrangian (i.e. an external source for the baryon current) while j_μ is interpreted as the expectation value of baryon current for the state corresponding to the particular solution we are looking at. To study the theory at finite chemical potential μ without any external source for the spatial components of the baryon current, we want to take

$$a_\nu = (\mu, 0, 0, 0) .$$

The scalar field equations of motion imply that asymptotically

$$\psi = \frac{\psi_1}{r^{\lambda_-}} + \frac{\psi_2}{r^{\lambda_+}} + \cdots , \tag{7.3}$$

where

$$\lambda_\mp = \frac{1}{2}(d \mp \sqrt{d^2 + 4m^2}) .$$

The holographic field theories we consider are defined by assuming $\psi_1 = 0$. In this case, λ_+ gives the dimension of the operator dual to ψ.[93] In this case, ψ_2 (which will be different for solutions corresponding to different states of the field theory) gives us the expectation value of the operator $\mathcal{O}$ in the field theory.

By the AdS/CFT correspondence, the field theory free energy corresponds to the Euclidean action of the solution. Thus, to investigate the field theory state which minimizes free-energy for given T and μ, we need to find the gravitational solution with boundary conditions given above which minimizes the Euclidean action. Note that we only consider solutions with translation invariance in t, x, y, z, and w. It would be interesting to investigate the possibility of inhomogeneous phases (or at least the stability of our solutions to inhomogeneous perturbations) but we leave this as a question for future work.

Calculating the action

In order to obtain finite results when calculating the gravitational action for a solution, it is important to include boundary contributions to the action. In terms of the Lorentzian metric, gauge field and scalar, the fully regulated expression that we require is [54]

$$\begin{aligned} S &= \lim_{r_M \to \infty} \left[- \int_{r<r_M} d^{d+1}x \sqrt{-g} \left\{ \mathcal{R} + \frac{d(d-1)}{L^2} - \frac{1}{4} F^2 - |D_\mu \psi|^2 - m^2 |\psi|^2 \right\} \right. \\ &\quad \left. + \int_{r=r_M} d^d x \sqrt{-\gamma} \left\{ -2K + \frac{2(d-1)}{L} - \frac{1}{L} \lambda_- |\psi|^2 \right\} \right] , \end{aligned}$$

where

$$\lambda_- = \frac{d}{2} - \frac{1}{2} \sqrt{d^2 + 4m^2} \, .$$

Here, γ is the metric induced on the boundary surface $r = r_M$, and K is defined as

$$K = \gamma^{\mu\nu} \nabla_\mu n_\nu \, ,$$

where n^μ is the outward unit normal vector at $r = r_M$. The scalar counterterm here is the appropriate one assuming that our boundary condition is to fix the coefficient of the leading term in the large r expansion of ψ. Since we are setting this term to zero, it turns out that the counterterm vanishes in the $r_M \to \infty$ limit.

[93] For a certain range scalar field masses in the range $-d^2/4 \leq m^2 \leq -d^2/4 + 1$, it is also consistent to define a theory by fixing $\psi_2 = 0$. In this case, the dimension of the dual operator is λ_-. We consider this case briefly in section 4.2.

For all cases we consider, the metric takes the form

$$ds^2 = \frac{r^2}{L^2} dx_i^2 + g_{00}(r) dt^2 + g_{rr}(r) dr^2 + g_{ww}(r) dw^2 \ . \tag{7.4}$$

Assuming the Einstein equations are satisfied, we can show (by subtracting a term proportional to the xx component of the equation of motion) that the integrand in the first term may be written as a total derivative with respect to r

$$-\sqrt{-g}\left\{\mathcal{R} + \frac{d(d-1)}{L^2} - \frac{1}{4}F^2 - |D_\mu \psi|^2 - m^2|\psi|^2\right\} = \partial_r \left(\frac{2}{r g_{rr}}\sqrt{-g}\right) \ .$$

Using

$$n_\mu = (0, \ldots, 0, \sqrt{g_{rr}}) \ ,$$

we have

$$\begin{aligned} K &= \gamma^{\mu\nu}\nabla_\mu n_\nu \\ &= \gamma^{\mu\nu}\left\{-\Gamma^r_{\mu\nu} n_r\right\} \\ &= \gamma^{\mu\nu}\left\{\frac{1}{2} g^{rr}\frac{\partial g_{\mu\nu}}{\partial r}\sqrt{g_{rr}}\right\} \\ &= \frac{1}{2\sqrt{g_{rr}}}\gamma^{\mu\nu}\frac{\partial \gamma_{\mu\nu}}{\partial r} \\ &= \frac{1}{\sqrt{g_{rr}}}\frac{\partial \ln(\sqrt{-\gamma})}{\partial r} \end{aligned}$$

so that

$$\sqrt{-\gamma}(-2K) = -\frac{2}{\sqrt{g_{rr}}}\frac{\partial\sqrt{-\gamma}}{\partial r} \ .$$

Our final expression for the action density is

$$S/V_d = \frac{2}{r g_{rr}}\sqrt{-g}\Big|_{r_0}^{r_M} + \left\{-\frac{2}{\sqrt{g_{rr}}}\frac{\partial\sqrt{-\gamma}}{\partial r} + \frac{2(d-1)}{L}\sqrt{-\gamma}\right\}_{r=r_M} \ . \tag{7.5}$$

Action in terms of asymptotic fields

It is convenient to rewrite the expression (7.5), in terms of the asymptotic expansion of the fields. For the ansatz (7.4), and the boundary conditions appropriate to our case, we find

$$g_{tt} = -r^2 + \frac{g_{tt}^{(3)}}{r^3} + \ldots \ ,$$

$$\begin{aligned} g_{rr} &= \frac{1}{r^2} + \frac{g_{rr}^{(7)}}{r^7} + \dots \ , \\ g_{ww} &= r^2 + \frac{g_{ww}^{(3)}}{r^3} + \dots \ , \\ \psi &= \frac{\psi^{(3)}}{r^3} + \dots \ , \\ \phi &= \mu - \frac{\rho}{3r^3} + \dots \ . \end{aligned}$$

Inserting these expansions into our expression above for the action we find that (assuming the term at $r = r_0$ vanishes)

$$S = 5g_{ww}^{(3)} + 4g_{rr}^{(7)} - 5g_{tt}^{(3)} \ .$$

However, using the equations of motion, we find that $g_{ww}^{(3)} + g_{rr}^{(7)} - g_{tt}^{(3)} = 0$, so we can simplify to:

$$S = -g_{rr}^{(7)} \ . \tag{7.6}$$

Numerically, it can be a bit tricky to read off $g_{rr}^{(7)}$ because there is also a $1/r^8$ term in the expansion of g_{rr}. But using the equations of motion, we can find

$$g_{rr}^{(8)} = \frac{3}{4}(7 + m^2)(\psi^{(3)})^2 \ .$$

From this, it follows that the combination

$$-r^7 g_{rr}(r) + r^5 - \frac{3}{4}(7 + m^2) r^5 \psi^2(r)$$

behaves like

$$-g_{rr}^{(7)} + \mathcal{O}(1/r^3) \ .$$

So, we can numerically evaluate the action by taking

$$S \approx -r_*^7 g_{rr}(r_*) + r_*^5 - \frac{3}{4}(7 + m^2) r_*^5 \psi^2(r_*) \ ,$$

where r_* is taken to be large but not too close to the cutoff value.

7.3 Review: $\psi = 0$ solutions

We begin by considering the solutions for which the scalar field is set to zero.

7.3.1 AdS Soliton solution

At zero temperature and chemical potential, the simplest solution with our boundary conditions is pure AdS with periodically identified w. However, assuming antiperiodic boundary conditions for any fermions around the w circle, there is another solution with lower action. This is the AdS soliton [65], described by the metric (setting $L = 1$)

$$ds^2 = r^2 \left(-dt^2 + dx^2 + dy^2 + dz^2 + f(r)\, dw^2\right) + \frac{dr^2}{r^2 f(r)} , \tag{7.7}$$

where

$$f(r) = 1 - \frac{r_0^5}{r^5} . \tag{7.8}$$

As long as we choose the period $2\pi R$ for w such that

$$r_0 = \frac{2}{5\, R} \tag{7.9}$$

the solution smoothly caps off at $r = r_0$. This IR end of the spacetime corresponds in the field theory to the fact that we have a confined phase with a mass gap. The fluctuation spectrum about this solution corresponds to a discrete spectrum of glueball states in the field theory.

Starting from this solution, we can obtain a solution valid for any temperature and chemical potential, by periodically identifying the Euclidean time direction and setting $A_0 = \mu$ everywhere. Using (7.6) we find that the action for this solution is

$$S_{sol} = -r_0^5 = -\left(\frac{2}{5R}\right)^5 .$$

The negative value indicates that this solution is preferred over the pure AdS solution with action zero.

7.3.2 Reissner-Nordstrom black hole solution

For sufficiently large temperature and/or chemical potential, the AdS soliton is no longer the $\psi = 0$ solution with minimum action. The preferred solution is the planar Reissner-Nordstrom black hole, with metric

$$ds^2 = r^2 \left(-dt^2 f(r) + dx^2 + dy^2 + dz^2 + dw^2\right) + \frac{dr^2}{r^2 f(r)} , \tag{7.10}$$

where

$$f(r) = 1 - \left(1 + \frac{3\mu^2}{8r_+^2}\right)\frac{r_+^5}{r^5} + \frac{3\mu^2 r_+^6}{8r^8}\ , \tag{7.11}$$

the scalar potential is

$$\phi(r) = \mu\left(1 - \frac{r_+^3}{r^3}\right)\ ,$$

and w is periodically identified as before.

This solution has a horizon at $r = r_+$. The temperature of the solution (determined as the inverse period of the Euclidean time for which the Euclidean solution is smooth) is given in terms of r_+ by

$$T = \frac{1}{4\pi}\left(5r_+ - \frac{9\mu^2}{8r_+}\right)\ . \tag{7.12}$$

From (7.6), we find that the action for this solution is

$$S_{RN} = -r_+^5\left(1 + \frac{3}{8}\frac{\mu^2}{r_+^2}\right)\ .$$

Thus, we find that the black hole solution has lower action than the soliton for

$$r_+\left(1 + \frac{3}{8}\frac{\mu^2}{r_+^2}\right)^{\frac{1}{5}} > \frac{2}{5R}\ ,$$

where r_+ is determined in terms of T and μ by (7.12). This defines a curve in the $T-\mu$ plane that begins on the $\mu = 0$ axis at $T = 1/(2\pi R)$ and curves down to the $T = 0$ axis at $\mu = 2^{19/10}/(5^{1/2}3^{4/5}R) \approx 4.3547/(2\pi R)$, as shown in figure 7.4.

As usual, the existence of a horizon in this solution indicates that the corresponding field theory state is in a deconfined phase [141].

In the next sections, we consider solutions with nonzero scalar field. We will find that for large μ there exist solutions with nonzero scalar field that have lower action than the solutions we have considered, so the phase diagram of figure 7.4 will be modified.

7.4 Neutral scalar field: color superconductivity

In the case of a neutral scalar field, our simple model has no explicit source for the gauge field in the bulk, so homogeneous solutions with a non-trivial

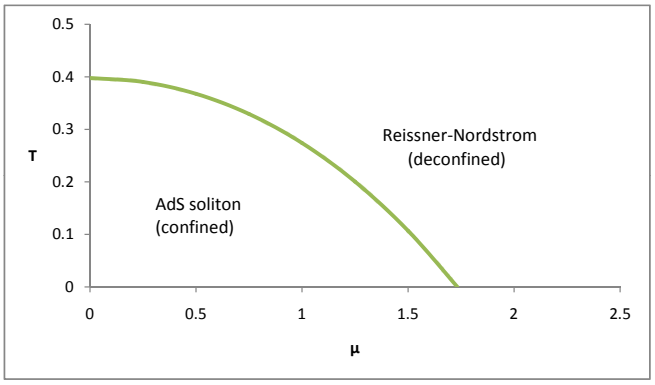

Figure 7.4: Phase diagram without scalar field, in units where $R = 2/5$.

static electric field (corresponding to a non-zero baryon number density in the field theory) necessarily have a horizon from which the flux can emerge[94].

To look for solutions of this form, we consider the ansatz[95]

$$\begin{aligned} ds^2 &= -g(r)e^{-\chi(r)}dt^2 + \frac{dr^2}{g(r)} + r^2(dw^2 + dx^2 + dy^2 + dz^2) \,, \\ A_t &= \phi(r) \,, \\ \psi &= \psi(r) \,. \end{aligned}$$

The scalar and Maxwell's equations that follow from the action (7.2) are

$$\psi'' + \left(\frac{4}{r} - \frac{\chi'}{2} + \frac{g'}{g}\right)\psi' - \frac{m^2}{g}\psi = 0 \,, \tag{7.13}$$

$$\phi'' + \left(\frac{4}{r} + \frac{\chi'}{2}\right)\phi' = 0 \,, \tag{7.14}$$

[94] In a more complete model, the source might be provided by some non-perturbative degrees of freedom in the theory, such as the wrapped D-branes that give rise to baryons in the Sakai-Sugimoto model.

[95] We could have considered a more complicated ansatz, with an extra undetermined function in front of dw^2. However, it is plausible that as for the $\psi = 0$ solution, the minimum action solution for the case where the w circle does not contract in the bulk is a periodic identification of the solution with non compact w and rotational invariance in the x, y, z, w directions.

while the Einstein equations are satisfied if

$$\chi' + \frac{r\psi'^2}{2} = 0 \,, \tag{7.15}$$

$$g' + \left(\frac{3}{r} - \frac{\chi'}{2}\right) g + \frac{re^{\chi}\phi'^2}{8} + \frac{m^2 r\psi^2}{4} - 5r = 0 \,. \tag{7.16}$$

These have two symmetries:

$$\tilde{\psi}(r) = \psi(ar) \,, \qquad \tilde{\phi}(r) = \frac{1}{a}\phi(ar) \,, \qquad \tilde{\chi}(r) = \chi(ar) \,, \qquad \tilde{g}(r) = \frac{1}{a^2} g(ar) \,, \tag{7.17}$$

arising from the underlying conformal invariance, and

$$\tilde{\chi} = \chi + \Delta \,, \qquad \tilde{\phi} = e^{-\frac{\Delta}{2}}\phi \,. \tag{7.18}$$

We would like to find solutions with a horizon at some $r = r_+$. The electric potential must also vanish at the horizon, and we are looking for solutions for which the leading falloff ψ_1 in (7.3) vanishes for the scalar. Also, multiplying the first equation (7.13) by g and evaluating at $r = r_+$ fixes $\psi'(r_+)$ in terms of $\psi(r_+)$ and $g'(r_+)$. Altogether, our boundary conditions are

$$g(r_+) = 0 \,, \qquad \phi(r_+) = 0 \,, \qquad \chi(\infty) = 0 \,, \qquad \psi_1 = 0 \,,$$

and

$$\psi'(r_+) = \frac{8m^2\psi(r_+)}{40r_+ - 2m^2 r_+^2\psi^2(r_+) - r_+ e^{\chi(r_+)}(\phi'(r_+))^2} \,.$$

The remaining freedom to choose r_+ and $\phi'(r_+)$ leads to a family of solutions with different T and μ. Explicitly, we have

$$\mu = \phi(\infty) \,, \qquad\qquad T = \frac{1}{4\pi} g'(r_+) e^{-\chi(r_+)/2} \,.$$

Note that solutions with the same T/μ are simply related by the scaling symmetry (7.17).

7.4.1 Numerical evaluation of solutions

To find solutions in practice, we can make use of the symmetries (7.17) to initially set $r_+ = 1$ and $\chi(0) = 0$ and solve the equations with boundary conditions

$$g(1) = 0 \,, \qquad \chi(0) = 0 \,, \qquad \phi(1) = 0 \,, \qquad \phi'(1) = E_0 \,, \qquad \psi(1) = \psi_0 \,,$$

and

$$\psi'(1) = \frac{8m^2\psi_0}{40 - 2m^2\psi_0^2 - E_0^2} \ .$$

We can integrate the ϕ and χ equations explicitly to obtain

$$\begin{aligned} \chi(r) &= -\int_0^r d\tilde{r}\frac{1}{2}\tilde{r}\left(\frac{\partial\psi}{\partial r}\right)^2 \ , \\ \phi(r) &= E_0\int_1^r \frac{d\tilde{r}}{\tilde{r}^4}e^{-\frac{1}{2}\chi(\tilde{r})} \ , \end{aligned}$$

leaving the remaining equations

$$\begin{aligned} \psi'' + (\frac{4}{r} + \frac{r\psi'^2}{4} + \frac{g'}{g})\psi' - \frac{m^2}{g}\psi &= 0 \ , \\ g' + \frac{3g}{r} + \frac{gr}{4}\psi'^2 + \frac{E_0^2}{8r^7} + \frac{m^2r\psi^2}{4} - 5r &= 0 \ . \end{aligned}$$

We use E_0 as a shooting parameter to enforce $\psi_1 = 0$, and find one solution for each ψ_0. From these solutions, we apply the symmetry (7.18) with $\Delta = -\chi(\infty)$ to restore $\chi(\infty) = 0$ and finally use the symmetry (7.17) to scale to the desired temperature or chemical potential.

Using this method, we find that solutions exist for scalar mass in the range $-25/4 \leq m^2 \leq 5$, which is exactly the range of masses for which the scalar is stable in the asymptotic region but unstable in the near-horizon region.[96] For a given m^2 in this range, solutions exist in the region $T/\mu < \gamma(m^2)$, where $\gamma(m^2)$ is a dimensionless number depending on m^2 (which we evaluate in the next section). The value of $\gamma(m^2)$ is remarkably small for all m^2 in the allowed range. For example, with $m^2 = -6$ (not particularly close to the limiting value $m^2 = -5$), we have $\gamma \approx .00006333$. It would be interesting to understand better how this small dimensionless number emerges since the setup has no small parameters. From the bulk point of view it is presumably related to the warping between IR and UV regions of the geometry.[97] From the boundary viewpoint, the low critical temperature may be explained by the BKL scaling [74, 76, 80] near a quantum critical point[98].

[96] Solutions of this form were first found in lower dimensions in [60]. The zero-temperature limit of such solutions were considered in [67].

[97] By considering the alternate quantization mentioned in section 2 and fine-tuning the mass so that the dual operator has the smallest possible dimension consistent with unitarity in the dual field theory, we can obtain γ as large as 0.0151, so even under the most favorable circumstances, the critical T/μ is quite small.

[98] We thank D.T. Son for pointing this out to us.

For a given T and μ, we can use (7.6) to evaluate the action for the solution and compare this with the action for the soliton and/or Reissner-Nordstrom solution with the same T and μ. We find that the action for the new solutions is always less than the action for the Reissner-Nordstrom solutions, and is also less than the action for the soliton solutions for chemical potential in a region $\mu > \mu_c(T)$. Thus, the solutions with scalar field represent the equilibrium phase in the region $T/\mu < \gamma, \mu > \mu_c(T)$, as shown in figures 7.1- 7.3 above.

The transition between the deconfined and superconducting phases is second order, while the transition between confined and superconducting phases is first order. The place where these phase boundaries meet represents a triple point for the phase diagram where the three phases (confined, deconfined, superconducting) can coexist.

7.4.2 Critical temperature

For fixed m^2, the value of $\psi(0)$ in the solutions increases from zero at $T/\mu = \gamma$, diverging as $T/\mu \to 0$. Since ψ is small everywhere near $T/\mu = \gamma$, the critical value of T/μ will be the value where the ψ equation, linearized around the Reissner-Nordstrom background, has a solution with the correct boundary conditions. Thus, we consider the equation

$$\psi'' + (\frac{4}{r} + \frac{g'}{g})\psi' - \frac{m^2}{g}\psi = 0 \ , \tag{7.19}$$

where (setting $r_+ = 1$)

$$g(r) = r^2 - \left(1 + \frac{3\mu^2}{8}\right)\frac{1}{r^3} + \frac{3\mu^2}{8r^6} \ ,$$

and find the value $\mu = \mu_c$ for which the equation admits a solution with boundary conditions $\psi(1) = 1$ (we are free to choose this), $\psi'(1) = m^2/g'(1)$ and the right falloff ($\psi_1 = 0$) at infinity.[99]

The choice $r_+ = 1$ implies that $T = (5 - 9\mu^2/8)/(4\pi)$, so we have $\gamma = (5 - 9\mu_c^2/8)/(4\pi\mu_c)$. The results for $\gamma(m^2)$ are plotted in figure 7.5. For comparison, we also considered the theory defined with the alternate

[99] To obtain a very accurate result, we first find a series solution ψ_{low} near $r = 1$ with $\psi(1) = 1$ (we are free to choose this) and $\psi'(1) = m^2/g'(1)$ and find a series solution ψ_{high} for large r with the correct fall-off ($\psi_1 = 0$) at infinity. Starting with ψ_{low} and ψ'_{low} at some $r = r_1$ where the low r series solution is still very accurate, we then numerically integrate up to $r = r_2$ where the large r series is very accurate and then find μ for which $\psi'_{num}(r_2)/\psi_{num}(r_2) = \psi'_{high}/\psi_{high}$.

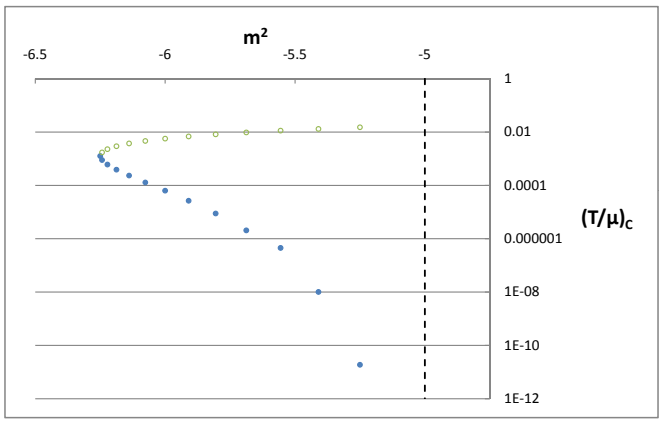

Figure 7.5: Critical T/μ vs m^2 of neutral scalar (filled circles). Mass is above BF bound asymptotically but below BF bound in near-horizon region of zero-temperature background solution in the range $-6.25 \leq m^2 < -5$. Unfilled circles represent critical values in the theory with alternate quantization of the scalar field, possible in the range $-6.25 \leq m^2 < -5.25$.

quantization ($\psi_2^\infty = 0$) of the bulk scalar field (mentioned in section 2). As we see in figure 7.5, the critical temperatures are somewhat larger in this case, but still much smaller than 1 relative to μ.

7.4.3 Properties of the superconducting phase

In the superconducting phase, it is interesting to ask how the charge density and free energy behave as a function of chemical potential. Since the solutions (as for the planar RN-black hole solutions) are trivially related to solutions where the w direction is non-compact, and since the underlying theory has a conformal symmetry, physical quantities in this phase (or in the RN phase) behave as $\mu^n F(T/\mu)$ for some non-trivial function F and a power n.[100] At the critical value of T/μ, we have a second order transition from the RN phase to the phase with scalar, so the free energy and its derivatives, and other physical quantities such as the density, are continuous

[100] If the solutions instead depended on the circle direction in a non-trivial way, we might have a general function of RT and $R\mu$.

across the transition. Thus, the relevant function F in these cases will be the same for the two phases across the transition. We find that the function F for either the charge density or the free energy changes very little between the very small value of T/μ where the the transition occurs and the $T \to 0$ limit. Thus, to a good approximation, we find that the density and free energy behave in the superconducting phase in the same way as for the zero temperature limit of the RN phase. For R=2/5, we have

$$\rho \approx 0.320\mu^4 \ ,$$

while

$$G \approx -.064\mu^5 \ .$$

In both cases, the behavior at large μ is governed by the underlying 4+1 dimensional conformal field theory.

7.5 Charged scalar field: flavor superconductivity

In this section, we generalize our holographic model to the case where the scalar field is charged under the gauge field in the bulk. As we discussed in the introduction, this implies that the dual field theory includes some low-dimension gauge-invariant operator with charge, so the charge in this case is more naturally thought of as some isospin-type charge (since the smallest gauge-invariant operators carrying baryon charge have dimensions of order N).

A significant qualitative difference in this case is that a scalar field condensate acts as a source for the electric field in the bulk, so it is possible to have solutions with no horizon carrying a finite charge density in the field theory. This gives the possibility of a fourth phase in which the scalar field condenses in the soliton background.

To obtain the action for the charged scalar case, we begin with the action (7.2) and make the replacement $\partial_\mu\psi \to \partial_\mu\psi - iqA_\mu\psi$. The results of the previous section correspond to $q = 0$.

7.5.1 Low-temperature horizon free solutions with scalar

Above some critical value of μ, there exist horizon-free geometries with a scalar field condensate. The solutions may be parameterized by the magnitude of the scalar at the IR tip of the geometry, and we will find a single solution for each such value. To determine these geometries, we need to take

into account back-reaction on the metric. The most general solution with the desired properties can be described by the ansatz

$$\begin{aligned} ds^2 &= r^2(e^{A(r)}B(r)dw^2 + dx^2 + dy^2 + dz^2 - e^{C(r)}dt^2) + \frac{dr^2}{r^2 B(r)} , \\ A_t &= \phi(r) , \\ \psi &= \psi(r) , \end{aligned} \tag{7.20}$$

where we demand $A(\infty) = C(\infty) = 0$ and $B(\infty) = 1$. As for the soliton geometry, we expect that the w circle is contractible in the bulk so that $B(r_0) = 0$ for some r_0. For the geometry to be smooth at this point, the periodicity of the w direction must be chosen so that

$$2\pi R = \frac{4\pi e^{-A(r_0)/2}}{r_0^2 B'(r_0)} . \tag{7.21}$$

Starting from the action (7.2) with scalar derivatives replaced by covariant derivatives, the scalar and Maxwell equations are:

$$\psi'' + \left(\frac{6}{r} + \frac{A'}{2} + \frac{B'}{B} + \frac{C'}{2}\right)\psi' + \frac{1}{r^2 B}\left(\frac{e^{-C}(q\phi)^2}{r^2} - m^2\right)\psi = 0 , \tag{7.22}$$

$$\phi'' + \left(\frac{4}{r} + \frac{A'}{2} + \frac{B'}{B} - \frac{C'}{2}\right)\phi' - \frac{2\psi^2 q^2 \phi}{r^2 B} = 0 . \tag{7.23}$$

Following [68], we find that the Einstein equations give:

$$A' = \frac{2r^2 C'' + r^2 C'^2 + 4rC' + 4r^2\psi'^2 - 2e^{-C}\phi'^2}{r(8 + rC')} , \tag{7.24}$$

$$C'' + \frac{1}{2}C'^2 + \left(\frac{6}{r} + \frac{A'}{2} + \frac{B'}{B}\right)C' - \left(\phi'^2 + \frac{2(q\phi)^2\psi^2}{r^2 B}\right)\frac{e^{-C}}{r^2} = 0 , \tag{7.25}$$

$$\begin{aligned} B'\left(\frac{4}{r} - \frac{C'}{2}\right) + B\left(\psi'^2 - \frac{1}{2}A'C' + \frac{e^{-C}\phi'^2}{2r^2} + \frac{20}{r^2}\right) + \\ \frac{1}{r^2}\left(\frac{e^{-C}(q\phi)^2\psi^2}{r^2} + m^2\psi^2 - 20\right) = 0 . \end{aligned} \tag{7.26}$$

These equations have two scaling symmetries,

$$\begin{aligned} \tilde{\psi}(r) = \psi(ar) , \qquad \tilde{\phi}(r) = \frac{1}{a}\phi(ar) , \qquad \tilde{A}(r) = A(ar) , \\ \tilde{B}(r) = B(ar) , \qquad \tilde{C}(r) = C(ar) , \end{aligned} \tag{7.27}$$

and

$$\tilde{C} = C + \Delta , \qquad \tilde{\phi} = e^{\frac{\Delta}{2}}\phi . \tag{7.28}$$

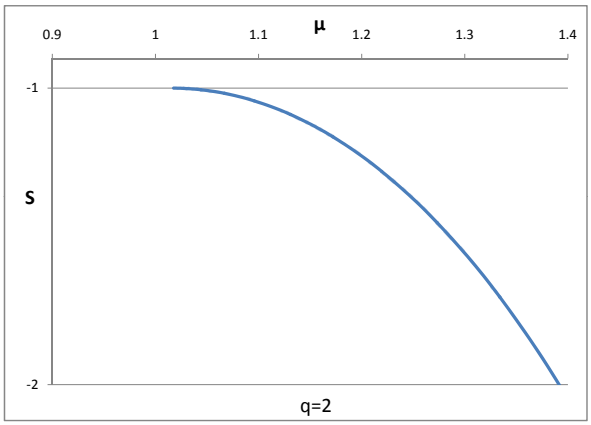

Figure 7.6: Action vs chemical potential for soliton with scalar solutions, taking $m^2 = -6$ and $q = 2$.

Numerical evaluation of solutions

To find solutions, we first use the scaling symmetries to fix $r_0 = 1$ and $C(r_0) = 0$. For each value of $\psi(1)$, we use $\phi(1)$ as a shooting parameter, choosing the value so that ψ has the desired behavior for large r. From the solution obtained in this way, we can use (7.28) with $\Delta = -C(\infty)$ to obtain the desired boundary condition $C(\infty) = 0$ in the rescaled solution. From (7.21), we see that the choice $r_0 = 1$ corresponds to a periodicity for the w direction equal to

$$2\pi R = \frac{4\pi e^{-A(1)/2}}{B'(1)} \,. \tag{7.29}$$

which will generally be different for solutions corresponding to different values of $\psi(1)$. In order to obtain solutions corresponding to our chosen value $R = 2/5$ (such that the action for the soliton solution is -1) we use the scaling (7.27), taking $a = B'(1)/5e^{-A(\infty)/2}$. After all the scalings, we calculate the chemical potential and action (making use of (7.6)) as

$$\mu = \phi(\infty) \,, \qquad\qquad S = [B]_{\frac{1}{r^5}} \,.$$

The action is plotted against chemical potential for various values of q in figures 7.6, 7.7, and 7.8 taking the example of a mass just above the BF bound, $m^2 = -6$.

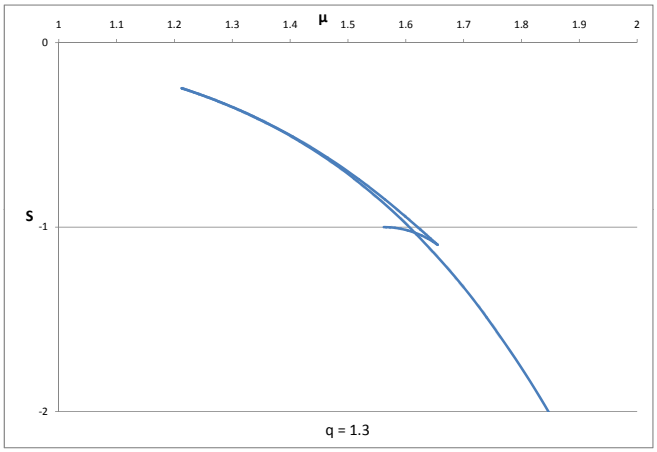

Figure 7.7: Action vs chemical potential for soliton with scalar solutions, taking $m^2 = -6$ and $q = 1.3$.

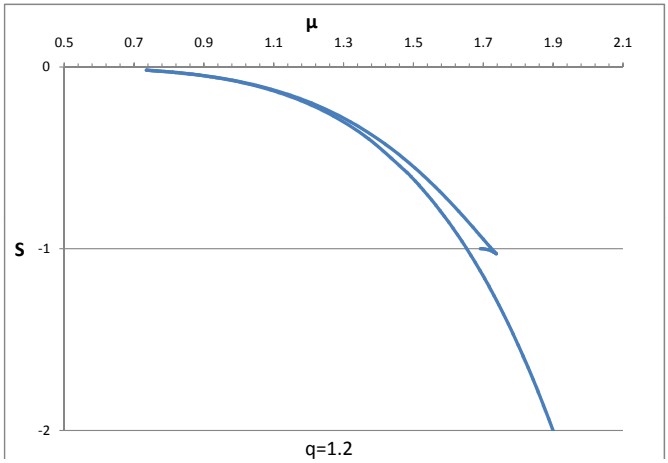

Figure 7.8: Action vs chemical potential for soliton with scalar solutions, taking $m^2 = -6$ and $q = 1.2$.

We find that for large enough values of q, the chemical potential increases monotonically and the action decreases monotonically as we increase $\psi(r_0)$. This implies that we have a second order transition to the superconducting phase at a critical value, which can be determined by a linearized analysis (see appendix A) to be $\mu \approx 1.0125/q$.

Below $q \approx 1.35$, the chemical potential is no longer monotonic in $\psi(r_0)$. We see that for $q = 1.3$, this results in a second order phase transition at $\mu \approx 1.558$, followed by a first order phase transition at $\mu \approx 1.616$ (taking $R = 2/5$). For smaller q (e.g. $q = 1.2$ in figure 7.8), we simply have a first order transition to the superconducting phase at a value of chemical potential that is less than the value for the solution with infinitesimal scalar field. All of these results are completely analogous to the lower-dimensional results of [68].

7.5.2 Hairy black hole solutions

At high temperatures, the w circle is no longer contractible, and we assume that (as for the solutions without scalar field) the solution can be obtained by periodic identification of a solution with boundary $R^{4,1}$ instead of $R^{3,1} \times S^1$. Thus, we take the ansatz

$$\begin{aligned} ds^2 &= -g(r)e^{-\chi(r)}dt^2 + \frac{dr^2}{g(r)} + r^2(dw^2 + dx^2 + dy^2 + dz^2) \,, \\ A_t &= \phi(r) \,, \\ \psi &= \psi(r) \,. \end{aligned}$$

The scalar and Maxwell's equations are

$$\psi'' + \left(\frac{4}{r} - \frac{\chi'}{2} + \frac{g'}{g}\right)\psi' + \frac{1}{g}\left(\frac{e^{\chi}q^2\phi^2}{g} - m^2\right)\psi = 0 \,, \tag{7.30}$$

$$\phi'' + \left(\frac{4}{r} + \frac{\chi'}{2}\right)\phi' - \frac{2q^2\psi^2}{g}\phi = 0 \,, \tag{7.31}$$

while the Einstein equations are satisfied if

$$\chi' + \frac{r\psi'^2}{2} + \frac{re^{\chi}q^2\phi^2\psi^2}{2g^2} = 0 \,, \tag{7.32}$$

$$g' + \left(\frac{3}{r} - \frac{\chi'}{2}\right)g + \frac{re^{\chi}\phi'^2}{8} + \frac{m^2r\psi^2}{4} - 5r = 0 \,. \tag{7.33}$$

These have two symmetries:

$$\tilde{\psi}(r) = \psi(ar) \,, \qquad \tilde{\phi}(r) = \frac{1}{a}\phi(ar) \,, \qquad \tilde{\chi}(r) = \chi(ar) \,, \qquad \tilde{g}(r) = \frac{1}{a^2}g(ar) \,, \tag{7.34}$$

and

$$\tilde{\chi} = \chi + \Delta \,, \qquad \tilde{\phi} = e^{-\frac{\Delta}{2}}\phi \,. \tag{7.35}$$

As we did for $q = 0$, we would like to find solutions with a horizon at some $r = r_+$. The electric potential must also vanish at the horizon, and we are looking for solutions for which the leading falloff ψ_1 in (7.3) vanishes for the scalar. Also, multiplying the first equation (7.30) by g and evaluating at $r = r_+$ fixes $\psi'(r_+)$ in terms of $\psi(r_+)$ and $g'(r_+)$. Altogether, our boundary conditions are

$$g(r_+) = 0 \,, \qquad \phi(r_+) = 0 \,, \qquad \chi(\infty) = 0 \,, \qquad \psi_1 = 0 \,,$$

and

$$\psi'(r_+) = \frac{8m^2\psi(r_+)}{40r_+ - 2m^2 r_+^2\psi^2(r_+) - r_+ e^{\chi(r_+)}(\phi'(r_+))^2} \,.$$

The remaining freedom to choose r_+ and $\phi'(r_+)$ leads to a family of solutions with different T and μ. Explicitly, we have

$$\mu = \phi(\infty) \,, \qquad\qquad T = \frac{1}{4\pi}g'(r_+)e^{-\chi(r_+)/2} \,.$$

Solutions with the same T/μ are simply related by the scaling symmetry (7.34).

Numerical evaluation of solutions

To find solutions in practice, we can make use of the symmetries (7.34, 7.35) to initially set $r_+ = 1$ and $\chi(0) = 0$ and solve the equations with boundary conditions

$$g(1) = 0 \,, \qquad \chi(0) = 0 \,, \qquad \phi(1) = 0 \,, \qquad \phi'(1) = E_0 \,, \qquad \psi(1) = \psi_0 \,,$$

and

$$\psi'(1) = \frac{8m^2\psi_0}{40 - 2m^2\psi_0^2 - E_0^2} \,.$$

We use E_0 as a shooting parameter to enforce $\psi_1 = 0$, and find one solution for each ψ_0. From these solutions, we apply the symmetry (7.35) with $\Delta = -\chi(\infty)$ to restore $\chi(\infty) = 0$ and finally use the symmetry (7.34) to scale to the desired temperature or chemical potential.

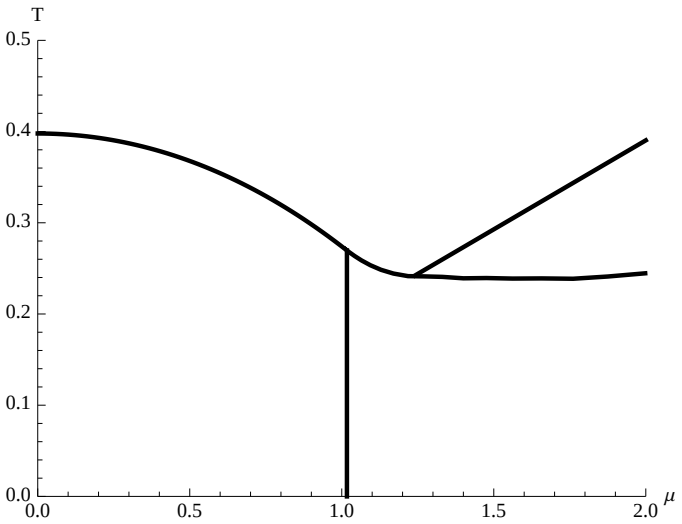

Figure 7.9: Phase diagram for $m^2 = -6$ and $q = 2$. Clockwise from the origin, the phases correspond to the AdS soliton (confined), RN black hole, black hole with scalar, and soliton with scalar.

7.5.3 Phase diagrams

At a generic point in the phase diagram, we can have up to four solutions (AdS soliton, planar RN black hole, soliton with scalar, black hole with scalar), or more in cases where there is more than one solution of a given type.

To map out the phase diagram, we evaluate the action for the various solutions using the methods of section 2. The equilibrium phase corresponds to the solution with lowest action. The phase diagrams for $q = 1.3$ and $q = 2$ (in the case $m^2 = -6$) are shown in figures 7.9 and 7.10/7.11).

For large q, the condensation of the scalar field occurs in a region of the phase diagram where the back-reaction is negligible, so the phase diagram may be understood here (for $\mu \sim 1/q$) by treating the gauge field and scalar on a fixed background (the Schwarzschild black hole). The resulting phase diagram is shown in figure (7.12).

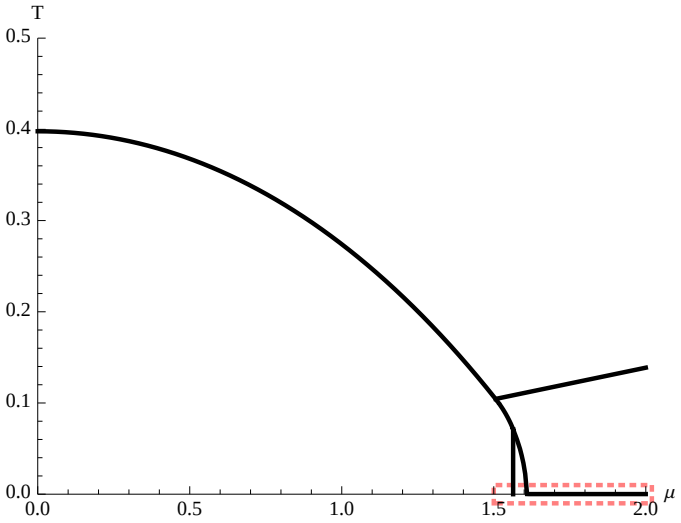

Figure 7.10: Phase diagram for $m^2 = -6$ and $q = 1.3$. Clockwise from the origin, the phases correspond to the AdS soliton (confined), RN black hole, black hole with scalar, and soliton with scalar.

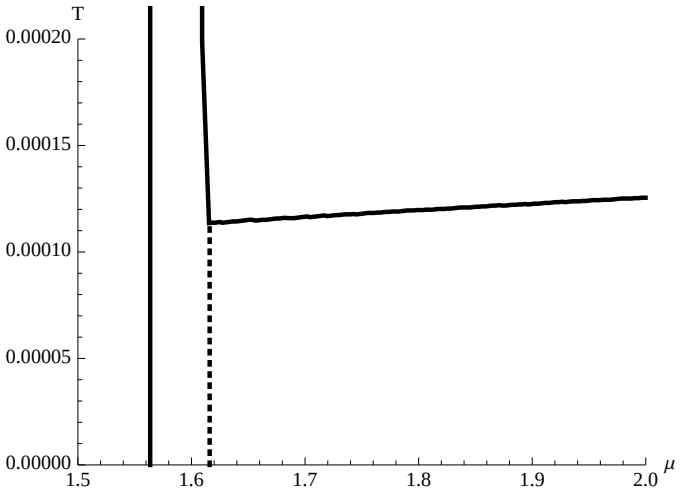

Figure 7.11: Small temperature region of phase diagram for $m^2 = -6$ and $q = 1.3$. Dashed line represents a first order transition within the soliton with scalar phase.

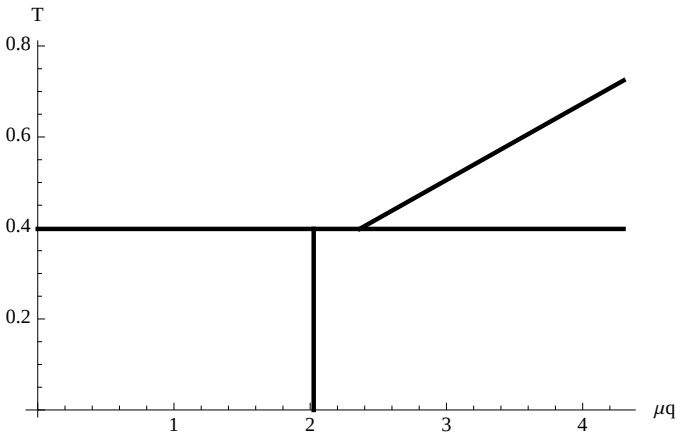

Figure 7.12: Phase diagram for large q, $m^2 = -6$.

7.6 Discussion

In this note, we have investigated the phase structure for a simple class of holographic systems which we have argued have the minimal set of ingredients to holographically describe the phenomenon of color superconductivity. Even in these simple models, we find a rich phase structure with features similar to the conjectured behavior of QCD at finite temperature and baryon chemical potential. It would be useful to verify the thermodynamic stability (and also the stability towards gravitational perturbations) of the phases that we have identified. This could indicate regions of the phase diagram where we have not yet identified the true equilibrium phase for the model, for example since our ansatz might be too symmetric.

We have calculated some of the basic thermodynamic observables, but it would be interesting to investigate more fully the physical properties of the various phases and establish more definitively a connection between the phase we find at large μ and small temperature and the physics of color superconductivity.

Apart from the $\psi\psi\psi^\dagger\psi^\dagger$ condensate that we can see directly using the ingredients of our model, there are various other features that characterize a color superconductivity phase [5]. Typically, the breaking of gauge symmetry is accompanied by some breaking of exact or approximate flavor symmetries. Thus, the superconducting phase has a low-energy spectrum characterized by Goldstone bosons or pseudo-Goldstone bosons associated with the broken flavor symmetries, together with massive vector bosons as-

sociated with the spontaneously broken gauge symmetry. It would therefore be interesting to analyze the spectrum of fluctuations in our model to compare with these expectations.

A caveat related to looking for features associated with the global flavor symmetries (and their breaking) in our model is that we may not have included enough ingredients in our bottom-up approach for all these features to be present. In simple models where the flavor degrees of freedom are associated with probe branes, there are explicit gauge fields in the bulk dual to the global symmetry current operators. However, in fully back-reacted solutions (appropriate for studying $N_f \sim N_c$), these branes are replaced by a modified geometry with additional fluxes (for an explicit example of such solutions, see [37]). In these solutions (which we are trying to model in our approach), it is less clear how to identify the global symmetry group from the gravity solution, but presumably it has to do with some detailed properties of the geometry. Thus, it is possible that the Goldstone modes associated with broken flavor symmetries correspond to fluctuations in some fields (e.g. form-fields) that we have not included.

The color superconducting condensate also breaks the global baryon number symmetry, so there should be an associated Goldstone boson related to the phase of the condensate, and associated superfluidity phenomena. In other holographic models with superfluidity, the condensate is dual to a charged scalar field in the bulk and the Goldstone mode is related to fluctuations in the phase of this field. However, as we mentioned in the introduction, the baryon operator has dimension of order N, so we do not expect a light charged scalar field in the bulk. In a more complete top-down model, the baryon operator may be related to some non-perturbative degrees of freedom (such as D-branes) in the bulk, and it may be necessary to have a model with these degrees of freedom included in order to directly see the Goldstone mode from the bulk physics. Related to these observations, it may be interesting to probe our model with D-branes (put in by hand), in order to make the relation to microscopic physics more manifest, and to help gain a better understanding of the phenomenological parameters of our model.

There are a number of variants on the model that would be interesting to study. First, the breaking of scale-invariance, implemented in our model by the varying circle direction in the bulk, could be achieved in other ways, replacing g_{ww} with a more general scalar field, as in the model of [36]. In the setup of that paper, the transition between confined and deconfined phases was found to exhibit crossover behavior at small chemical potential, a feature expected in the real QCD phase diagram and expected generally

for massive quarks with sufficiently large N_f/N_c. It would be interesting to look for an even more realistic holographic model by incorporating features of the model we have studied here and the model of [36].

It would also be interesting to look at the effects of a Chern-Simons term for the bulk gauge field. In [104] and [111], it was shown that such a term (with sufficiently large coefficient) gives rise to an instability toward inhomogeneous phases, perhaps associated with the chiral density wave phase believed to exist at large density in QCD with $N_c \ll N_f$ [35, 125]. It is interesting to investigate the interplay between these inhomogeneous instabilities and the superconducting instabilities discussed in the present chapter. It would also be interesting to consider more general actions (such as Born-Infeld) for the gauge field, interaction terms for the scalar field in the bulk, or other couplings between the scalar field and gauge field.

Finally, once the technical challenges of writing down fully back-reacted solutions for top-down models of holographic QCD with $N_f \ N_c$ have been overcome, it will be interesting to see whether the basic features we find here are manifested in the more complete string-theoretic models. If certain features are found to be universal, these might taken as qualitative predictions for the QCD phase diagram, or at least motivate an effort to understand whether these features are also present in the phase diagram of real-world QCD.

Chapter 8

Conclusion

In this thesis I showed how the AdS/CFT correspondence can not only be used to address deep questions in quantum gravity and the nature of space-time, but also as a powerful tool to construct strongly coupled field theory models ranging from relativistic fluids to QCD-like theories.

Part I of this thesis was focused on a fundamental question regarding the holographic principle, i.e.: characterizing the precise map between bulk and boundary degrees of freedom. At first glance, simply by realizing how fundamentally different the physics of these two sides seem, I argued that such a map is highly non trivial, most likely non local and even possibly not well behaved. However, as discussed in chapters 2, 3, and 4, there are good reasons to believe that, while still non trivial, such map does follow certain general rules and it is not arbitrarily non local.

By direct use of entanglement entropy on the field theory side, and its holographic realization on the gravity side, I was able to set an upper limit on the size of the bulk region dual to a portion of the boundary. This bulk region, I believe, should contain enough information to allow for the reconstruction of every physical observer within the causal development of the region of interest on the boundary, as discussed in chapter 2. It is interesting to point out that, as indicated by the scaling of entropy in space-times with gravity, quantum gravity seems to be highly redundant in its information storing, a fact that is not only supported by the holographic principle, but directly present in my discussion on the bulk to boundary map and partial information retrieval.

Moreover, I addressed how a potential counter argument mentioned in chapter 2, arising from high central densities boson stars, was avoided by noticing that these objects are believed to be unstable and, therefore, physically forbidden — as argued in chapter 3.

In addition, in chapter 4 I provided a detailed discussion of Rindler wedges of AdS space, their mathematical formulation as hyperbolic black holes, and how entanglement is a fundamental piece for the existence of a holographic space-time. In this chapter it was also observed how entanglement between boundary degrees of freedom had a dramatic influence on the

shape and even topology of the gravity dual. Moreover, I argued how the micro states of certain black holes can be understood as isolated patches of space-time with pathological horizons — as indicated by their divergent energy momentum tensors — that, nonetheless, when ensembled together can lead to a smooth, larger, space-time.

In part II of this thesis I shifted focus to some practical uses of the AdS/CFT correspondence. I started by looking at how small perturbations of the metric field of certain gravity solutions can have a direct interpretation as a relativistic fluid on the field theory side. This result is known as the fluid / gravity correspondence and can be used in a perturbative manner to compute higher order corrections to the relativistic Navier-Stokes equation, as well as to directly study the dynamics of such metric perturbations solely from the gravity theory point of view.

In chapter 5, with the hope of capturing a more general set of solutions, subject only to the most basic physical constraints, I went further and relaxed the conditions imposed on the perturbations usually considered in the fluid/ gravity correspondence literature. What I observed was how certain features of the bulk metric had a direct and dramatic consequence on the types of field theory solutions we obtained on the boundary. Conversely, I showed how demanding that the boundary theory only obeyed the basic conservations laws was not enough to ensure a well behaved bulk dual; these, in turn, are most likely related to out of equilibrium, or unstable boundary solutions that are out of the scope of the techniques employed.

Next, in chapter 6, I discussed how generic holographic field theories can be constructed from a relatively simple gravity model in a bottom up as well as a top down approach. Not only I was able to define such theories, but the extension to finite temperature and finite chemical potential — both notoriously hard in conventional field theory — was both natural and (relatively) easy to be dealt with.

In this chapter I discussed both numerical and analytical analysis of a variety of holographic models and was able to identify their major differences and similarities. For models based on Dp-Dq brane systems I computed the exact relation between charge and chemical potential in the field theory and found that it reproduced some well known results in the literature. Additionally, I generalized the results to an arbitrary Dp-Dq brane ansatz. For the bottom up approach I opted for a numerical analysis of the density versus chemical potential relation in different dimensions, with different field contents and with or without back reaction, the results of which were summarized in table 6.2.

Finally, as an extension of the bottom up approach discussed in chapter

6, in chapter 7 I analyzed a holographic model that showcases a much richer phase diagram, describing, at least qualitatively, the phenomenon of colour super conductivity predicted by QCD.

To accomplish this I built a bottom up holographic model that included a neutral scalar field coupled to gravity. This model not only has the well known Hawking-Page transition in the bulk — from an AdS soliton to a Reissner-Nordstrom black hole — which in the context of holographic field theory is interpreted as a confinement - deconfinement transition, but I also observed a second phase transition, since now not only temperature, but also chemical potential is a free solution parameter.

Moreover, the discussion was extended to charged scalar fields coupled to gravity — which I argued could potentially model the phenomena of flavour superconductivity — and uncovered an even richer phase diagram. This phase new diagram was shown to be highly dependent on the parameters of the theory, and changed dramatically when the mass or charge of the scalar field were changed.

In this thesis I showed how the AdS/CFT correspondence can address deep ingrained issues of quantum gravity, as well as be used to build realistic models of strongly coupled field theories. All of the projects discussed in this thesis are part of very rich and active fields of research and many of the results obtained throughout this thesis served as stepping stones for further advancing our knowledge of the holographic principle, the nature of space-time, and holographic models of field theories.

While the subjects addressed in this thesis continue to evolve, a thorough understanding of the holographic principle and the AdS/CFT correspondence, as well a fully working — tractable — model of strongly coupled field theories such as QCD still eludes physicist. Nevertheless, progress in this field has been steady and I humbly believe the thesis presented here contributed positively to furthering our understanding of such questions.

Bibliography

[1] Ofer Aharony, Steven S. Gubser, Juan Martin Maldacena, Hirosi Ooguri, and Yaron Oz. Large N field theories, string theory and gravity. *Phys.Rept.*, 323:183–386, 2000.

[2] Ofer Aharony, Jacob Sonnenschein, and Shimon Yankielowicz. A holographic model of deconfinement and chiral symmetry restoration. *Annals Phys.*, 322:1420–1443, 2007.

[3] Mark G. Alford, Krishna Rajagopal, and Frank Wilczek. QCD at finite baryon density: Nucleon droplets and color superconductivity. *Phys.Lett.*, B422:247–256, 1998.

[4] Mark G. Alford, Krishna Rajagopal, and Frank Wilczek. Color flavor locking and chiral symmetry breaking in high density QCD. *Nucl.Phys.*, B537:443–458, 1999.

[5] Mark G. Alford, Andreas Schmitt, Krishna Rajagopal, and Thomas Schfer. Color superconductivity in dense quark matter. *Rev.Mod.Phys.*, 80:1455–1515, 2008.

[6] Mohsen Alishahiha, Andreas Karch, Eva Silverstein, and David Tong. The dS/dS correspondence. *AIP Conf.Proc.*, 743:393–409, 2005.

[7] Martin Ammon, Johanna Erdmenger, Matthias Kaminski, and Patrick Kerner. Flavor Superconductivity from Gauge/Gravity Duality. *JHEP*, 0910:067, 2009.

[8] Martin Ammon, Johanna Erdmenger, Matthias Kaminski, and Patrick Kerner. Superconductivity from gauge/gravity duality with flavor. *Phys.Lett.*, B680:516–520, 2009.

[9] Martin Ammon, Johanna Erdmenger, Shu Lin, Steffen Muller, Andy O'Bannon, et al. On Stability and Transport of Cold Holographic Matter. *JHEP*, 1109:030, 2011.

[10] Daniel Arean, Pallab Basu, and Chethan Krishnan. The Many Phases of Holographic Superfluids. *JHEP*, 1010:006, 2010.

[11] Dumitru Astefanesei and Eugen Radu. Boson stars with negative cosmological constant. *Nucl.Phys.*, B665:594–622, 2003.

[12] Dumitru Astefanesei and Eugen Radu. Boson stars with negative cosmological constant. *Nucl.Phys.*, B665:594–622, 2003.

[13] J. Babington, J. Erdmenger, Nick J. Evans, Z. Guralnik, and I. Kirsch. Chiral symmetry breaking and pions in nonsupersymmetric gauge / gravity duals. *Phys.Rev.*, D69:066007, 2004.

[14] Vijay Balasubramanian and Per Kraus. A Stress tensor for Anti-de Sitter gravity. *Commun.Math.Phys.*, 208:413–428, 1999.

[15] Vijay Balasubramanian, Michael B. McDermott, and Mark Van Raamsdonk. Momentum-space entanglement and renormalization in quantum field theory. *Phys.Rev.*, D86:045014, 2012.

[16] T. Banks. Holographic Space-time from the Big Bang to the de Sitter era. *J.Phys.*, A42:304002, 2009.

[17] Pallab Basu, Jianyang He, Anindya Mukherjee, and Hsien-Hang Shieh. Superconductivity from D3/D7: Holographic Pion Superfluid. *JHEP*, 0911:070, 2009.

[18] Pallab Basu, Anindya Mukherjee, and Hsien-Hang Shieh. Supercurrent: Vector Hair for an AdS Black Hole. *Phys. Rev.*, D79:045010, 2009.

[19] Pallab Basu, Fernando Nogueira, Moshe Rozali, Jared B. Stang, and Mark Van Raamsdonk. Towards A Holographic Model of Color Superconductivity. *New J.Phys.*, 13:055001, 2011.

[20] Oren Bergman, Gilad Lifschytz, and Matthew Lippert. Holographic Nuclear Physics. *JHEP*, 11:056, 2007.

[21] Sayantani Bhattacharyya, Veronika E Hubeny, Shiraz Minwalla, and Mukund Rangamani. Nonlinear Fluid Dynamics from Gravity. *JHEP*, 0802:045, 2008.

[22] N.D. Birrell and P.C.W. Davies. Quantum Fields in Curved Space. *Cambridge Monogr.Math.Phys.*, 1982.

[23] Raphael Bousso, Ben Freivogel, Stefan Leichenauer, Vladimir Rosenhaus, and Claire Zukowski. Null Geodesics, Local CFT Operators and AdS/CFT for Subregions. 2012.

[24] Raphael Bousso, Stefan Leichenauer, and Vladimir Rosenhaus. Lightsheets and AdS/CFT. *Phys.Rev.*, D86:046009, 2012.

[25] Peter Breitenlohner and Daniel Z. Freedman. Positive Energy in anti-De Sitter Backgrounds and Gauged Extended Supergravity. *Phys.Lett.*, B115:197, 1982.

[26] Peter Breitenlohner and Daniel Z. Freedman. Stability in Gauged Extended Supergravity. *Annals Phys.*, 144:249, 1982.

[27] Yves Brihaye, Betti Hartmann, and Sardor Tojiev. Stability of charged solitons and formation of boson stars in 5-dimensional Anti-de Sitter space-time. 2013.

[28] D. Buchholz, C. D'Antoni, and K. Fredenhagen. The universal structure of local algebras. *Comm. Math. Phys.*, 111:123 – 135, 1987.

[29] Horacio Casini, Marina Huerta, and Robert C. Myers. Towards a derivation of holographic entanglement entropy. *JHEP*, 1105:036, 2011.

[30] Heng-Yu Chen, Koji Hashimoto, and Shunji Matsuura. Towards a Holographic Model of Color-Flavor Locking Phase. *JHEP*, 1002:104, 2010.

[31] Bartlomiej Czech, Joanna L. Karczmarek, Fernando Nogueira, and Mark Van Raamsdonk. Rindler Quantum Gravity. *Class.Quant.Grav.*, 29:235025, 2012.

[32] Bartlomiej Czech, Joanna L. Karczmarek, Fernando Nogueira, and Mark Van Raamsdonk. The Gravity Dual of a Density Matrix. *Class.Quant.Grav.*, 29:155009, 2012.

[33] Bartlomiej Czech, Joanna L. Karczmarek, Fernando Nogueira, and Mark Van Raamsdonk. The Gravity Dual of a Density Matrix. *Class.Quant.Grav.*, 29, 2012.

[34] Sebastian de Haro, Sergey N. Solodukhin, and Kostas Skenderis. Holographic reconstruction of space-time and renormalization in the AdS / CFT correspondence. *Commun.Math.Phys.*, 217:595–622, 2001.

[35] D.V. Deryagin, Dmitri Yu. Grigoriev, and V.A. Rubakov. Standing wave ground state in high density, zero temperature QCD at large N(c). *Int.J.Mod.Phys.*, A7:659–681, 1992.

[36] Oliver DeWolfe, Steven S. Gubser, and Christopher Rosen. A holographic critical point. *Phys.Rev.*, D83:086005, 2011.

[37] Eric D'Hoker, John Estes, and Michael Gutperle. Exact half-BPS Type IIB interface solutions. II. Flux solutions and multi-Janus. *JHEP*, 0706:022, 2007.

[38] Xi Dong, Bart Horn, Shunji Matsuura, Eva Silverstein, and Gonzalo Torroba. FRW solutions and holography from uplifted AdS/CFT. *Phys.Rev.*, D85:104035, 2012.

[39] Xi Dong, Bart Horn, Eva Silverstein, and Gonzalo Torroba. Micromanaging de Sitter holography. *Class.Quant.Grav.*, 27:245020, 2010.

[40] Vladimir Dzhunushaliev, Vladimir Folomeev, Ratbay Myrzakulov, and Douglas Singleton. On the stability of spherically symmetric and wormhole solutions supported by the sine-Gordon ghost scalar field. *Phys.Rev.*, D82:045032, 2010.

[41] Roberto Emparan. AdS / CFT duals of topological black holes and the entropy of zero energy states. *JHEP*, 9906:036, 1999.

[42] Johanna Erdmenger, Matthias Kaminski, Patrick Kerner, and Felix Rust. Finite baryon and isospin chemical potential in AdS/CFT with flavor. *JHEP*, 0811:031, 2008.

[43] Johanna Erdmenger, Matthias Kaminski, and Felix Rust. Holographic vector mesons from spectral functions at finite baryon or isospin density. *Phys.Rev.*, D77:046005, 2008.

[44] Thomas Faulkner, Monica Guica, Thomas Hartman, Robert C. Myers, and Mark Van Raamsdonk. Gravitation from Entanglement in Holographic CFTs. *JHEP*, 1403:051, 2014.

[45] L.H. Ford and Thomas A. Roman. Averaged energy conditions and quantum inequalities. *Phys.Rev.*, D51:4277–4286, 1995.

[46] K. Fredenhagen. On the modular structure of local algebras of observables. *Comm. Math. Phys.*, 97:79 – 89, 1985.

[47] Ben Freivogel, Veronika E. Hubeny, Alexander Maloney, Robert C. Myers, Mukund Rangamani, et al. Inflation in AdS/CFT. *JHEP*, 0603:007, 2006.

[48] Ben Freivogel, Yasuhiro Sekino, Leonard Susskind, and Chen-Pin Yeh. A Holographic framework for eternal inflation. *Phys.Rev.*, D74:086003, 2006.

[49] Sijie Gao and Robert M. Wald. Theorems on gravitational time delay and related issues. *Class.Quant.Grav.*, 17:4999–5008, 2000.

[50] Simon A. Gentle, Mukund Rangamani, and Benjamin Withers. A Soliton Menagerie in AdS. *JHEP*, 1205:106, 2012.

[51] Steven B. Giddings and Donald Marolf. A Global picture of quantum de Sitter space. *Phys.Rev.*, D76:064023, 2007.

[52] S. Goldstein, J. L. Lebowitz, Tumulka R., and N. Zanghì. Canonical Typicality. *Phys. Rev. Lett.*, 96:050403, 2006.

[53] S. S. Gubser, Igor R. Klebanov, and Alexander M. Polyakov. Gauge theory correlators from non-critical string theory. *Phys. Lett.*, B428:105–114, 1998.

[54] Steven S. Gubser. Breaking an Abelian gauge symmetry near a black hole horizon. *Phys.Rev.*, D78:065034, 2008.

[55] Umut Gursoy, Elias Kiritsis, Liuba Mazzanti, Georgios Michalogiorgakis, and Francesco Nitti. Improved Holographic QCD. *Lect.Notes Phys.*, 828:79–146, 2011.

[56] Alex Hamilton, Daniel N. Kabat, Gilad Lifschytz, and David A. Lowe. Holographic representation of local bulk operators. *Phys.Rev.*, D74:066009, 2006.

[57] Alex Hamilton, Daniel N. Kabat, Gilad Lifschytz, and David A. Lowe. Local bulk operators in AdS/CFT: A Boundary view of horizons and locality. *Phys.Rev.*, D73:086003, 2006.

[58] Sean A. Hartnoll. Lectures on holographic methods for condensed matter physics. *Class.Quant.Grav.*, 26:224002, 2009.

[59] Sean A. Hartnoll, Christopher P. Herzog, and Gary T. Horowitz. Building a Holographic Superconductor. *Phys. Rev. Lett.*, 101:031601, 2008.

[60] Sean A. Hartnoll, Christopher P. Herzog, and Gary T. Horowitz. Holographic Superconductors. *JHEP*, 0812:015, 2008.

[61] Idse Heemskerk, Donald Marolf, Joseph Polchinski, and James Sully. Bulk and Transhorizon Measurements in AdS/CFT. *JHEP*, 1210:165, 2012.

[62] C. P. Herzog, P. K. Kovtun, and D. T. Son. Holographic model of superfluidity. *Phys. Rev.*, D79:066002, 2009.

[63] Norio Horigome and Yoshiaki Tanii. Holographic chiral phase transition with chemical potential. *JHEP*, 01:072, 2007.

[64] Gary T. Horowitz. Introduction to Holographic Superconductors. 2010.

[65] Gary T. Horowitz and Robert C. Myers. The AdS / CFT correspondence and a new positive energy conjecture for general relativity. *Phys.Rev.*, D59:026005, 1998.

[66] Gary T. Horowitz and Matthew M. Roberts. Holographic Superconductors with Various Condensates. *Phys. Rev.*, D78:126008, 2008.

[67] Gary T. Horowitz and Matthew M. Roberts. Zero Temperature Limit of Holographic Superconductors. *JHEP*, 0911:015, 2009.

[68] Gary T. Horowitz and Benson Way. Complete Phase Diagrams for a Holographic Superconductor/Insulator System. *JHEP*, 1011:011, 2010.

[69] Sanle Hu, James T. Liu, and Leopoldo A. Pando Zayas. Charged Boson Stars in AdS and a Zero Temperature Phase Transition. 2012.

[70] Veronika E. Hubeny. Extremal surfaces as bulk probes in AdS/CFT. *JHEP*, 1207:093, 2012.

[71] Veronika E. Hubeny. Extremal surfaces as bulk probes in AdS/CFT. *JHEP*, 093, 2012.

[72] Veronika E. Hubeny and Mukund Rangamani. Causal Holographic Information. *JHEP*, 1206:114, 2012.

[73] Veronika E. Hubeny, Mukund Rangamani, and Tadashi Takayanagi. A Covariant holographic entanglement entropy proposal. *JHEP*, 0707:062, 2007.

[74] Nabil Iqbal, Hong Liu, Mark Mezei, and Qimiao Si. Quantum phase transitions in holographic models of magnetism and superconductors. *Phys.Rev.*, D82:045002, 2010.

[75] W. Israel. Thermo field dynamics of black holes. *Phys.Lett.*, A57:107–110, 1976.

[76] Kristan Jensen, Andreas Karch, Dam T. Son, and Ethan G. Thompson. Holographic Berezinskii-Kosterlitz-Thouless Transitions. *Phys.Rev.Lett.*, 105:041601, 2010.

[77] P. Jetzer. Stability of charged boson stars. *Phys.Lett.*, B231:433, 1989.

[78] Philippe Jetzer. Boson stars. *Phys.Rept.*, 220:163–227, 1992.

[79] Daniel Kabat, Gilad Lifschytz, and David A. Lowe. Constructing local bulk observables in interacting AdS/CFT. *Phys.Rev.*, D83:106009, 2011.

[80] David B. Kaplan, Jong-Wan Lee, Dam T. Son, and Mikhail A. Stephanov. Conformality Lost. *Phys.Rev.*, D80:125005, 2009.

[81] Vadim Kaplunovsky, Dmitry Melnikov, and Jacob Sonnenschein. Baryonic Popcorn. 2012.

[82] Andreas Karch and Emanuel Katz. Adding flavor to AdS / CFT. *JHEP*, 0206:043, 2002.

[83] D. J. Kaup. Klein-Gordon Geon. *Phys.Rev.*, 172:13311342, 1968.

[84] Keun-Young Kim, Sang-Jin Sin, and Ismail Zahed. Dense hadronic matter in holographic QCD. 2006.

[85] Igor R. Klebanov and Edward Witten. AdS/CFT correspondence and symmetry breaking. *Nucl. Phys.*, B556:89–114, 1999.

[86] Shinpei Kobayashi, David Mateos, Shunji Matsuura, Robert C. Myers, and Rowan M. Thomson. Holographic phase transitions at finite baryon density. *JHEP*, 02:016, 2007.

[87] Martin Kruczenski, David Mateos, Robert C. Myers, and David J. Winters. Towards a holographic dual of large-N(c) QCD. *JHEP*, 05:041, 2004.

[88] Nima Lashkari, Michael B. McDermott, and Mark Van Raamsdonk. Gravitational Dynamics From Entanglement "Thermodynamics". 2013.

[89] Andrew R. Liddle and Mark S. Madsen. The Structure and formation of boson stars. *Int.J.Mod.Phys.*, D1:101–144, 1992.

[90] Steven L. Liebling and Carlos Palenzuela. Dynamical Boson Stars. *Living Rev.Rel.*, 15:6, 2012.

[91] Jorma Louko, Donald Marolf, and Simon F. Ross. On geodesic propagators and black hole holography. *Phys.Rev.*, D62:044041, 2000.

[92] Juan Martin Maldacena. The Large N limit of superconformal field theories and supergravity. *Adv.Theor.Math.Phys.*, 2:231–252, 1998.

[93] Juan Martin Maldacena. Eternal black holes in anti-de Sitter. *JHEP*, 0304:021, 2003.

[94] Gautam Mandal and Takeshi Morita. Gregory-Laflamme as the confinement/deconfinement transition in holographic QCD. *JHEP*, 1109:073, 2011.

[95] David Mateos, Robert C. Myers, and Rowan M. Thomson. Holographic phase transitions with fundamental matter. *Phys. Rev. Lett.*, 97:091601, 2006.

[96] Samir D. Mathur. Fuzzballs and the information paradox: A Summary and conjectures. 2008.

[97] Samir D. Mathur. The Information paradox and the infall problem. *Class.Quant.Grav.*, 28:125010, 2011.

[98] Samir D. Mathur. Black Holes and Beyond. *Annals Phys.*, 327:2760–2793, 2012.

[99] Samir D. Mathur and Christopher J. Plumberg. Correlations in Hawking radiation and the infall problem. *JHEP*, 1109:093, 2011.

[100] Shunji Matsuura. On holographic phase transitions at finite chemical potential. *JHEP*, 0711:098, 2007.

[101] John McGreevy. Holographic duality with a view toward many-body physics. *Adv.High Energy Phys.*, 2010:723105, 2010.

[102] Larry McLerran and Robert D. Pisarski. Phases of cold, dense quarks at large N(c). *Nucl.Phys.*, A796:83–100, 2007.

[103] Shiraz Minwalla. Restrictions imposed by superconformal invariance on quantum field theories. *Adv. Theor. Math. Phys.*, 2:781–846, 1998.

[104] Shin Nakamura, Hirosi Ooguri, and Chang-Soon Park. Gravity Dual of Spatially Modulated Phase. *Phys.Rev.*, D81:044018, 2010.

[105] Shin Nakamura, Yunseok Seo, Sang-Jin Sin, and K.P. Yogendran. A New Phase at Finite Quark Density from AdS/CFT. *J.Korean Phys.Soc.*, 52:1734–1739, 2008.

[106] Giuseppe Nardulli. Effective description of QCD at very high densities. *Riv.Nuovo Cim.*, 25N3:1–80, 2002.

[107] Tatsuma Nishioka, Shinsei Ryu, and Tadashi Takayanagi. Holographic Superconductor/Insulator Transition at Zero Temperature. *JHEP*, 1003:131, 2010.

[108] Fernando Nogueira. Extremal Surfaces in Asymptotically AdS Charged Boson Stars Backgrounds. *Phys.Rev.*, D87(10):106006, 2013.

[109] Fernando Nogueira and Jared B. Stang. Density versus chemical potential in holographic field theories. *Phys.Rev.*, D86:026001, 2012.

[110] Carlos Nunez, Angel Paredes, and Alfonso V. Ramallo. Unquenched Flavor in the Gauge/Gravity Correspondence. *Adv.High Energy Phys.*, 2010:196714, 2010.

[111] Hirosi Ooguri and Chang-Soon Park. Spatially Modulated Phase in Holographic Quark-Gluon Plasma. *Phys.Rev.Lett.*, 106:061601, 2011.

[112] Renaud Parentani. The Energy momentum tensor in Fulling-Rindler vacuum. *Class.Quant.Grav.*, 10:1409–1416, 1993.

[113] L. Pestov and G. Uhlmann. Two Dimensional Compact Simple Riemannian manifolds are Boundary Distance Rigid. *Annals of Math.*, 161:1089–1106, 2005.

[114] S. Popescu, A. J. Short, and A. Winter. Entanglement and the foundations of statistical mechanics. *Nature Physics*, 2:754 – 758, 2006.

[115] Krishna Rajagopal and Frank Wilczek. The Condensed matter physics of QCD. 2000.

[116] Moshe Rozali, Hsien-Hang Shieh, Mark Van Raamsdonk, and Jackson Wu. Cold Nuclear Matter In Holographic QCD. *JHEP*, 01:053, 2008.

[117] R. Ruffini and S. Bonazzola. Systems of self gravitating particles in general relativity and the concept of an equation of state. *Phys.Rev.*, 187:17671783, 1969.

[118] Shinsei Ryu and Tadashi Takayanagi. Holographic derivation of entanglement entropy from AdS/CFT. *Phys.Rev.Lett.*, 96:181602, 2006.

[119] Shinsei Ryu and Tadashi Takayanagi. Holographic derivation of entanglement entropy from AdS/CFT. *Phys.Rev.Lett.*, 96, 2006.

[120] Tadakatsu Sakai and Shigeki Sugimoto. Low energy hadron physics in holographic QCD. *Prog.Theor.Phys.*, 113:843–882, 2005.

[121] Kenji Sakamoto and Kiyoshi Shiraishi. Boson stars with large selfinteraction in (2+1)-dimensions: An Exact solution. *JHEP*, 9807:015, 1998.

[122] Kenji Sakamoto and Kiyoshi Shiraishi. Exact solutions for boson fermion stars in (2+1)-dimensions. *Phys.Rev.*, D58:124017, 1998.

[123] Omid Saremi and Dam Thanh Son. Hall viscosity from gauge/gravity duality. *JHEP*, 1204:091, 2012.

[124] F.E. Schunck and E.W. Mielke. General relativistic boson stars. *Class.Quant.Grav.*, 20:R301–R356, 2003.

[125] E. Shuster and D.T. Son. On finite density QCD at large N(c). *Nucl.Phys.*, B573:434–446, 2000.

[126] Dam T. Son and Andrei O. Starinets. Viscosity, Black Holes, and Quantum Field Theory. *Ann.Rev.Nucl.Part.Sci.*, 57:95–118, 2007.

[127] M.A. Stephanov. QCD phase diagram: An Overview. *PoS*, LAT2006:024, 2006.

[128] Andrew Strominger. The dS / CFT correspondence. *JHEP*, 0110:034, 2001.

[129] Leonard Susskind. The World as a hologram. *J.Math.Phys.*, 36:6377–6396, 1994.

[130] Leonard Susskind. Addendum to Fast Scramblers. 2011.

[131] Leonard Susskind, Larus Thorlacius, and John Uglum. The Stretched horizon and black hole complementarity. *Phys.Rev.*, D48:3743–3761, 1993.

[132] B. Swingle. Entanglement Renormalization and Holography. *Phys.Rev.D*, D86:065007, 2012.

[133] Gerard 't Hooft. Dimensional reduction in quantum gravity. *THU-93-26*, 1993.

[134] Mark Van Raamsdonk. Black Hole Dynamics From Atmospheric Science. *JHEP*, 0805:106, 2008.

[135] Mark Van Raamsdonk. Comments on quantum gravity and entanglement. 2009.

[136] Mark Van Raamsdonk. Building up spacetime with quantum entanglement. *Gen.Rel.Grav.*, 42:2323–2329, 2010.

[137] Mark Van Raamsdonk. A patchwork description of dual spacetimes in AdS/CFT. *Class.Quant.Grav.*, 28:065002, 2011.

[138] Mark Van Raamsdonk and Kevin Whyte. Baryon charge from embedding topology and a continuous meson spectrum in a new holographic gauge theory. *JHEP*, 1005:073, 2010.

[139] Aron C. Wall. Maximin Surfaces, and the Strong Subadditivity of the Covariant Holographic Entanglement Entropy. 2012.

[140] Edward Witten. Anti-de Sitter space and holography. *Adv. Theor. Math. Phys.*, 2:253–291, 1998.

[141] Edward Witten. Anti-de Sitter space, thermal phase transition, and confinement in gauge theories. *Adv.Theor.Math.Phys.*, 2:505–532, 1998.

[142] Edward Witten. Baryons and branes in anti de Sitter space. *JHEP*, 07:006, 1998.

otsep1000

Appendix A

Appendix to Chapter 4

A.1 Coordinate transformations

In this appendix, we show that a conformal transformation between the boundary of some Poincare patch and Minkowski space maps diamond-shaped regions as in Figure 4.4 to complementary Rindler wedges of Minkowski space. We also argue that there is another conformal transformation that maps one of these diamond-shaped regions to hyperbolic space times time.

Starting with the cylinder $S^d \times R$ in coordinates

$$ds^2 = -dT^2 + dR^2 + \sin^2 R \, d\Omega_{d-1}^2, \tag{A.1}$$

the change of coordinates

$$\tan \frac{T \pm R}{2} = t \pm r \tag{A.2}$$

followed by the conformal transformation

$$ds^2 \to \frac{1}{4} \left((r-t)^2 + 1\right) \left((r+t)^2 + 1\right) ds^2 \tag{A.3}$$

takes the region $D_P = \{-\pi < T < \pi, R < \pi - |T|\}$ to Minkowski space with metric

$$ds^2 = -dt^2 + dr^2 + r^2 d\Omega_{d-1}^2 \, . \tag{A.4}$$

The region D_P forms the boundary of a Poincare patch in AdS. If p_i and p_f are any points on the past and future boundaries of D_P (the past and future tips of a diamond-shaped region as in Figure 4.4), then the forward and backward lightcones from p_i and p_f divide D_P into four regions, as in Figure 4.4. After the transformation to Minkowski space, the space is still divided into four regions by lightcones, but since p_i and p_f map to the infinite past and infinite future, these lightcones become intersecting lightlike planar hypersurfaces. After a Poincare transformation, these can be mapped to the surfaces $x = t$ and $x = -t$ that bound Rindler wedges of Minkowski space, with the region $D(p_i, p_f)$ (the region bounded by the

forward lightcone from p_i and the backward lightcone from p_f) mapping to one of the wedges. As an example, the transformation above, without any additional Poincare transformation, maps the domain of dependence of the $\theta < \pi/2$ hemisphere of the $T = 0$ sphere to the Rindler wedge $x > 0, |t| < x$.

To map $D(p_i, p_f)$ to $H^d \times R$ using a conformal transformation, we can combine a map $D(p_i, p_f)$ to a Rindler wedge of Minkowski space as above, with a map back to a region $|T| < T_0, R < T_0 - |T|$ (the causal development of a ball in the $T = 0$ sphere), with a third conformal transformation (given explicitly in [29]) to $H^d \times R$. We note in particular [29] that in the map from the Rindler wedge to $H^d \times R$, the Rindler Hamiltonian maps to the generator of time translations.

Appendix B

Appendix to Chapter 7

B.1 Large charge limit

In this appendix, we analyze the case of large q. This is particularly simple, since in this limit, the back-reaction of the scalar and the gauge field on the metric go to zero in the region of the phase diagram where transitions to the superconducting phases occur. Explicitly, we can show that in the limit $q \to \infty$ with $q\mu$ fixed, the gauge field and scalar field decouple from the equations for the metric, but still give rise to a nontrivial phase structure. To investigate this, we need only consider the scalar field and gauge field equations on the fixed background spacetimes corresponding to low temperatures (the soliton geometry) and high temperatures (the Schwarzschild black hole).

Low Temperature

Starting from the action (7.2) for the scalar field and gauge field on the soliton background (7.7), we find that the equations of motion are (setting $L = 1$)

$$\begin{aligned} \phi'' + \left(\frac{f'}{f} + \frac{4}{r}\right)\phi' - \frac{2q^2}{r^2 f}\psi^2\phi &= 0\,, \\ \psi'' + \left(\frac{f'}{f} + \frac{6}{r}\right)\psi' + \frac{q^2}{r^4 f}\phi^2\psi - \frac{m^2}{r^2 f}\psi &= 0\,, \end{aligned}$$

where f is defined in (7.8).

These equations have two scaling symmetries related to the conformal symmetry of the boundary field theory and to the absence of back-reaction in our large charge limit. Given a solution $(\phi(r), \psi(r), r_0, q, m)$, we can check that the scaling

$$(\phi(r), \psi(r), r_0, q, m) \to (\beta\phi(\alpha r), \beta\alpha\psi(\alpha r), \frac{r_0}{\alpha}, \frac{q}{\alpha\beta}, m)$$

sends solutions to solutions. For our calculations, we will use this to set $r_0 = q = 1$.

Multiplying these equations by f and taking the limit $r \to r_0 = 1$, we find that regular solutions must obey

$$\begin{aligned} \phi'(1) &= \frac{2\psi^2(1)\phi(1)}{5} , \\ \psi'(1) &= \frac{\psi(1)}{5}\left(m^2 - \phi^2(1)\right) . \end{aligned}$$

We have two remaining parameters, $\psi(0)$ and $\phi(0)$. One of these can be fixed by demanding that the "non-normalizible" mode of ψ vanishes at infinity, while different values of the remaining parameter correspond to different values of μ.

Employing numerics, we find that for a fixed value of m^2, there is some critical value of μ above which solutions with a condensed scalar field exist.

In order to determine the critical value $\mu_c(m^2)$, we use the fact that the field values go to zero as we approach the critical μ from above. Thus, at the critical μ, the equations above linearized around the background solution $\phi = \mu$ should admit a solution with the correct boundary conditions. The linearized equations decouple from each other, so we need only study the ψ equation. This becomes

$$\psi'' + \left(\frac{6r^5 - 1}{r(r^5 - 1)}\right)\psi' + \frac{r(\mu^2 - m^2 r^2)}{r^5 - 1}\psi = 0 .$$

We can take $\psi(1) = 1$ without loss of generality, so the boundary condition for ψ' becomes

$$\psi'(1) = \frac{1}{5}(m^2 - \mu^2) .$$

Given m^2, we now find μ^2 by demanding that the leading asymptotic mode (ψ_1) of ψ vanishes. Our results for the critical μ as a function of m^2 are shown in figure B.1.

High temperature

The high temperature geometry relevant to the limit of large q with μq fixed is the $\mu \to 0$ limit of the Reissner-Nordstrom geometry (7.10), which gives the planar AdS-Schwarzschild black hole (with one of the spatial directions compactified). This is the relevant background for $T > 1/(2\pi R)$.

Explicitly, we have

$$ds^2 = r^2\left(-dt^2 f(r) + dx^2 + dy^2 + dz^2 + dw^2\right) + \frac{dr^2}{r^2 f(r)} ,$$

where

$$f(r) = 1 - \frac{r_+^5}{r^5} \ .$$

Here, r_+ is related to the temperature by

$$r_+ = \frac{4\pi T}{5} \ .$$

The equations of motion in this background are

$$\psi'' + \left(\frac{f'}{f} + \frac{6}{r}\right)\psi' + \frac{q^2}{r^4 f^2}\phi^2\psi - \frac{m^2}{r^2 f}\psi \quad = \quad 0 \ .$$

The equations have the same scaling symmetry as before, so we can set $r_+ = q = 1$ for numerics. Here, the choice $r_+ = 1$ corresponds to $T = 1/(2\pi R)$, where R is the radius chosen in the previous section by setting $r_0 = 1$. In this case, the boundary conditions are

$$\phi(1) = 0 \ , \qquad\qquad \psi'(1) = \frac{m^2 L^2 \psi(1)}{5} \ .$$

To determine the physics at other temperatures, we can fix q and R and use the scaling to adjust the temperature.

For any values of parameters, we have a solution

$$\psi = 0 \ , \qquad \phi(r) = \mu(1 - \frac{1}{r^3}) \ .$$

corresponding to the pure Reissner-Nordstrom background in the probe limit.

As in the low temperature phase, we find a critical value $\mu_c = F(m^2)$ (or, restoring temperature dependence, $\mu_c = \frac{T}{T_c}F(m^2)$) for each choice of m^2, above which there is another solution with nonzero ψ. This critical μ may again be determined by a linearized analysis, from which we obtain the equation

$$\psi'' + \left(\frac{6r^5 - 1}{r(r^5 - 1)}\right)\psi' + \left(\frac{\mu^2(r^3 - 1)^2}{r^4(r^5 - 1)^2} - \frac{m^2 r^3}{r^5 - 1}\right)\psi = 0 \ .$$

We can set $\psi(1) = 1$ without loss of generality, and this requires

$$\psi'(1) = \frac{m^2}{5} \ .$$

These can be solved numerically to find $F(m^2)$, and our results (with the low temperature results) are plotted in figure B.1.

A sample phase diagram, for the case $m^2 = -6$ is shown in figure 7.12.

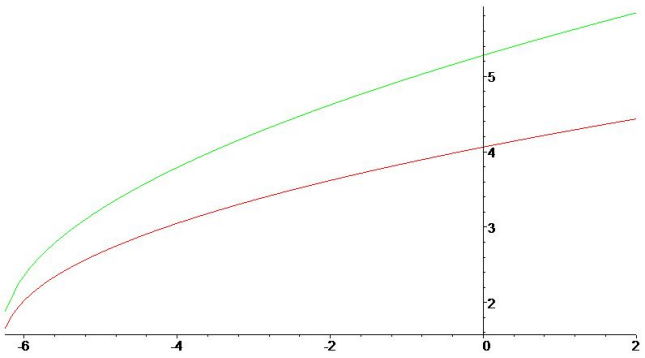

Figure B.1: Critical values of μq vs m^2 for scalar condensation in large q limit. The top curve is the critical value for μ in black hole phase (just above the transition temperature), while the bottom curve is the critical μ in low temperature phase.

B.1.1 Order of phase transitions in the probe limit

To complete this section, we verify analytically that the action for solutions with scalar field in the probe limit is always less than the corresponding unperturbed solution. In this limit we neglect the gravity back reaction of the gauge fields and scalar. The on-shell action in this approximation is given by

$$\frac{S}{T^d} = \int d^{d+1}x \, \sqrt{-g} g^{tt} g^{rr} \frac{A_t'^2}{2} \, . \tag{B.1}$$

We have used the fact that the scalar action is quadratic and vanishes on-shell once the boundary value of scalar is kept to zero [10]. Writing the action in this simple form gives us information about the relative free energy of the different phases.

The solution for A_t in the superconducting phase may be written as

$$A_t^S = A_t^0 + \delta A_t \, , \tag{B.2}$$

where $\delta A_t \to 0$ in the IR region of the bulk and near the boundary. A_t^0 is the value of A_t in the normal phase. Then, from eq. (B.1) we get

$$\frac{S_{new}}{T^d V} = \frac{S_{old}}{T^d V} + 2 \int dr \sqrt{-g} g^{rr} g^{tt} \partial_r A_t^0 \partial_r (\delta A_t) + \int \sqrt{-g} g^{rr} g^{tt} \frac{(\delta A_t)'^2}{2} \, . \tag{B.3}$$

The cross term between A_t^0 and δA_t vanishes after integrating by parts and then using the eom of A_t^0. Hence

$$\delta S = S_{new} - S_{old} = (T^d V) \int \sqrt{-g} g^{rr} g^{tt} \frac{(\delta A_t)'^2}{2} dr < 0 \text{as} g^{tt} < 0. \quad \text{(B.4)}$$

Therefore if a phase with non-trivial scalar condensate exists it will always have a lower free energy than the normal phase and the associated transition will be of second order.

The introduction of gravity may give rise to a positive term in the on-shell action and the nature of phase transition may change.

B.2 Critical μ for solutions with infinitesimal charged scalar

To find the critical μ at which solutions with infinitesimal scalar field exist, we find the value of μ for which the linearized scalar equation about the appropriate background admits a solution with the right boundary conditions at infinity.

At low temperatures, this gives (setting $r_0 = 1$)

$$\psi'' + \left(\frac{g'}{g} + \frac{4}{r}\right)\psi' + \frac{1}{g}\left(\frac{q^2\phi^2}{r^2} - m^2\right)\psi \,,$$
$$g(r) = r^2 - \frac{1}{r^3} \,, \qquad \phi = \mu \,,$$

while for the RN black hole background (setting $r_+ = 1$) we have

$$\psi'' + \left(\frac{g'}{g} + \frac{4}{r}\right)\psi' + \frac{1}{g}\left(\frac{q^2\phi^2}{g} - m^2\right)\psi \,,$$
$$g(r) = r^2 - \left(1 + \frac{3\mu^2}{8}\right)\frac{1}{r^3} + \frac{3\mu^2}{8r^6} \,,$$
$$\phi = \mu\left(1 - \frac{1}{r^3}\right) \,.$$

More general values of r_0 or r_+ can be restored by the scaling symmetry.

For $m^2 = -6$, we find a critical value of μ in the low-temperature case given by $\mu_{low} q = 5.089/(2\pi R)$. At high temperatures, the critical solutions exist T/μ when has a critical value as plotted in figure B.2.

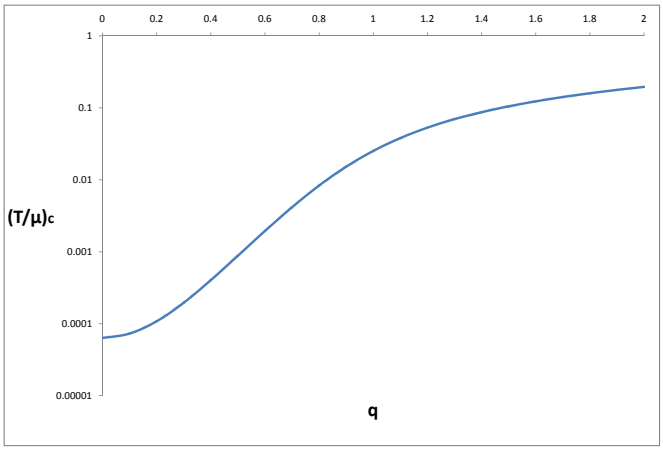

Figure B.2: Critical T/μ vs charge q for condensation of $m^2 = -6$ scalar field in Reissner-Nordstrom background.